

Reprogramming bacterial nanocompartments into light-triggered nanoreactors

by

Dennis Johanna Diaz Rincon

A thesis submitted in fulfilment of the requirements for the degree of
Doctor of Philosophy

Supervisors:

A/Prof. Anwar Sunna

Dr. Andrew care



MACQUARIE
University
SYDNEY · AUSTRALIA

Department of Molecular Sciences
Macquarie University
Sydney, Australia
December 2019

Table of contents

TABLE OF CONTENTS.....	II
ABSTRACT	IV
STATEMENT OF ORIGINALITY	VI
ACKNOWLEDGEMENTS.....	VII
POSTER PRESENTATIONS.....	IX
ORAL PRESENTATIONS AND PATENT	X
AWARDS.....	XI
LIST OF PUBLICATIONS.....	XII
LIST OF ABBREVIATIONS.....	XIII
AIMS AND SCOPE OF THIS THESIS	XVIII
.....	1
.....	1
CHAPTER 1: BIOENGINEERING STRATEGIES FOR PROTEIN-BASED NANOPARTICLES.....	1
INTRODUCTION	2
CHAPTER2: REPROGRAMMING ENCAPSULIN INTO A LIGHT-ACTIVATABLE NANOREACTOR FOR THE “ON DEMAND” GENERATION OF REACTIVE OXYGEN SPECIES.....	33
INTRODUCTION	34
CONTRIBUTIONS TO MANUSCRIPT 1	35
<i>Introduction.....</i>	38
<i>Materials and methods.....</i>	40
<i>Results.....</i>	44
<i>Discussion</i>	53
<i>References</i>	58
SUPPLEMENTARY INFORMATION.....	63

CHAPTER 3: ENGINEERING ENCAPSULINS AS ROS-GENERATING NANOCOMPARTMENTS.....	69
INTRODUCTION	70
CONTRIBUTION TO MANUSCRIPT 2	71
<i>ABSTRACT</i>	73
<i>Introduction</i>	74
<i>Materials and methods</i>	76
<i>Results</i>	80
<i>Discussion</i>	87
<i>References</i>	90
<i>Supplementary information</i>	94
CHAPTER 4: ENGINEERING ENCAPSULIN FOR THE LOADING AND CONTROLLED RELEASE OF DRUGS.....	97
<i>Introduction</i>	98
<i>Materials and methods</i>	100
<i>Results and Discussion</i>	104
<i>Conclusions</i>	113
<i>References</i>	114
CHAPTER 5: SUMMARY AND FUTURE PERSPECTIVES.....	116
APPENDIX A: ETHICS APPROVAL	127

Abstract

Encapsulins are protein-based nanocompartments found in 1-4% of known prokaryotes, which have a set of distinct physical and functional features that make them attractive as unique reaction chambers. They self-assemble from identical protein subunits into hollow spherical structures that are 18-44 nm in diameter and exhibit good colloidal properties and robust stability. During self-assembly, encapsulins selectively package and protect cargo proteins (native or foreign) tagged with a unique encapsulation signal peptide (ESig), offering an interchangeable system for the programmed encapsulation of ESig-tagged proteins. In addition, surface pore openings allow small molecules, like cellular oxygen, to enter the internal cavities of encapsulins, facilitating their interaction with the protein cargo. The outer surfaces of encapsulins are also highly adaptable and can be genetically and/or chemically modified to further enhance their functionalities. In this thesis, I aimed to reprogram encapsulin nanocompartments to have light-activatable properties and functionalities that lend themselves to practical applications in biotechnology and biomedicine.

The fluorescent proteins KillerRed (KR) and mini-Singlet Oxygen Generator (mSOG) are unique biological photosensitizers that produce reactive oxygen species (ROS) when irradiated with light at specific wavelengths. I reprogrammed the native function of encapsulin (Enc) from the bacterium *Thermotoga maritima* by loading it with ESig-tagged KR or mSOG variants. All photosensitizer-loaded Encs were recombinantly produced in *Escherichia coli*, purified by chromatographic methods and were found to be ~25-30 nm in size, monodisperse and fluorescent. The red fluorescent protein KR is a Type I photosensitizer that generates mainly superoxide ion ($O_2^{\cdot-}$) under green/yellow light irradiation. Upon activation with green light, KR-loaded Enc produced similar amounts of ROS as free KR, while unloaded Enc produced no ROS. These results show that KR can be packaged inside Enc without affecting its photosensitizing functions. Alternatively, the green fluorescent flavoprotein mSOG is a Type II photosensitizer that produces singlet oxygen (1O_2) upon blue light irradiation. mSOG variants, mSOG1 and mSOG2, previously engineered for enhanced 1O_2 generation were loaded into Enc. All mSOG-loaded Encs produced measurable quantities of 1O_2 under blue light activation, with a

mSOG1-loaded Enc variant (Enc-mSOG1-ESig_T) shown to be the most effective. Based on these findings, the capacity for Enc-mSOG1-ESig_T to trigger photosensitized reactions was evaluated in a cellular model of lung cancer. Enc-mSOG1-ESig_T displayed no cytotoxicity in the dark, however, when activated with blue light, it caused a ~34% reduction in cancer cell viability. Thus, this work represents the first-time protein-based nanocompartments have been loaded with functional biological photosensitizers and shown the ability to act as light-triggerable 'nanoreactors'. Furthermore, their capacity to induce phototoxicity against cancer cells highlights their potential as an exciting new nanoplatform for the photodynamic therapy of cancer.

I also present preliminary work aimed at incorporating a light-triggered disassembly/reassembly mechanism into encapsulin for the loading and/or releasing its cargo. To achieve this function, I implemented a pH disassembly/reassembly approach to test the encapsulation of small-molecule drugs into *T. maritima* encapsulin. Additionally, protein modelling was used to identify three residues located at the interfaces of encapsulin subunits, which could be substituted with photo-responsive unnatural amino acids (UAA) (e.g azobenzene) to potentially mediate light-triggered disassembly/reassembly of the nanocompartment.

Statement of Originality

This work has not previously been submitted for a degree or diploma in any university. To the best of my knowledge and belief, the thesis contains no material previously published or written by another person except where due reference is made in the thesis itself.

(Signed) _____ Date: _____
Dennis Johanna Diaz Rincon

Acknowledgements

This thesis comprises three years of full-time research conducted in the Department of Molecular Sciences at Macquarie University from 2016 to 2019.

I would like to express my sincerest gratitude to my supervisors A/Prof Anwar Sunna and Dr Andrew Care for their patience, trust, optimism and support. Your guidance and lessons have helped me throughout this project.

Anwar, thank you for giving me the opportunity to join your research group and pursue my dreams, without your guidance, supervision and trust, completing this research would have been much more challenging.

I would like to specially thank Andrew for the all the time and effort he put into making this project successful. Your experience and attention to detail allowed me to grow as a scientist and researcher. Thank you for motivating to get out of my comfort zone to try new experiences like applying for grants, presenting in conferences and doing a pod-cast.

I would like to thank our collaborators Prof Ingemar André (Lund University, Sweden), Prof Sinisa Bjelic (Linneus University, Sweden) and Dr Victoria Peddie (University of Adelaide, Australia) for their contributions to this work.

Thank you to all the great people in my research group: Kerstin, Alex, Dominik, Rachit, Vinoth, Sandra, Kaitlin, India and Manuel. Thanks also to: Monica, Shibani, Alex, Tom, Niel, Heinrich, Hugh, Briardo, Elizabeth, Sameera, Elsa, Alejandro, Daniel, Laura, and all the other people that I have met and become friends with over these three years. I have learnt a lot from every one of you and I am very grateful for all the moments we shared together.

I acknowledge the international Macquarie University Research Excellence Scholarship (iMQRES), Sydney Vital Research Scholar Award and the Commonwealth Scientific and Industrial Research Organisation (CSIRO) Ph.D.

Scholarship Program in Synthetic Biology for funding this project and providing me with financial support. I would also like to acknowledge the Macquarie University Postgraduate Research Fund (PGRF) funding scheme in conjunction with the previously mentioned funding bodies for giving me the opportunity to present my research at national and international conferences.

I am also thankful to all my friends that could not be here with me, but they were always here for me regardless, their advice and motivation always kept me going.

Finally, I would like to thank my parents Lucia and Orlando for all the unconditional love and support. They have shaped the person I am today and because of them I have managed to achieve what I have thus far. I am immensely grateful to Ary for all his love, company, support and patience. Thank you for keeping me motivated and grounded, without you this journey would have been very difficult.

Poster presentations

Diaz D, Sunna A, and Care A. 2019. Shining a light on photosensitizing protein-based nanoparticles. Synthetic Biology Australasia Conference, Brisbane, Australia.

Diaz D, Sandra F, Sunna A, and Care A. 2019. Photosensitizing protein nanocages for photodynamic therapy. Biomimetics in Bioengineering Conference, Brisbane, Australia.

Diaz D, Sandra F, Sunna A, Care A. 2019. Developing protein nanocages as carriers for biological photosensitizers in cancer photodynamic therapy. 10th International Nanomedicine Conference. Sydney, Australia.

Boyton I, Goodchild S, Sandra F, **Diaz D**, Collins-Praino L.E, Care A. 2019. Characterizing the unique cargo-loading mechanisms of a protein-based nanoparticle. 10th International Nanomedicine Conference, Sydney, Australia.

Del Valle M, Goodchild S, Sandra F, **Diaz D**, Care A. 2019. Characterization of an encapsulin protein nanocage from *Alkaliphilus Metalliredigens*. 10th International Nanomedicine Conference, Sydney, Australia.

Wyllie K, Sandra F, **Diaz D**, Sunna A, Care A. 2019. Peptide-directed Encapsulation for Protein Delivery. 10th International Nanomedicine Conference, Sydney, Australia.

Diaz D, Care A, Sunna A. 2018. A novel protein-based nanoplatform for the localized and controlled delivery of drugs. Bionetwork Research Symposium. Sydney, Australia.

Diaz D, Care A, Sunna A. 2017. Protein nanocages for the localized and controlled delivery of drugs. Synthetic Biology Australasia Conference. Sydney, Australia.

Oral presentations and patent

Care A, **Diaz D**, Sandra F, and Vittorio O. 2019. Cages suitable for containing copper and methods for their use. **Patent**. *Provisional specification 2019902198*.

Diaz D, Sandra F, Sunna A, and Care A. 2019. Photosensitizing protein nanocages for photodynamic therapy. Biomimetics in Bioengineering Conference, Brisbane, Australia (Rapid Fire Talk).

Diaz D, Asensio X, Sunna A, and Care A. 2019. Bioengineering protein nanocompartments into photosensitizing nanoparticles. Bioengineering and Nanoscience Symposium, University of Sydney, Australia.

Diaz D, Care A, Sunna A. 2018. Engineering protein nanocages for targeted photodynamic therapy. 18th European Congress on Biotechnology (ECB) in Geneva, Switzerland.

Awards

- 2018** Macquarie University Postgraduate Research Fund (PGRF)
Value: 5,000 AUD
- 2018** Sydney Vital Research Scholar Award.
Value: 10,000 AUD
- 2018** Commonwealth Scientific and Industrial Research Organisation (CSIRO)
PhD Scholarship Program in Synthetic Biology. Approx.
Value: 40,000 AUD
- 2016** Three-year international Macquarie University Research Excellence
Scholarship, (iMQRES).
Approx. value: 200,000 AUD.

List of publications

This thesis includes one published article (see Chapter 1) and two manuscripts which were prepared for submission (see Chapters 2 and 3).

- 1) **Diaz D**, Care A, Sunna A. Bioengineering Strategies for Protein-Based Nanoparticles. *Genes* **2018**, 9 (7): p. 370.
(<https://doi.org/10.3390/genes9070370>)
- 2) **Diaz D**, Sandra F, Vidal X, Sunna A, Care A. Reprogramming encapsulin into a light-activatable nanoreactor for the “on demand” generation of reactive oxygen species. Prepared for submission to *Nature Communications*.
- 3) **Diaz D**, Vidal X. Sunna A, Care A. Engineering encapsulin as a ROS-generating nanocompartment. Prepared for submission to *Biomaterials Science and Engineering*.

List of Abbreviations

4-HPAA	4-hydroxyphenylacetaldehyde
AdhD	monomeric alcohol dehydrogenase D
ADP	Adenosine diphosphate
Aldox	Aldoxorubicin
ATP	Adenosine triphosphate
AzoPhe	Phenylalanine-4'-azobenzene
CALI	Chromophore-assisted light inactivation
CCMV	Cowpea
CD	circular dichroism
CelB	tetrameric β -glucosidase
CPMV	Cowpea mosaic virus
CPP	cell-penetrating peptide
CuAAC	copper-catalyzed azide–alkyne cycloaddition
Cyt cb562	C-type cytochrome
DAB	Diaminobenzidine
DCFH-DA	2',7'-dichlorodihydrofluorescein diacetate
DDS	Drug delivery systems
DHF	2'-7'-dichlorofluorescein
DLS	Dynamic light scattering
DMEM/F-12	Dulbecco's Modified Eagle Medium: Nutrient Mixture F-12
DNA	deoxyribonucleic acid
DOX	Doxorubicin
Dps	DNA-binding proteins
DyP	Dye decolorizing peroxidase
EGFP	Enhanced Green fluorescent protein

ELISA	Enzyme linked immunosorbent assays
EM	Electron microscopy
Em _{max}	Fluorescence emission maxima
Enc	His-tagged encapsulin from <i>T. maritima</i>
ESig	Encapsulation signal
ESig _T	Truncated Encapsulation signal
Ex _{max}	Fluorescence excitation maxima
FBS	Foetal bovine serum
FLP	Ferritin like proteins
FMN	Flavin mononucleotide Flavin mononucleotide and nicotinamide adenine dinucleotide
FMO	phosphate (NADPH)-dependent monooxygenase (FMO)
FRET	Fluorescence resonance energy transfer
GALK	ATP-dependent galactokinase
GFP	Green fluorescent protein
GLUK	ADP-dependent glucokinase
HA	Influenza virus haemagglutinin
HBc	Hepatitis B virus capsid protein
HCC	Hepatocellular carcinoma
HEK	Human embryonic kidney
HEPES	4-(2-hydroxyethyl)-1-piperazineethanesulfonic acid
HPV	Human papillomavirus
Hsp	Heat shock proteins
IgG	Immunoglobulin G
IMAC	Nickel-immobilized metal affinity chromatography
Insol	Insoluble
IPTG	Isopropyl- β -D-thiogalactopyranoside

KR	KillerRed
L	Peptide linker
LC%	Loading capacity
LS	Lumazine Synthase
mINT	minimal interaction domain
mKO	Monomeric KillerOrange
MnP	manganese peroxidase
mRNA	Messenger ribonucleic acid
mSOG	Mini Singlet oxygen generator
MTT	3-(4,5-dimethylthiazol-2-yl)-2,5-diphenyltetrazolium bromide
MVP	Major vault protein
NAD(P)H	Nicotinamide adenine dinucleotide (phosphate)
Native-PAGE	Native - polyacrylamide gel electrophoreses
NDDS	Nanoparticles-based drug delivery systems
nEnc	Unmodified (native) empty encapsulin from <i>Thermotoga maritima</i>
NHS	N-hydroxy-succinimides
Ni-NTA	nickel-nitrilotriacetic acid
NP	Nanoparticles
NPs	Nanoparticles
NS5A	Hepatitis C viral nonstructural protein 5A
OD	Optical density
PANAM	Polymers like polyamidoamine
PBS	Phosphate buffered saline
PC	Protein-based compartments
PCR	Polymerase chain reaction
PDT	Photodynamic therapy
PEG	Polyethylene glycol

pI	Isoelectric point
PLP	Pyridoxal phosphate
PNC	Protein nanocompartments
PNPs	Protein-based nanoparticles
PSA	Polystyrene sulfonic acid
RNA	Ribonucleic acid
ROS	Reactive oxygen species
RT	Room temperature
SAGEs	Self-assembling cage-like particles
SDS-PAGE	Sodium dodecyl sulphate - polyacrylamide gel electrophoreses
SEC	Size exclusion chromatography
sfGFP	Superfolder Green fluorescent protein
SN	SuperNova
Sol	Soluble
SOPP	Singlet oxygen photosensitizing protein
SOSG	Singlet Oxygen Sensor Green
StAv	Streptavidin
TEM	Transmission electron microscopy
TEP1	Telomerase-associated protein
TFP	Teal Fluorescent protein
TIV	Trivalent inactivated influenza vaccine
<i>Tm</i>	<i>Thermotoga maritima</i>
TnaA	Pyridoxal phosphate -dependent tryptophanase
tRNA	Transfer ribonucleic acid
U	Enzyme units
UAA	Unnatural amino acid
UAR-EMS	Uranyl acetate replacement stain

UV	Ultraviolet
VLP	Virus-like particle
VPARP	Vault poly(ADP-ribose) polymerase

Aims and scope of this thesis

The overarching aim of this thesis was to reprogram encapsulin nanocompartments to have light-activatable functionalities for practical applications in biotechnology and biomedicine. Specifically, the light-activated generation of reactive oxygen species (ROS) to enable the nanocompartment to drive photosensitization reactions; and light-triggered disassembly/reassembly to provide the nanocompartment with a mechanism to load and/or release cargo.

In order to achieve this aim, the specific objectives of this study included:

- i. Loading encapsulins with photosensitizing proteins that can be induced with light to produce ROS.
- ii. Evaluating the capacity and efficiency of photosensitizer-loaded encapsulins to generate ROS upon light-activation.
- iii. Determining the ability of ROS-generating encapsulins to trigger photosensitization reactions that reduce cancer cell viability an *in vitro* model of photodynamic therapy.
- iv. Incorporating photoresponsive unnatural amino acids into encapsulin's macrostructure to potentially mediate its light-induced disassembly/reassembly.

In total, this thesis is composed of five chapters, three of which have been published or prepared as manuscripts for submission to peer-reviewed journals. **Chapter 1** is a published review article that provides relevant background information on the topics investigated in this thesis. **Chapter 2** is a manuscript that reports the development of miniSinglet Oxygen Generator (miniSOG)-loaded encapsulins and their photosensitizing functions. **Chapter 3** is a manuscript that details the construction of ROS-generating KillerRed-loaded encapsulins and discusses their potential applications. **Chapter 4** outlines preliminary work performed to develop a light-triggered disassembly/reassembly mechanism for encapsulin that could mediate drug loading and/or release. Finally, a general summary and future perspectives for this work are provided in **Chapter 5**.

1

Bioengineering Strategies for Protein- Based Nanoparticles



Introduction

Protein-based nanoparticles (PNPs) self-assemble from multiple protein subunits into highly organised nanostructures. PNPs possess an array of physical and functional features that can be further engineered to develop new nanotechnologies, which can be applied in research and industry. The following article entitled “Bioengineering Strategies for Protein-Based Nanoparticles” provides an in-depth review of PNPs. It highlights the various classes and properties of PNPs, showcases the strategies available to modify them, and discusses their current and future applications.

This review was published as a peer-reviewed article in the journal *MDPI Genes*.

Review

Bioengineering Strategies for Protein-Based Nanoparticles

Dennis Diaz ¹, Andrew Care ^{1,2}  and Anwar Sunna ^{1,2,3,*} 

¹ Department of Molecular Sciences, Macquarie University, Sydney, NSW 2109, Australia; dennis.diaz-rincon@hdr.mq.edu.au (D.D.); andrew.care@mq.edu.au (A.C.)

² Australian Research Council Centre of Excellence for Nanoscale BioPhotonics, Macquarie University, Sydney, NSW 2109, Australia

³ Biomolecular Discovery and Design Research Centre, Macquarie University, Sydney, NSW 2109, Australia

* Correspondence: anwar.sunna@mq.edu.au; Tel.: +61-2-9850-4220

Received: 7 June 2018; Accepted: 17 July 2018; Published: 23 July 2018



Abstract: In recent years, the practical application of protein-based nanoparticles (PNPs) has expanded rapidly into areas like drug delivery, vaccine development, and biocatalysis. PNPs possess unique features that make them attractive as potential platforms for a variety of nanobiotechnological applications. They self-assemble from multiple protein subunits into hollow monodisperse structures; they are highly stable, biocompatible, and biodegradable; and their external components and encapsulation properties can be readily manipulated by chemical or genetic strategies. Moreover, their complex and perfect symmetry have motivated researchers to mimic their properties in order to create de novo protein assemblies. This review focuses on recent advances in the bioengineering and bioconjugation of PNPs and the implementation of synthetic biology concepts to exploit and enhance PNP's intrinsic properties and to impart them with novel functionalities.

Keywords: protein-based nanoparticles; bioengineering; nanobiotechnology; synthetic biology; biomedicine; biocatalysis; virus-like particle; nanocages

1. Introduction

Protein-based nanoparticles (PNPs) are present in all three domains of life, where they form highly organized supramolecular structures with unique biophysical properties. PNPs are composed of multiple copies of one or more types of monomeric protein building blocks (subunits), which self-assemble into highly organized hollow structures that are 10–100 nm in diameter [1]. Many PNPs exhibit sphere-shaped conformations with polyhedral symmetries, although some other shapes have been reported [2,3]. They possess at least one internal cavity and static and/or gated pores located in between protein subunits that give access to the cavity [4]. In nature, the internal cavities provide confined spaces that act as containers for enzymes and their substrates and byproducts; storage compartments for minerals; chaperones for the sequestration of partially unfolded proteins; and protective carriers for genetic material (e.g., viruses) [5,6].

Protein-based nanoparticles have many other useful attributes that make them highly attractive as biological nanomaterials. For instance, (i) they are soluble, monodisperse, biocompatible, and have robust structures [7]; (ii) they have three different interfaces that can be engineered to gain new functionalities (internal, external, and inter-subunit) [8]; (iii) the crystal structure, genetic, and molecular information of many PNPs are available, allowing for rational chemical and/or genetic modifications to be performed [9,10]; (iv) their uniform and highly repetitive structures enable the homogeneous incorporation and display of multiple copies of a moiety(ies) [11]. Additionally, scientists have gained new insights into the unique structural characteristics and self-assembly mechanisms of

natural PNPs, which have informed the design and construction of novel synthetic PNPs from natural oligomeric proteins and/or in silico designed protein sequences [12].

The ability of PNPs to encapsulate a diverse range of molecular cargoes (e.g., catalytic, therapeutic, or imaging agents) and their amenability to functionalization have led to their use in numerous practical applications [13]. Herein, we review the new and existing synthetic biology tools used to design and engineer functional PNPs, and also highlight their application in vaccine development, drug delivery, and biocatalysts.

2. Identification, Production, and Purification of Protein-Based Nanoparticles

The identification of PNPs has become easier due to the accessibility of genomic data and the development of powerful bioinformatics software for genome mining. For example, Giessen and Silver used this combined approach to identify 900 putative encapsulin systems in bacterial and archaeal genomes [14]. However, it should be noted that only a limited number of PNPs have been studied in-depth, including nonviral PNPs like ferritin, heat shock proteins (Hsp), DNA-binding proteins from starved cells (Dps), encapsulin, the E2 protein of pyruvate dehydrogenase, lumazine synthase, vault proteins, and virus-like particles (VLPs, which resemble viruses, but contain no viral genetic material and are therefore non-infectious) [15]. The structural features and natural functions of the most studied PNPs are summarized in Table 1.

Protein-based nanoparticles have been produced either in their natural hosts, as recombinant proteins in expression systems (e.g., bacteria, yeast, plants, and insect or mammalian cells), or by cell-free protein synthesis. As shown in Table 1, the majority of PNPs described in this review have been expressed and produced recombinantly in *Escherichia coli*. However, the functional expression of eukaryotic PNPs in *E. coli* remains a challenge because they often require complex protein folding and post-translational modifications [16]. For instance, due to these constraints, vault proteins and the cowpea mosaic virus (CPMV) VLP cannot be produced in *E. coli* and instead require insect cells and/or plant expression systems [17,18]. Selecting the most suitable production method can make a significant difference when it comes to achieving high production yields for PNPs. For example, the norovirus VLP exhibits low production yields in *E. coli* (1.5–3 mg/L). Expression of the same VLP in the yeast *Pichia pastoris* improved its yield by 200-fold, but production times increased (~50 h). Similar yields were then obtained within only four hours using a cell-free protein synthesis system (based on *E. coli* lysate) [19].

Due to their large macromolecular structures, PNP purification protocols tend to involve size exclusion chromatography (SEC) and/or differential centrifugation (e.g., sucrose gradient) steps [20,21]. To achieve higher PNP purity, SEC is generally combined with affinity chromatography, in which the PNP displays a pre-selected purification tag (e.g., histidine-tag), or ion-exchange, in which the outer surface charge of the PNP is exploited [22,23]. PNP purification protocols often require protein concentrating steps with polyethylene glycol (PEG, e.g., PEG8000) or ammonium sulfate precipitation [24,25]. In addition, depending on the thermal stability of a PNP, an initial heat treatment step (>60 °C) can be performed to precipitate the majority of production host proteins prior to any chromatographic techniques [26,27].

Table 1. Function, structure, and production of the most commonly used protein-based nanoparticles (PNPs).

	PNP	Native Organism	Biological Function	Geometry	Number of Subunits	Size (Diameter)	Heterologous Production	Ref.
Virus-like particles (VLPs)	CCMV ¹	Cowpea chlorotic mottle virus capsid protein	Plant virus	Icosahedral	182	28 nm	Plants; yeast; <i>Escherichia coli</i> ; <i>Pseudomonas fluorescens</i>	[11,28–30]
	CPMV ²	Cowpea mosaic virus capsid protein	Plant virus	Pseudo icosahedral	120 Large (L) and 120 Small (S)	28 nm	Insect cells; plants	[31,32]
	HBc ³	Hepatitis B virus capsid protein	Human virus	Icosahedral	180 or 240	30 nm or 34 nm	Mammalian cells; insect cells; plants; yeast; <i>E. coli</i> ; cell-free	[33–38]
	MS2	Enterobacteriaceae	Bacteriophage	Icosahedral	180	26 nm	Yeast; <i>E. coli</i> ; cell-free	[39–41]
	P22	<i>Salmonella typhimurium</i>	Bacteriophage	Icosahedral	420	60 nm	<i>E. coli</i>	[42]
	Q β	<i>E. coli</i>	Bacteriophage	Icosahedral	180	28 nm	Yeast; <i>E. coli</i> ; cell-free	[43–45]
Non-viral PNPs	Dps ⁴ (mini-ferritin)	Archaea; Bacteria (e.g., <i>Listeria innocua</i>)	Involved in oxidative and starvation responses	Tetrahedral	12	9 nm	<i>E. coli</i>	[46,47]
	E2	<i>Bacillus stearothermophilus</i>	Core of the pyruvate dehydrogenase multienzyme complex	Dodecahedral	60	24 nm	<i>E. coli</i>	[48]
	Encapsulin	Archaea; Bacteria	Involved in oxidative stress response	Icosahedral	60 or 180	20–40 nm	Mammalian cells; yeast; <i>E. coli</i>	[49–52]
	Ferritin (maxi-ferritin)	Archaea; Bacteria; Eukarya	Iron storage	Octahedral	24	12 nm	Mammalian cells; insect cells; yeast; <i>E. coli</i>	[53–58]
	Hsp ⁵	Archaea; Bacteria; Eukarya (e.g., <i>Methanococcus jannaschii</i>)	Chaperone	Octahedral	24	12 nm	<i>E. coli</i>	[59,60]
	Lumazine synthase	Archaea; Bacteria; Eukarya (e.g., <i>Aquifex aeolicus</i>)	Mediates the biosynthesis of riboflavin	Icosahedral	60	15.4 nm	<i>E. coli</i>	[61,62]
	Vault protein	Eukarya	Involved in signaling and immune responses	39-fold dihedral	78 Major vault protein	Diameter: 40 nm Length: 67 nm	Insect cells; cell-free	[63–66]

¹ Cowpea chlorotic mottle virus, ² Cowpea mosaic virus, ³ Hepatitis virus, ⁴ DNA-binding proteins from starved cells, ⁵ Heat shock proteins.

3. Rational Design of Protein-Based Nanoparticles

In the redesign of natural protein assemblies, it is important to understand how proteins fold and maintain their structure, and how their natural arrangement relates to their function. Protein-based nanoparticles exhibit complex, yet genetically modifiable protein architectures. The genetic, molecular, and structural (including crystal structures) data of some PNPs are readily accessible. This information, in conjunction with new computational tools for molecular design and engineering, makes PNPs ideal candidates for rational redesign [67]. Ferritins are one of the most well-studied PNPs and are regularly engineered to have enhanced or new functionalities. Kim and co-workers used 3D modeling and simulation tools (e.g., Modeller V 9.19, PEP-FOLD, and Pymol) to predict the length of an “intrinsically disordered peptide” (referred to as XTEN) required to optimally cover the surface of ferritin [68]. Ferritin subunits displaying C-terminal XTENs (with differing lengths) and their capacity to assemble into ferritin PNPs was simulated *in silico*. The four best XTEN-displaying ferritin variants were selected and successfully expressed in *E. coli*. The variants were further modified to display targeting peptides and affibodies for pharmacokinetic studies *in vivo* (mice). The engineered ferritin variants showed superior binding avidity and selectivity, enhanced pharmacokinetic profiles, slower clearance rates, and improved targeting, which are important aspects in therapeutic applications (e.g., drug delivery). This study clearly demonstrates the potential of rational design tools to optimize the modification of PNPs, thus enhancing their functionality in a specific application [68,69].

Redesigning native protein assemblies can be challenging because they have evolved to be marginally stable, meaning that even the subtlest modifications to their protein sequence can lead to protein unfolding and/or aggregation [70–72]. Accordingly, studies using rational design to alter PNPs' natural properties, such as stability under different conditions (e.g., pH, temperature, and ionic strength), pore size, shell size, and shape, are less common. The rational design of artificial hollow PNPs can be generally achieved via three methods: the fusion approach; domain swapping; and metal-directed self-assembly. In the fusion approach, two (or more) different proteins that are individually capable of self-assembling into oligomers are fused together via a small linker domain that matches the chosen symmetry. Thus, identical copies of the resulting fusion protein self-assemble into the pre-designed particle or biomaterial [73,74]. This strategy was used by Lai et al. to construct tetrahedral PNPs from two different oligomeric protein domains (a dimer and a trimer) joined together by an α -helical linker [75]. In this study, an idealized molecular model was created *in silico* to help identify potential mutation sites to improve the PNP's structural asymmetry. In the domain-swapping approach, a secondary structural domain of one protein is substituted with the corresponding domain located within another protein, resulting in an intertwined oligomer [76]. Metal-directed self-assembly involves the construction of new protein interfaces that arise from the coordination of metal ions that have large binding energies [77]. Employing these two strategies, Miyamoto et al. obtained a novel C-type cytochrome (Cyt *cb*₅₆₂) cage structure, in which three domain-swapped Cyt *cb*₅₆₂ dimers formed a cage by the coordination of amino acids to Zn²⁺ metal ions [76].

Coiled-coil peptides are structural motifs within proteins that bind one another via hydrophobic interactions, thus mediating protein oligomerization. Consequently, coiled-coil peptides have been used in the development of new PNPs. For example, Fletcher et al. described *de novo* coiled-coil peptides designed to form two different oligomer states that, once mixed, were able to arrange into ~100 nm unilamellar self-assembling cage-like particles (SAGEs) [78].

Recent advances in computational design have allowed the *de novo* design of protein–protein interfaces [73]. The Baker's lab has developed the Rosetta software as a computational tool for protein structure prediction and design [79]. Using Rosetta, they redesigned dimeric, trimeric, and pentameric protein oligomers (Figure 1A,B) to act as building blocks for the assembly of megadalton-scale icosahedral PNPs. To achieve this, three architectural types (I53, I52, and I32) were formed from pairwise combinations of the dimeric/trimeric and pentameric oligomers (Figure 1C). These were then used to model novel PNPs by fitting protein oligomers with similar crystal structures in the Protein Data Bank (PDB, <http://www.rcsb.org/pdb/>) or *de novo* designed protein oligomers. The resulting designs

were sorted based on different selection criteria, including interface area, predicted binding energies, and shape complementarity. A number of designs were selected and expressed recombinantly in *E. coli*, and those capable of self-assembly into PNPs were further characterized. Ten designs were found to self-assemble and form PNP structures (26–31 nm diameters) that matched their predicted/ modeled architectures. The de novo designed I53-50 (Figure 1D) exhibited superior single-subunit stability and assembly kinetics similar to those of viral capsids [80].

In more recent work, additional positively charged residues were incorporated into the internal cavity surface of I53-50, allowing it to package its own negatively charged mRNA genome (Figure 1F), thus generating a synthetic “nucleocapsid” (I53-50-v1) (Figure 1E). To determine whether the nucleocapsid could be evolved to acquire more virus-like properties, combinatorial libraries of nucleocapsid variants were produced in *E. coli*. The variants were subjected to sequential rounds of selection (Figure 1G), first against RNase for enhanced genome packaging (more than 133-fold higher); second to blood and RNase at body temperature (37 °C) for increased stability in blood (from less than 3.7% to 71% of the packaged RNA was protected from degradation following six hours of treatment) and in vivo (mice) to increase blood circulation times (from less than 5 min to over 4.5 h) (Figure 1H). This study shows that PNPs can be de novo designed and that their properties can be evolved further, thus providing an exciting opportunity to create non-natural PNPs with novel functionalities [81].

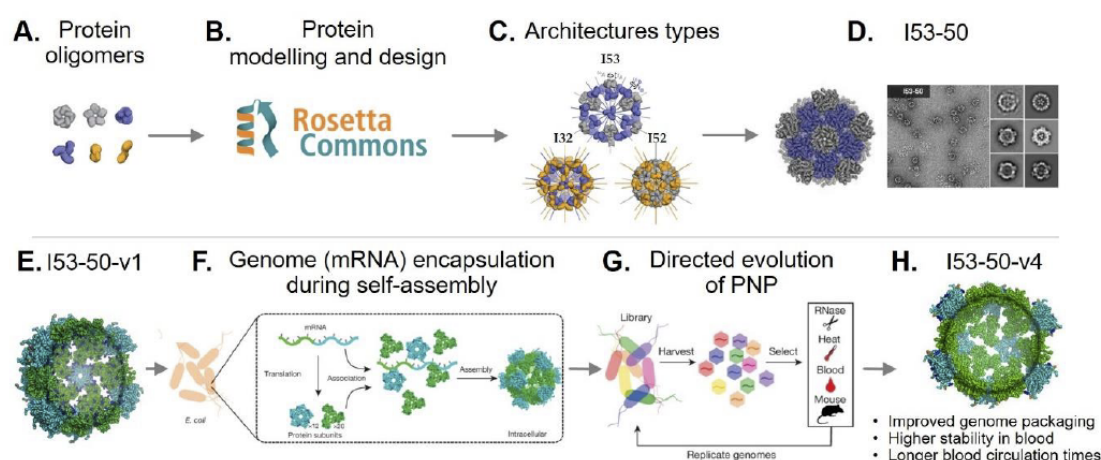


Figure 1. Rational design and directed evolution of a synthetic nucleocapsid. (**Upper panel**) Diagram showing the in silico design process and subsequent production of a de novo PNP. (A) Pentameric (gray), trimeric (blue), and dimeric (yellow) protein oligomers selected for rational design. (B) The Rosetta software was employed in the in silico design of new PNPs. (C) Rosetta-predicted PNP architecture types. (D) Design model I53-50 and its corresponding negative-stain electron micrograph, showing that the obtained structure matched the predicted in silico model. Adapted with permission of [80]. (**Lower panel**) Synthetic nucleocapsid design and evolution. (E) Model of the I53-50-v1. Pentamers (cyan) and trimers (green). (F) Nucleocapsids are capable of encapsulating their own genome (mRNA) during self-assembly in *Escherichia coli*. (G) *E. coli* is transformed with a library of synthetic nucleocapsid variants. All variants are purified together from cell lysates and selected against RNase, heat, blood, and in vivo blood circulation. The mRNA inside the selected capsids variants is then obtained and amplified using quantitative reverse transcription PCR (RT-qPCR), re-cloned to construct a new library, and transformed into *E. coli* for another round of selection. (H) After several rounds of evolution, an improved version of the original nucleocapsid was obtained (I53-50-v4). Adapted with permission of [81].

4. Bioengineering Functional Protein-Based Nanoparticles

The functional properties of a PNP can be custom engineered to meet the requirement of a particular application by modification of their interfaces via bioconjugation and/or genetic engineering (see Figure 2). Since the genetic, structural, and biochemical properties of many PNPs are well known, this information can be used to design and select the best functionalization strategy for a specific PNP and its intended application [9,10]. In this section, we provide an overview of various bioconjugation and genetic engineering strategies (and combinations thereof) used to functionalize PNPs for a diverse range of bioapplications. Table 2 summarizes the functionalization methods, encapsulation strategies, and reported cargo molecules for a selection of PNPs.

4.1. Bioconjugation

The functionalization of PNPs using bioconjugation strategies is effective for the attachment of various moieties that cannot be introduced via genetic modification. This includes large moieties (e.g., antibodies) that may disrupt PNP self-assembly, and non-biological moieties (e.g., small-molecule drugs) that cannot be produced in heterologous hosts (e.g., *E. coli*) [7,82].

4.1.1. Noncovalent Bioconjugation of Protein-Based Nanoparticles

The nonspecific physical adsorption of moieties onto PNP surfaces requires no complex chemical reactions and has been used to encapsulate cargoes and/or functionalize PNPs outer surfaces. For example, cationic polymers like polyamidoamine (PANAM) have been electrostatically bound to the negatively charged cowpea chlorotic mottle virus (CCMV) VLP capsid, resulting in the formation of hexagonal higher-order structures. Large-sized polymers (>20 positive charges) maintained their affinity towards the VLP at high salt concentrations. However, under the same conditions, midsized polymers (8–9 positive charges) lost their affinity, while small-sized polymers (<4 positive charges) could not form complexes even at low salt concentrations [83]. Although the simplicity of physical adsorption is an attractive strategy to functionalize PNPs, it relies on weak noncovalent interactions that are easily disrupted and may cause the disassociation of moieties from the PNP surface in complex fluids (e.g., blood).

4.1.2. Covalent Bioconjugation of Protein-Based Nanoparticles

The covalent bioconjugation of functional moieties to PNPs is achieved by exploiting reactive groups of the naturally occurring amino acids exposed on their inner or outer surfaces. This approach forms highly stable bonds leading to strong irreversible interactions between the involved molecules [84]. Commonly used crosslinking agents in the bioconjugation of PNPs include maleimides for cysteine thiols; *N*-hydroxy-succinimides (NHS) for lysine amines; and carbodiimides for glutamate or aspartate carboxylates [85]. These agents have been extensively applied to bioconjugate PNPs to antibodies [86], fluorescent dyes [87,88], folic acid [89], cell-targeting and cell-penetrating peptides [90], and small-molecule drugs [91]. However, bioconjugation techniques often suffer from poor selectivity and low reproducibility and can result in moieties attached with altered conformations and random orientations, causing a reduction/loss of their function [13,92]. Furthermore, some bioconjugation processes are highly complex and require abrasive chemical reagents (e.g., organic solvents) and high temperatures, which may reduce a PNP's stability.

Recently, click chemistry reactions have been shown as a viable functionalization technique for PNPs. This strategy denotes a set of reactions that are fast, straightforward, specific, and efficient. The copper-catalyzed azide–alkyne cycloaddition (CuAAC) reaction is a reliable technique that relies on the presence of alkynes and azides in the PNP and the moiety to conjugate [93]. These reactive groups have been introduced into PNPs mainly by residue-specific replacement using amino acid analogues (e.g., azidohomoalanine or homopropargylglycine) and unnatural amino acids (UAAs) [94].

This approach has been used by Finn and co-workers to bind carbohydrate-based ligands, fluorogenic dyes, proteins, and polymers to Q β VLP [95–97].

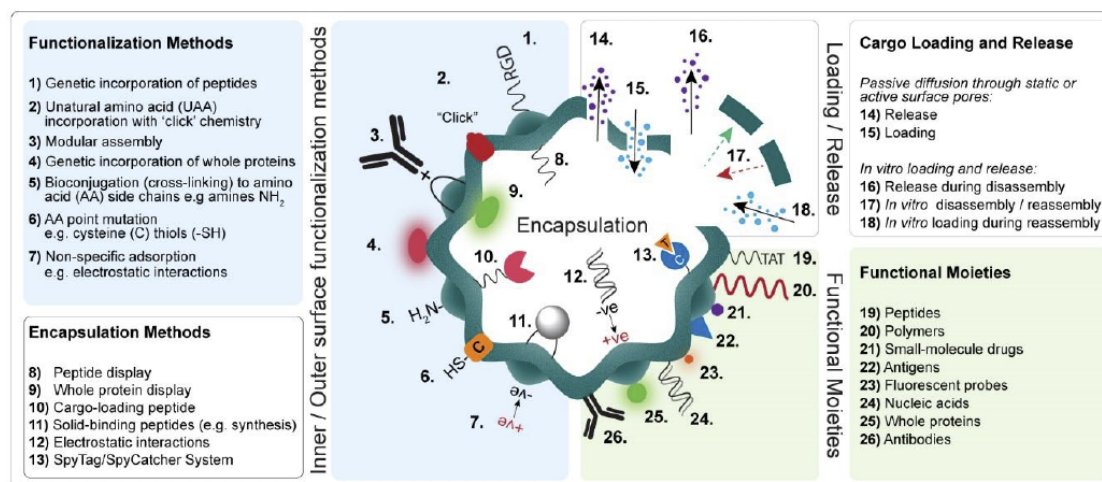


Figure 2. Illustration showing the various approaches used to functionalize PNPs with different functional moieties, and the strategies employed to encapsulate, load, and release cargo molecules. RGD, cell-binding motif (Arg-Gly-Asp); TAT, human immunodeficiency virus (HIV-1) cell-penetrating peptide (CPP); +ve, positive; -ve: negative.

4.2. Genetically Engineered Protein-Based Nanoparticles

Genetic modification of PNPs allows for the precise control over the number, position, and distribution of incorporated moiety(ies) [11]. Accordingly, genetic modification alone or in combination with bioconjugation techniques (as described above) is fast becoming the preferred strategy for engineering functional PNPs.

4.2.1. Peptide and Protein Display

Functional peptides or proteins can be genetically fused to the N- or C-terminus, or within loop regions of PNP subunits that are known to be exposed on their outer surface. Some examples include: the N-terminus of the lumazine synthase from *Brucella* spp., which has been fused to immunogenic peptides [98]; the C-terminus of the Hsp from *Methanococcus jannaschii* fused to the tumor-targeting peptide RGD-4C (Cys-Asp-Cys-Arg-Gly-Asp-Cys-Phe-Cys) [87]; and the loop at the 42 position of encapsulin, which was fused to a His-tag [99].

Recently, the functional display of whole proteins on the outer surface of PNPs has been reported [100,101]. For example, atomic structural analysis of a grapevine fanleaf VLP revealed several amino acid residues at the C-terminus of the VLP's subunit that were externally exposed and not involved in any of the protein–protein interactions integral to the VLP's self-assembly. This region was then modified to successfully display red or green fluorescent proteins on the outer surface of the VLP without disrupting its assembly and stability [100]. Similarly, the C-terminus of de novo designed T33-21 subunit was genetically fused to two different antifreeze proteins, resulting in their individual functional display on the assembled PNP's outer surface. Both antifreeze PNPs exhibited improved antifreeze activities relative to their monomeric counterparts [101].

4.2.2. Modular Assembly

The genetic incorporation of large moieties into PNPs can disrupt their self-assembly and stability and is therefore limited to peptides and small proteins. To overcome this, modular assembly strategies have been developed that allow the indirect attachment of large moieties to the outer surfaces of

PNP surfaces. For example, a peptide that binds the fragment crystallizable (Fc)-region of antibodies has been introduced onto the outer surface of ferritin using genetic engineering. This Fc-binding peptide was then shown to act as an effective anchorage point for the modular attachment of large and structurally complex immunoglobulin G (IgG) antibodies to the PNP [102].

Another modular assembly strategy for antibody display is based on the high affinity of the streptavidin (StAv)–biotin binding system, which is widely used in biology and medicine as a molecular adaptor. Currently, biotin can be covalently linked to a variety of molecules (e.g., proteins, peptides, nucleotides, carbohydrates, metals), and these biotinylated molecules bind to StAv with high affinity to form a conjugate [103]. This approach was used to develop a functionalized Janus PNP [104]. Briefly, a tetrapeptide was genetically fused to Dps from *Listeria innocua* to be displayed externally. The tetrapeptide was employed to immobilize Dps to thiol-reactive beads. Then, biotin was linked to the accessible tetrapeptides on the Dps surface for subsequent StAv binding. The resulting StAv-functionalized Dps PNPs were released from the beads, leaving the non-biotinylated subunits available for further functionalization. This functionalization platform allows the attachment of any biotinylated moiety to the PNP, enabling various applications. For example, targeting of *Staphylococcus aureus* was achieved by a fluorescein-labeled StAv-functionalized Dps, which displayed a biotinylated monoclonal antibody against protein A expressed on the cell surface of *S. aureus*.

A similar approach to modular incorporation of molecules is enzymatic labeling with sortase A. Sortases are found in Gram-negative bacteria, where they are crucial in the covalent binding of proteins to the peptidoglycan cell wall. Sortase A from *S. aureus* can catalyze the peptide bond formation between a protein containing a Leu-Pro-X-Thr-Gly (LPXTG) motif and a peptide with a polyglycine sequence (at the N-terminus). The latter can be decorated with any molecule accessible to chemical synthesis (e.g., fluorophores, crosslinkers, and biomolecules) or other recombinant proteins or peptides [105,106]. This allows for the site-specific modification of proteins at either the N- or C-terminus or internal loops and the formation of cyclized (poly)peptides [106]. For example, sortase A-mediated bioconjugation has been used to attach thermoresponsive biopolymers, cellulose-degrading enzymes, fluorescent proteins, antigens, and fluorescent probes to a range of PNPs [82,107,108]. This technique represents a viable alternative to purely chemical crosslinking or genetic engineering methods and offers several advantages. These advantages include the ability to perform reactions under mild physiological conditions, fewer modification requirements on the target protein, and, since sortases that recognize different amino acid motives are available, it can be orthogonal. Nevertheless, although there is a minimal requirement for prior genetic modification of the protein of interest, several factors potentially affecting the efficiency of labeling, such as flexibility, accessibility, and intrinsic structure of the target region for modification, should be considered [106].

Genetic engineering of PNPs can be used also to improve the specificity and uniformity of bioconjugation strategies by introducing point mutations, aimed at changing and/or removing standard reactive residues, or to introduce unnatural amino acids (UAAs) for subsequent chemical conjugations. Generally, Cys and/or Lys residues are either introduced or removed from the surface of PNPs to improve the selectivity of covalent bioconjugation and to better control the number of functional moieties to be displayed on their surfaces. For example, the incorporation of Cys allowed the thiol-mediated attachment of chromophores, nanogold, and biotin onto the external surface of CMPV [109]. Additionally, mutating natural Cys to other nonreactive amino acids can be used to eliminate nonspecific functionalization that may hinder the PNP macrostructure. An example of this was the substitution of one intrinsic Cys, located at the interface between encapsulin subunits, that could make the structure unstable upon bioconjugation of the anticancer drug doxorubicin (DOX) to an externally displayed Cys [9].

Another strategy to broaden the reactive groups for functionalization beyond the 20 naturally occurring amino acids is the incorporation of UAAs. Generally, two approaches can be used for the metabolic incorporation of UAAs into proteins, namely the residue-specific and the site-specific strategies. Residue-specific methods involve the global (or partial) replacement of the standard amino

acid, not just in the protein of interest but in all proteins within the host system [110]. This approach relies on the structural resemblance between the analogue and the standard amino acid. However, other approaches can be applied to improve the incorporation of the analog UAA, such as overexpression or mutations of aminoacyl-tRNA synthetases and the reassignment of sense codons [111]. The site-specific method allows replacement of a single residue while maintaining access to the other 20 standard amino acids. In this approach, the incorporation of the UAA requires an evolved transfer RNA (tRNA)/aminoacyl-tRNA synthetase pair able to first, respond to a nonsense (e.g., amber codon) or four-base codon, and second, recognize the desired UAA [110,112]. The amber codon suppression is one of the most popular and well-established techniques for UAA insertion into proteins. This approach has been used successfully by Francis and collaborators to introduce aminophenylalanine into the MS2 VLP, mediating the covalent bioconjugation of fluorophore-labeled aminophenol-containing DNA, DNA aptamers, and antibodies [20,113,114].

4.2.3. Encapsulation of Foreign Cargoes

The internal cavities of PNPs have the capacity to encapsulate, carry, and protect both native and non-native molecular cargo. Molecular cargo are typically loaded inside PNPs via (i) diffusion, in which cargo molecules move through static (i.e., small molecules like ions, water, organic molecules) or gated pores (which open and close in response to specific conditions) located at the interfaces between PNP subunits that give access to the internal cavity [4]; (ii) *in vitro* loading, in which a disassembled PNP undergoes reassembly in the presence of the molecular cargo, thus encapsulating it; or (iii) *in vivo* loading, in which molecular interactions between the internal cavity surfaces of a PNP and cargo components facilitate encapsulation during PNP *in vivo* self-assembly [115]. When selecting the best strategy to load cargo into a PNP, it is important to consider the size of the cargo in relation to the size of the outer pores and/or internal cavity. Another important aspect is potential leakage of the cargo (e.g., via pores) after encapsulation and the possible nonspecific interactions between the cargo and the PNP's outer surface, which may prevent efficient loading.

Optimization of the loading process conditions should be considered to favor the accessibility of the cargo to the PNP's inner cavity (e.g., disassembly/reassembly conditions) and to avoid the cargo's instability. Finally, the stability of the cargo and PNPs under storage and application conditions should be compatible. In this section, we focus on other genetic modifications that can be used to aid the loading of molecules inside PNP cavities that have not been discussed in previous sections of this review.

In nature, the surface of the interior cavity of PNPs often displays an intrinsic affinity towards their natural cargo molecule, enabling the encapsulation of molecules with similar properties [1]. For instance, some VLPs have positively charged interior surfaces, and their electrostatic interactions with negatively charged nucleic acid enhance the self-assembly of the capsid subunits around its natural cargo (i.e., RNA/DNA). This mechanism has been exploited to encapsulate negatively charged non-native cargo into empty capsids (i.e., VLPs), including nonviral RNA, polyanions, and nanoparticles (NPs) (e.g., thiolalkylated tetraethylene glycol-coated gold NPs) [39]. Furthermore, the charge of a non-native cargo can be specifically modified to facilitate its encapsulation within some PNPs, thus eliminating the need for any PNP modification. For example, the positively charged DOX has been co-encapsulated with polystyrenesulfonic acid (PSA). Polystyrenesulfonic acid is negatively charged and mediates the loading of DOX into the positively charged interior of the hibiscus chlorotic ringspot virus VLP [116].

Table 2. Methods used to bioengineer the most commonly used PNPs for a range of bioapplications.

	PNP	In Vitro Loading Mechanism	Cov Biocon ¹	Point Mut ²	UAA ³	Pep Disp ⁴	Prot Disp ⁵	Modul Assem ⁶	Encapsulated Cargo		Applications	Ref.
									Diffusion ⁷	In Vitro	In Vivo	
VLPs	CCMV	pH; Ionic strength	•	•		•	•			Metals; small-molecule drugs; nucleic acids; organic polymers		Drug delivery; vaccines; bioimaging; prodrug activation; biocatalysis [30,117–124]
	CPMV		•	•		•	•		Metals; fluorescent probes; biotin; organic polymers			Drug delivery; vaccines; bioimaging [31,91,125–129]
	HBc	Denaturants	•	•	•	•	•	•		Metals; small-molecule drugs; fluorescent probes; nucleic acids		Drug delivery; vaccines; bioimaging [37,130–135]
	MS2	pH; Denaturants	•	•	•	•	•		Fluorescent probes; photosensitizers	Metals; small-molecule drugs; nucleic acids	Proteins	Drug delivery; vaccines; bioimaging; biocatalysis [114,136–140]
	P22	pH	•	•		•		•	Metals; fluorescent probes; biotin; organometallic polymers	Proteins	Proteins; peptides; epitopes; nucleic acids	Drug delivery; vaccines; nanomaterial synthesis; biocatalysis; solubility enhancement [107,141–146]
	Qβ	pH; Denaturants	•	•	•	•	•		Fluorescent probes; cationic polymers	Metals; small-molecule drugs; fluorescent probes; nucleic acids	Proteins	Drug delivery; vaccines; bioimaging; nanomaterial synthesis [24,97,132,137,147,148]
	Dps		•			•		•	Metals			Drug delivery; nanomaterial synthesis [104,149,150]
	E2	Denaturants	•	•		•	•	•	Small-molecule drugs; fluorescent probes	Nucleic acids		Drug delivery; vaccines; biocatalysis; antibody purification [48,82,151–156]
	Encapsulin	pH; Denaturants	•	•		•	•		Metals	Proteins	Proteins	Drug delivery; bioimaging; immunotherapy; antimicrobials; biocatalysis [9,50–52,157–159]

Table 2. Cont.

PNP	In Vitro Loading Mechanism	Cov Biocon ¹	Point Mut ²	UAA ³	Pep Disp ⁴	Prot Disp ⁵	Modul Assem ⁶	Encapsulated Cargo			Applications	Ref.
								Diffusion ⁷	In Vitro	In Vivo		
Ferritin	pH	•	•	•	•		•	Metals; small-molecule drugs	Bioactive compounds; metals; small-molecule drugs	Metals	Solubility enhancement; drug delivery; vaccines; bioimaging; immunotherapy; nanomaterial synthesis	[27,102,160–169]
Hsp	Temperature	•	•		•	•		Metals	Metals; small-molecule drugs; dyes; fluorescent probes		Drug delivery; nanomaterial synthesis; biocatalysis	[59,87,170–172]
LS	Ionic strength	•	•		•	•	•		Proteins		Drug delivery; vaccines; bioimaging; biocatalysis	[62,98,173–177]
Vault	“Breathing mechanism”	•			•				Metals; proteins; epitopes; antigens	Proteins	Solubility enhancement; drug delivery; vaccines; bioimaging; immunotherapy; bioremediation	[178–187]

¹ Covalent bioconjugation; ² Point Mutation; ³ Unnatural amino acid incorporation; ⁴ Peptide display; ⁵ Whole protein display; ⁶ Modular assembly; ⁷ Pore-mediated diffusion.

Other PNPs show more complex *in vivo* loading mechanisms for the encapsulation of their native cargo which are based on specific interactions between interior surface regions and unique components of their native cargoes. These mechanisms have been adapted to facilitate the loading of non-native molecules. For example, the encapsulation of MS2 genomic RNA can be attained via noncovalent interactions between the capsid subunits and the 19-nucleotide specific MS2 cistron, known as the pac site. In the case of Q β phage, this process is mediated by a 29-nucleotide RNA hairpin, known as the Q β hairpin [39,44]. The fusion of the pac site and Q β hairpin to therapeutically relevant microRNAs (miRNAs) and interference RNAs (iRNAs) has allowed their encapsulation inside MS2 and Q β , respectively [24,90].

Similarly, certain non-virus derived PNPs present unique encapsulation mechanisms. For instance, enzymes that are naturally targeted inside encapsulin can be encapsulated via a C-terminal extension of 30–40 amino acids, referred to as a cargo-loading peptide (CLP). The CLP selectively binds to hydrophobic pockets located on the cavity surface of encapsulin [21]. Foreign cargo proteins, such as fluorescent proteins and enzymes (e.g., firefly luciferase and Aro10p pyruvate decarboxylase) tagged with full or truncated CLP sequences, have been loaded successfully inside encapsulins *in vivo* and/or *in vitro* [49–51,188].

The mammalian vault protein comprises three proteins—a major vault protein (MVP), a vault poly(ADP-ribose) polymerase (VPARP), and a telomerase-associated protein (TEP1). The vault macrostructure is formed by MVP, which in solution shows transient open and closed states (“breathing” mechanism), allowing the encapsulation of the other two vault-associated proteins [178]. It has been shown that a C-terminal minimal interaction domain (mINT) of 162 amino acids, which binds to MVP’s inner surface, allows the encapsulation of VPARP [179]. Rome and co-workers have genetically fused the mINT domain to various proteins (i.e., green fluorescent protein (GFP), luciferase, chlamydial epitopes, antitumor cytokines and antigens), allowing their *in vitro* loading into MVP [179–182,189]. To further extend the loading properties of mINT to inorganic compounds, a gene construct of mINT was designed to contain an N-terminal 31-amino acid extension that included a His-tag. The His-tag in the protein was used to bind gold-Ni-nitrilotriacetic acid (NTA) particles, and the resulting complex was successfully internalized inside the vault capsule. This mINT–gold complex can potentially capture any His-tagged protein and facilitate their loading inside the vault protein, thus avoiding any need for prior genetic fusion of cargo proteins to mINT [183].

Further studies have involved the encapsulation of hydrophobic drugs inside vaults via the fusion of a small amphipathic α -helix derived from the hepatitis C viral nonstructural protein 5A (NS5A) to the N-terminus of MVP, which is exposed on the inner surface. This modification creates a lipophilic setting in the vault protein’s cavity, which allows the reversible association of several hydrophobic therapeutic molecules, including retinoic acid, amphotericin B, and bryostatins 1. However, no association was observed with the hydrophilic drug DOX [184]. Recently, Shang et al. reported that the fusion of NS5A to the C-terminus of hepatitis B virus subunit (HBc) improved the encapsulation capability of the hydrophobic form of DOX inside HBc [134], confirming the properties of NS5A to bind and facilitate the loading of hydrophobic therapeutic compounds inside PNPs.

In another approach, the Douglas group used the intrinsic features of the P22 VLP to develop a supramolecular platform for several applications ranging from material sciences to biomedicine [190,191]. The P22 bacteriophage capsid naturally self-assembles from multiple copies of a capsid subunit with the aid of a scaffolding protein (SP). The C-terminus of the SP interacts noncovalently with the interior of the capsid, resulting in its incorporation, and this process guides the assembly of the capsid via the head-full mechanism. It has been shown that a completely modified SP protein in which the last few C-terminus residues are conserved still maintains the ability to lead the assembly of a native-like P22 capsid [42]. Also, SP-tagged proteins can be *in vivo* loaded into P22 [42]. Douglas and collaborators have used the P22 SP encapsulation method to load monomeric and oligomeric enzymes. The tetrameric β -glucosidase enzyme, CelB, and monomeric alcohol dehydrogenase D (AdhD) from *Pyrococcus furiosus* were individually loaded inside P22 VLP [115,145].

Additionally, this strategy has allowed for multiple enzymes, linked together with flexible spacers, to be collectively loaded inside P22 VLP. The co-encapsulated enzymes remained active and were able to perform a sequential enzymatic reaction *in vitro* (further details can be found in Section 5.2) [143].

Some PNPs do not have loading mechanisms (e.g., lumazine synthase and E2), or their native encapsulation mechanism is limited to a certain molecule (e.g., VLPs affinity to nucleic acids). In these cases, other genetic engineering strategies must be developed to facilitate the encapsulation of different cargo. A straightforward approach to encapsulate proteins inside a PNP was designed for lumazine synthase. The interior surface was engineered to provide a negatively charged environment inside the PNP by mutating four residues per monomer to glutamate. This resulted in the specific encapsulation of GFP carrying a positively charged tag (deca-arginine) at its C-terminus. This approach allows for the general encapsulation of other tagged proteins [192].

Other loading strategies are based on the specific interactions between two peptides. Giessen et al. used the well-known SpyTag/SpyCatcher system [193]—in which the peptide (SpyTag) forms an amide bond to its protein partner (SpyCatcher)—to package two enzymes involved in the biosynthesis of indigo dye inside MS2 [139]. Herein, SpyTag was expressed inside an MS2 capsid (SpyMS2), allowing the *in vivo* loading and covalent attachment of SpyCatcher-tagged enzymes [139]. Encapsulation of the two-enzyme indigo biosynthetic pathway improved the production of indigo dye *in vivo* (*E. coli*) and *in vitro* [139].

A similar loading approach was developed for CCMV VLPs. Usually, the loading of cargo inside CCMV is mainly performed by *in vitro* disassembly/reassembly with or without conjugation to DNA tags [118,120]. However, to control the encapsulation of enzymes inside CCMV, a noncovalent anchoring moiety was used to attach the target protein to the subunit before reassembly. A heterodimeric coiled-coil protein was employed as the anchor. The coiled-coil sequences were bound to the C-terminus of enhanced GFP (EGFP) (E-coil) and the N-terminus of CMMV capsid subunits (K-coil). The resulting EGFP–subunit complex was mixed with different concentrations of wild-type (wt) subunits to allow the reassembly of the capsid. This encapsulation method provided some control over the loading of EGFP per capsid by altering the ratios of wt and EGFP subunits and resulted in loads of up to 15 EGFP proteins per capsid [194].

4.2.4. Interface Engineering

The self-assembly of PNPs relies on optimally balanced energetics that occur in part from the complex and dynamic interplay of amino acids at the interfaces between their subunits [195]. Understanding the underlying molecular mechanisms of self-assembly for supramolecular entities is complicated, particularly if their structures are highly symmetrical and homo-oligomeric, like most PNPs. To date, the self-assembly of PNPs has been investigated using various biophysical characterization techniques that rely on understanding the folding process of oligomeric proteins by chemical denaturation kinetics, as well as the calorimetric quantitation of thermal denaturation (e.g., differential scanning calorimetry, isothermal titration calorimetry, and pressure perturbation calorimetry). The chemical and thermal unfolding of protein oligomers can also be monitored by nuclear magnetic resonance and circular dichroism (CD) spectroscopy. These techniques in conjunction with structural and functional analysis, such as X-ray crystallography and mutation-related studies, can help elucidate the self-assembly and disassembly mechanisms of PNPs [196,197]. In-depth studies into the self-assembly of horse ferritin have revealed that subunits need to be completely folded to provide complementary interfaces for dimer formation. Based on these studies, a self-assembly mechanism for ferritin was proposed, in which dimers interact to form tetramers and hexamers. Subsequently, two hexamers can form one dodecamer, and two dodecamers self-assemble into the final 24-mer structure [196]. Studies on the pH disassembly of ferritin show that the 24-mer structure becomes unstable at pH 3.4. Different intermediate structures are formed during the dissociation process, starting with the formation of particles with two holes, followed by headphone-like structures,

and finally resulting in mostly trimers and some monomers. Increasing the pH to neutral allowed the reassembly process of a nanoparticle with two hole defects [198].

As previously discussed in Section 4.2.3 in vitro disassembly processes have been exploited for cargo loading. The disassembly of certain PNPs can be initiated by pH [50,198], metals [199], reducing agents [130], ionic strength [119], or a combination thereof [117]. For example, encapsulin has been shown to disassemble in vitro under highly acidic or alkaline conditions, as well as in presence of high concentrations of denaturing agents (e.g., 7 M guanidine hydrochloride) [50]. To trigger their subsequent reassembly, optimal assembly conditions needed to be re-established (e.g., through dialysis). It has also been shown that the pH-driven disassembly/reassembly properties of PNPs can be altered by genetically modifying the interface between their subunits. For instance, ferritin disassembles at pH 2 and reassembles at pH 7. Such acidic pH can be a harsh condition for drug loading, especially when most bioactive compounds are unstable at extremely acidic pH. To allow a more amenable environment for cargo-loading, Chen et al. modified the 4-fold axis interface in ferritin by cleaving the last 23 amino acids at the C-terminus. This modified ferritin disassembled at a pH of 4.0 and was used to successfully encapsulate the bioactive compound curcumin inside ferritin [58].

The localized and controlled release of a drug enhances its therapeutic efficacy while reducing its harmful side effects. However, drug release from PNP cavities tends to be poorly controlled, working by simple diffusion and/or biodegradation. The ability to disassemble in specific physiological conditions is a crucial property required in the design of PNP-based drug delivery systems (DDSs). PNPs have been engineered to disassemble at acidic pH (5.0), which causes the release of their cargo upon cell internalization via endocytosis [151]. As an example, amino acids located at the N-terminus of E2 were deleted to cluster histidines at the interface between subunits. Repulsive interactions between histidines at acidic pH resulted in the destabilization of the E2 macrostructure [151]. E2 has also been modified to exhibit an inverse pH-sensitive self-assembly [200]. The synthetic GALA peptide, which consists of variable amino acid repeats of Glu-Ala-Leu-Ala, switches its conformation with changes in pH. GALA was used to replace a C-terminal α -helix known to be required for self-assembly of the E2 macrostructure. At pH 7.0, the GALA peptide is in the extended coil form, and thus, the modified E2 is disassembled. Lowering the pH to 4.0 switched GALA to its helix form, allowing the reassembly of the PNP. This process was shown to be reversible [200].

5. Application of Protein-Based Nanoparticles in Biomedicine and Biotechnology

In this section, we describe selected examples that show the progress made thus far in the development of PNPs as platforms for vaccine development, drug delivery, and biocatalysis. The reader is referred to other reviews for more information about the potential applications of PNPs in other fields, such as diagnostic imaging [201], biomineralization [202], and nanomaterial synthesis [203].

5.1. Biomedical Applications of Protein-Based Nanoparticles

5.1.1. Vaccine Development

Natural and synthetic PNPs have potential use in biomedicine as vaccines and as DDSs. While modifications on the outside of PNPs have been shown to be a viable strategy for vaccine development, the encapsulation of target molecules inside PNPs remains a more challenging option. For example, VLPs have been successfully developed and introduced as vaccines. In these VLPs, which lack genetic material, the outer surface is chemically or genetically modified to introduce a large number of anchoring points to which antigens can be connected to increase their immunogenicity [204]. In another example, HBc particles, which have the ability to serve as carriers of foreign B cell and cytotoxic T lymphocytes epitopes [205], have been used to genetically display antigens for malaria [206], tuberculosis [207], human papillomavirus (HPV) 16 cytotoxic T lymphocytes epitope E7 [208], and dengue virus type 2 [209]. Few VLP-based vaccines are commercially available worldwide, including vaccines against HPV (Gardasil[®], Cervarix[®], and Gardasil9[®]) and hepatitis B

virus (Engerix[®] and third-generation Sci-B-Vac[™]). Other VLP-based vaccine candidates are in different stages of preclinical and clinical trials [15,210].

Nonviral PNPs can also be modified to display immunogenic epitopes that can be used potentially for vaccine development and immunotherapy [181,182]. One good example is *Helicobacter pylori* ferritin. Structural analysis of this protein revealed that the insertion of a heterologous protein—the influenza virus haemagglutinin (HA) subunit—near the N-terminus would allow HA to assume the physiologically relevant trimeric viral spike. The resulting fusion protein, ferritin–HA, was expressed in mammalian cells to achieve the glycosylation and post-translational modifications characteristic of viral proteins. Figure 3A shows transmission electron microscopy (TEM) images of ferritin–HA with spikes protruding from the spherical PNP. The protective immune response of ferritin–HA was compared with that obtained with trivalent inactivated influenza vaccine (TIV) in mice and ferrets. In the presence of the adjuvant Ribi, immune response indicators, such as hemagglutination inhibition (HAI), neutralization (IC₉₀, Figure 3B) and ELISA titers, were significantly increased with ferritin–HA in both animal models. Additionally, the sera of immunized animals were used to assess the extent of neutralization against a panel of H1N1 pseudotyped viruses. Ferritin–HA elicited a major increment in influenza protection compared to the commercial vaccine (TIV, Figure 3C) [162]. Recently, this same platform was used to display HA stem-only (stem being the conserved region of HA glycoprotein) immunogens. Six iterative cycles of structure-based design were necessary to achieve H1HA stabilized stem immunogens that were later fused to ferritin. The HA stem-only ferritin vaccine exhibited antibody-mediated cross-immune protection against the H5H1 virus in mice and ferrets. This work represents an interesting platform for the potential development of universal influenza vaccines [163].

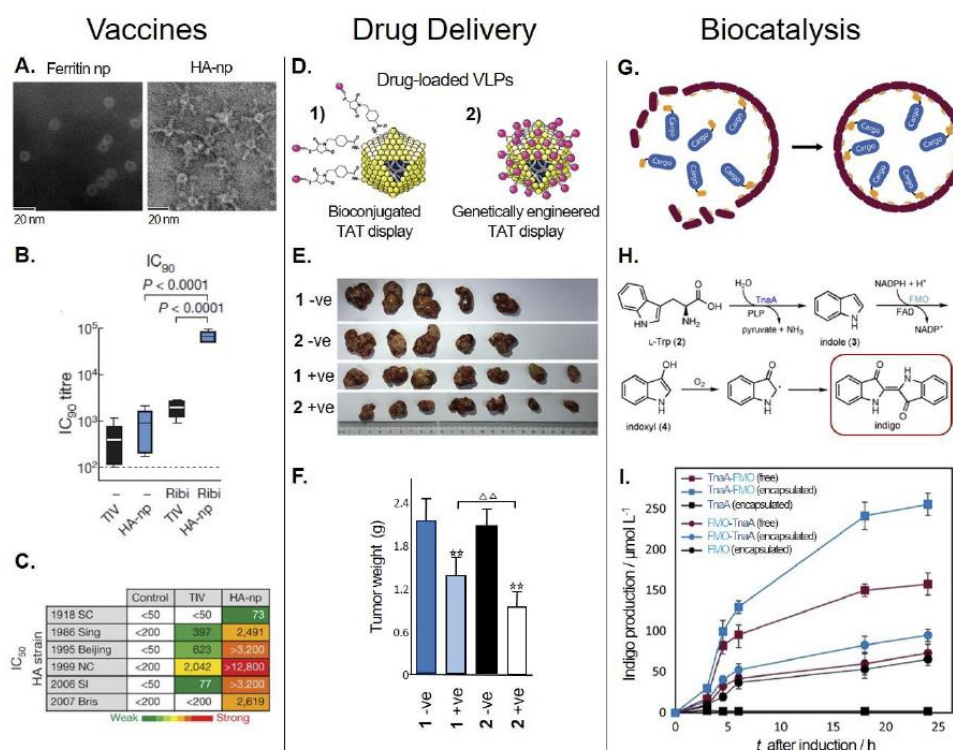


Figure 3. Examples of the bioapplications of PNPs. (Left panel) Vaccines: Development of a PNP-based influenza vaccine. (A) Transmission electron microscopy (TEM) image showing unmodified ferritin nanoparticles (np) (left) and modified ferritin np with visible hemagglutinin (HA) spikes (HA-np) (right). (B) Comparison of the immunogenicity (in mice) of trivalent inactivated influenza vaccine (TIV, control) or HA-np, without (–) or with adjuvant (Ribi). Neutralization titers (IC₉₀) were determined

by measuring the concentration of antibody required to inhibit viral entry by 90%. (C) Table showing the neutralization (IC_{50} values) of immune sera induced by TIV or HA-np (with Ribi) against a range of H1N1 pseudotyped influenza viruses. Heat map is a colored gradient, from green (weak) to yellow to red (strong), reflecting the neutralization strength. Adapted with permission of [162]. (Middle panel) Drug delivery: A PNP-based microRNA delivery system for targeted cancer therapy. (D) MS2 VLPs loaded with an anticancer microRNA (miR122) and modified to display a cell-penetrating peptide (TAT) by either (1) bioconjugation (crosslinking); or (2) genetic engineering. (E) Tumors isolated from mouse models of hepatocellular carcinoma (HCC) after three weeks of treatment with either of the modified VLPs, which were loaded with miR122 (+ve) or a noncoding miRNA control (−ve). (F) Tumor weights after treatment with modified VLPs. Data compared with their negative controls (−ve) are represented by: $\star\star p < 0.01$; data from the genetically modified VLPs (2 +ve) treated group compared with the bioconjugated (crosslinked) VLPs treated group (1 +ve) are represented by: $\Delta\Delta p < 0.01$. Adapted with permission of [92]. (Right panel) Biocatalysis: In vivo loading of multiple enzymes inside PNPs for biocatalysis. (G) Genetic incorporation of the SpyCatcher/SpyTag system into the internal cavity of the MS2 VLP, which facilitates the loading of cargo tagged with either SpyCatcher or SpyTag during MS2 self-assembly in vivo. (H) Diagram of the sequential two-enzyme (i.e., pyridoxal phosphate (PLP)-dependent tryptophanase (TnaA) and flavin mononucleotide and nicotinamide adenine dinucleotide phosphate (NADPH)-dependent monooxygenase (FMO)) biosynthetic pathway for the production of indigo from L-tryptophan (L-Trp). (I) In vivo indigo production of *E. coli* strains expressing either of the encapsulated polycistronic operons (containing both enzymes): “TnaA + FMO” or “FMO + TnaA”, and their respective controls: free and single encapsulated enzymes. Adapted with permission of [139].

5.1.2. Drug Delivery Systems

Conventional drug-based therapy lacks targeting and proper biodistribution, resulting in undesired side effects and a reduction in clinical efficacy [211]. In order to avoid these complications and provide an effective and localized treatment to patients, drugs must be targeted specifically, distributed, and controllably released at their primary site-of-action (e.g., tumors).

Drug delivery systems aim to minimize these limitations by altering a drug's solubility, pharmacokinetics, and biodistribution [212]. Emerging nanotechnologies, in particular, NPs, show great promise as DDSs for cancer treatment [213]. Yet, very few synthetic NPs have advanced to become approved clinical therapies. This is due to their significant limitations, which include physicochemical heterogeneity, problematic functionalization, instability in physiological solutions, poor tumor penetration, and toxicity in biological systems [214]. The use of PNPs as nanocarriers is a promising alternative to synthetic NPs for the development of “smart” delivery systems. PNPs can be designed and produced to trigger the release of their cargo in response to changes in pH, chemical stimuli, redox potential, and temperature [215]. Most of the development of PNP delivery systems have focused on the treatment of cancer and the loading of cancer drugs inside PNPs in combination with targeting peptides. For example, in vitro studies showed no significant difference in the cytotoxic effect of RGD-targeted DOX-loaded HBc (RGD-HBc-NS5A/dox), DOX-loaded HBc without RGD (HBc-NS5A/dox), and free DOX. However, in vivo assays performed on mice xenografted with B16F10 tumors showed that RGD-HBc-NS5A/dox had significantly higher tumor growth inhibition (90.7%) compared to HBc-NS5A/dox (78.5%) and free DOX (72.1%). Furthermore, in vivo (mice) assessment of the potential systematic toxicity of RGD-HBc-NS5A/dox indicated that these nanocarriers were safe and displayed no observable hepatotoxicity or nephrotoxicity [134].

Other therapeutic molecules that have been loaded inside PNPs include miRNAs. miRNAs are endogenous noncoding RNAs that can negatively regulate the gene expression of specific messenger RNAs (mRNAs) by inhibiting their translation or degradation. miRNA interference has been shown to have therapeutic properties in cancer and other diseases [216]. MS2 VLPs have been used as a vehicle

for the targeted delivery of miRNA. For instance, MS2 was loaded with miR146a (MS2-miR146a), while the human immunodeficiency virus (HIV-1) cell-penetrating peptide (CPP) TAT was chemically crosslinked to its outer surface to facilitate uptake by different cell lines. The delivery system was able to induce miRNA expression both in vitro and in vivo [90]. The MS2-miR146a platform has shown other therapeutic effects by delaying the progression of systemic lupus erythematosus in mice [138] and repressing osteoclast differentiation [217].

This platform was improved further by Wang et al., who used phage surface display to genetically incorporate the HIV-1 TAT peptide and load another type of therapeutic miRNA (miR122) inside MS2 for the treatment of HCC [92]. The miR122-MS2 displaying TAT, by either bioconjugation (crosslinking) or genetic engineering, was evaluated for its therapeutic performance (Figure 3D). This delivery system was able to cross the cellular membrane and efficiently deliver miR122 to cancer cell lines (Hep3B, HepG2, and Huh7 HCC). Also, it was observed that the inhibition of invasion and induction of apoptotic rate in vitro, as well as tumor growth, weight, and proliferative capability in vivo (mice), showed significantly better results ($p < 0.01$ or 0.05) when using MS2-miR122 with the genetically incorporated TAT CPP compared to the chemically crosslinked variant (Figure 3E,F). This could be explained by the constant copy number of subunits forming the MS2 VLP, resulting in equal numbers of TAT peptides expected on the VLP's surface. On the other hand, the TAT peptides bioconjugated on the native MS2 VLP relies on a more unstable crosslinking chemistry that may result in variable amounts of TAT on the VLPs. Therefore, a higher amount of evenly distributed TAT peptides could increase the efficiency of MS2 VLP uptake, causing a better inhibitory effect [92].

5.2. Biocatalysis

In nature, enzymatic pathways are compartmentalized into subcellular lipid-based structures or small protein-based compartments [115]. They contribute to confining enzymes and substrates in close proximity to allow faster conversion rates, protecting enzymes from degradation or inactivation, keeping toxic byproducts from damaging cell functions, and maintaining metabolic homeostasis [115]. Encapsulation of enzymes inside engineered PNPs is a novel approach towards fabricating catalytically active nanomaterials with unique properties [115]. Many PNPs have been used to encapsulate enzymes and perform catalytic reactions that in vivo would otherwise produce toxic or highly unstable chemicals. For example, the enzyme Aro10p catalyzes the decarboxylation of 4-hydroxyphenylpyruvate (4-HPP) to 4-hydroxyphenylacetaldehyde (4-HIPAA) [218]. 4-HIPAA can further react with dopamine via a cyclization reaction to form norcoclaurine, an intermediate for the production of benzyloquinoline alkaloids [219,220]. However, 4-HIPAA production in yeast is challenging due to the toxicity effects associated with aldehyde reactivity [221,222]. To address this limitation, Lau et al. encapsulated Aro10p inside encapsulin. The resultant encapsulin–Aro10p complex showed enzymatic activity with 4-HPP in vitro, resulting in spontaneous cyclization of 4-HIPAA with dopamine to produce norcoclaurine [51].

Encapsulation can be applied also as a strategy to increase enzyme stability. Accordingly, manganese peroxidase (MnP)—an enzyme important in the bioremediation of water contaminated with aromatic compounds—was encapsulated inside vault PNPs. The enzyme was encapsulated via fusion to the mINT domain that interacts with the surface inside the vault. The vault-encapsulated MnP not only retained peroxidase activity, but they also displayed higher phenol biodegradation and higher stability towards thermal inactivation when compared to the free enzyme [187].

Some PNPs, such as VLPs, have been studied extensively to exploit their potential as catalytic nanoreactors. For example, Douglas and co-workers made use of synthetic biology tools to develop P22 as a platform for biocatalysis. They showed that P22 was able to encapsulate the tetrameric protein CelB—a β -glucosidase that hydrolyzes a wide variety of beta-linked disaccharides—from the hyperthermophile *P. furiosus*. The in vivo assembly and encapsulation resulted in P22 VLPs within high numbers of tetrameric CelB (~80 monomers per capsid). This high packaging density of CelB had no effect on the enzyme's overall activity [115].

Recently, the P22 VLP system was developed further to achieve the efficient co-encapsulation of a multi-enzyme system capable of performing a coupled cascade of reactions [143]. The selected enzymes carry out sequential reactions in the sugar metabolism of the archaeon *P. furiosus*. The first enzyme is CelB, the second enzyme is the monomeric ATP-dependent galactokinase (GALK), and the third enzyme is the dimeric ADP-dependent glucokinase (GLUK). GALK and GLUK phosphorylate galactose to galactose-1-phosphate, and glucose to glucose-6-phosphate, respectively [223,224]. The design of the multi-enzyme system focused on the ability of CelB to break down lactose into galactose and glucose, which are then used as substrates for the other two enzymes. Additionally, ATP can be coupled to be a cofactor for both GALK and GLUK (once ADP is formed). For co-encapsulation of the enzymes, a gene construct was generated containing the enzymes linked together via flexible spacers. The fusion allows for co-encapsulation of enzymes in a defined ratio. Two protein fusions were evaluated and the effect of gene positioning inside the fusion was assessed, one containing two enzymes (CelB and GLUK) and the other with three enzymes (CelB, GLUK, and GALK). The encapsulated CelB-GLUK construct (CelB-GLUK-P22) showed no difference in enzyme activities compared to the single encapsulated enzymes (GLUK-P22 and CelB-P22, respectively). However, GLUK-CelB-P22 exhibited eight-fold CelB activity reduction compared to CelB-P22. Also, the production yield of GLUK-CelB-P22 decreased two-fold in comparison to CelB or GLUK-P22. These results indicate that the arrangement of enzymes within the fusion can have important effects on both VLP assembly and enzyme activity. The two and three co-encapsulated enzymes were able to perform the cascade reaction, showing similar kinetic parameters to the results achieved by a mixture of equal ratios of single encapsulated enzymes [143].

Enzyme catalytic rate declines have been reported also after encapsulation. Rate declines have been attributed to macromolecular crowding, protein conformational change restrictions during the enzymatic reaction, diffusion of product from the enzyme–substrate complex, and differences in activity coefficients between a native enzyme and an enzyme–substrate complex [42,225]. Also, the colocalization of enzymes does not always achieve enhanced yield activities. Therefore, understanding how the balance of each enzyme’s kinetic parameters and the interenzyme distance affect the flux of intermediates in an enzymatic cascade plays an important role in the design of more complex synthetic pathways [143].

The above examples were performed *in vitro* at small scales, and they required purification of all the components involved in the reaction. However, *in vivo* encapsulation and production seems to be better suited for a low-cost industrial manufacture of chemicals at large scale. For example, Giessen et al. encapsulated the two-enzyme biosynthetic pathway for the commercially relevant indigo dye inside MS2 (Figure 3G) [139]. The enzymes were packaged inside MS2 using the previously described SpyTag/SpyCatcher system (Section 4.2.3). During the biosynthetic pathway of indigo dye (Figure 3H), the pyridoxal phosphate (PLP)-dependent tryptophanase (TnaA) converts L-tryptophan to indole, which is oxidized to indoxyl by the flavin mononucleotide and nicotinamide adenine dinucleotide phosphate (NADPH)-dependent monooxygenase (FMO). Deep blue indigo is formed by the dimerization of indoxyl in the presence of molecular oxygen [226,227]. Two different polycistronic constructions were assessed (TnaA-FMO and FMO-TnaA) and the production of indigo dye was evaluated *in vitro* and *in vivo* (*E. coli*). *In vivo* production was compared between strains expressing the SpyMS2 (encapsulated) or the wt MS2 (wtMS2, free) along the pathway. The order of the genes in the constructions was found to be very important. As shown in Figure 3I, when the pathway was encapsulated, the TnaA-FMO strain outperformed the FMO-TnaA strain, achieving 100% higher production of indigo dye. Also, the production of indigo dye with encapsulated enzymes showed a 60% increase in indigo dye production despite their slightly lower amount of soluble TnaA/FMO compared to the wtMS2 strain (Figure 3I). Furthermore, the encapsulated enzymes displayed higher stability and maintained their initial activity at 25 °C for seven days, whereas free enzymes lost more than 90% of their initial activities under these conditions. The improvement in production of indigo

dye could be attributed to the increased local concentration of intermediates and enhancement of enzyme stability upon encapsulation [139].

6. Conclusions and Future Perspectives

Protein-based nanoparticles have the capacity to be re-engineered, with countless reports detailing the attachment of a diverse range of functional small molecules and macromolecules to their inner and outer surfaces. Various genetic modification and/or bioconjugation techniques have been established to develop PNP-based platforms for applications in drug delivery, nanomaterial synthesis, vaccines, and biocatalysis [12]. However, predicting the effects these modifications have on a PNPs' structural stability and its ability to self-assemble is an ongoing challenge.

The interfaces between subunits are the most poorly understood PNP surface, but arguably the most important and promising one, as PNP self-assembly, disassembly, and reassembly, and also their surface pores, are dependent upon it. Thus, unraveling the underlying mechanisms of PNP self-assembly and the processes driving pore opening and closing is essential for the controlled loading/release and the transfer of cargo molecules in and out of the PNP's cavity. This knowledge will expedite the translation of PNPs into drug delivery applications, in which spatial and temporal control of the release of a drug enhances its therapeutic efficacy and also minimizes any harmful off-target side effects. Additionally, this information can help create more efficient synthetic biocatalytic nanoreactors by enabling better regulation of substrate and/or product flux through PNP surface pores.

Finally, new *in silico* tools that allow the accurate prediction of protein structure and assembly, in combination with high-throughput characterization techniques, will pave the way towards the production of functional PNPs that are tailored to their ultimate application.

Funding: D.D. is supported by an international Macquarie University Research Excellence Scholarship, Sydney Vital Research Scholar Award and the Commonwealth Scientific and Industrial Research Organisation (CSIRO) Ph.D. Scholarship Program in Synthetic Biology. A.C. is supported by a Cancer Institute New South Wales Early Career Fellowship (Project Number: ECF171114) and the Australian Research Council (CE140100003).

Conflicts of Interest: The authors declare no conflict of interest.

References

1. Molino, N.M.; Wang, S.W. Caged protein nanoparticles for drug delivery. *Curr. Opin. Biotechnol.* **2014**, *28*, 75–82. [[CrossRef](#)] [[PubMed](#)]
2. Kato, K.; Tanaka, H.; Sumizawa, T.; Yoshimura, M.; Yamashita, E.; Iwasaki, K.; Tsukihara, T. A vault ribonucleoprotein particle exhibiting 39-fold dihedral symmetry. *Acta Crystallogr.* **2008**, *64*, 525–531. [[CrossRef](#)] [[PubMed](#)]
3. Mosayebi, M.; Shoemark, D.K.; Fletcher, J.M.; Sessions, R.B.; Linden, N.; Woolfson, D.N.; Liverpool, T.B. Beyond icosahedral symmetry in packings of proteins in spherical shells. *Proc. Natl. Acad. Sci. USA* **2017**, *114*, 9014–9019. [[CrossRef](#)] [[PubMed](#)]
4. Rother, M.; Nussbaumer, M.G.; Renggli, K.; Bruns, N. Protein cages and synthetic polymers: A fruitful symbiosis for drug delivery applications, bionanotechnology and materials science. *Chem. Soc. Rev.* **2016**, *45*, 6213–6249. [[CrossRef](#)] [[PubMed](#)]
5. Cornejo, E.; Abreu, N.; Komeili, A. Compartmentalization and organelle formation in bacteria. *Curr. Opin. Cell Biol.* **2014**, *26*, 132–138. [[CrossRef](#)] [[PubMed](#)]
6. Schoonen, L.; van Hest, J.C. Functionalization of protein-based nanocages for drug delivery applications. *Nanoscale* **2014**, *6*, 7124–7141. [[CrossRef](#)] [[PubMed](#)]
7. Li, F.; Wang, Q. Fabrication of nanoarchitectures templated by virus-based nanoparticles: Strategies and applications. *Small* **2014**, *10*, 230–245. [[CrossRef](#)] [[PubMed](#)]
8. Bhaskar, S.; Lim, S. Engineering protein nanocages as carriers for biomedical applications. *Npg Asia Mater.* **2017**, *9*. [[CrossRef](#)]
9. Moon, H.; Lee, J.; Min, J.; Kang, S. Developing genetically engineered encapsulin protein cage nanoparticles as a targeted delivery nanopatform. *Biomacromolecules* **2014**, *15*, 3794–3801. [[CrossRef](#)] [[PubMed](#)]

10. Giessen, T.W. Encapsulins: Microbial nanocompartments with applications in biomedicine, nanobiotechnology and materials science. *Curr. Opin. Chem. Biol.* **2016**, *34*, 1–10. [[CrossRef](#)] [[PubMed](#)]
11. Lee, E.J.; Lee, N.K.; Kim, I.S. Bioengineered protein-based nanocage for drug delivery. *Adv. Drug Deliv. Rev.* **2016**, *106*, 157–171. [[CrossRef](#)] [[PubMed](#)]
12. Lai, Y.T.; King, N.P.; Yeates, T.O. Principles for designing ordered protein assemblies. *Trends Cell Biol.* **2012**, *22*, 653–661. [[CrossRef](#)] [[PubMed](#)]
13. Raeeszadeh-Sarmazdeh, M.; Hartzell, E.; Price, J.V.; Chen, W. Protein nanoparticles as multifunctional biocatalysts and health assessment sensors. *Curr. Opin. Chem. Eng.* **2016**, *13*, 109–118. [[CrossRef](#)]
14. Giessen, T.W.; Silver, P.A. Widespread distribution of encapsulin nanocompartments reveals functional diversity. *Nat. Microbiol.* **2017**, *2*, 1–11. [[CrossRef](#)] [[PubMed](#)]
15. Roldao, A.; Mellado, M.C.; Castilho, L.R.; Carrondo, M.J.; Alves, P.M. Virus-like particles in vaccine development. *Expert Rev. Vaccines* **2010**, *9*, 1149–1176. [[CrossRef](#)] [[PubMed](#)]
16. Farrokhi, N.; Hrmova, M.; Burton, R.A.; Fincher, G.B. Heterologous and Cell-Free Protein Expression Systems. In *Plant Genomics: Methods and Protocols*; Gustafson, J.P., Langridge, P., Somers, D.J., Eds.; Humana Press: Totowa, NJ, USA, 2009; pp. 175–198.
17. Rome, L.H.; Kickhoefer, V.A. Development of the vault particle as a platform technology. *ACS Nano* **2013**, *7*, 889–902. [[CrossRef](#)] [[PubMed](#)]
18. Rohovie, M.J.; Nagasawa, M.; Swartz, J.R. Virus-like particles: Next-generation nanoparticles for targeted therapeutic delivery. *Bioeng. Transl. Med.* **2017**, *2*, 43–57. [[CrossRef](#)] [[PubMed](#)]
19. Sheng, J.; Lei, S.; Yuan, L.; Feng, X. Cell-free protein synthesis of norovirus virus-like particles. *RSC Adv.* **2017**, *7*, 28837–28840. [[CrossRef](#)]
20. ElSohly, A.M.; Netirojjanakul, C.; Aanei, I.L.; Jager, A.; Bendall, S.C.; Farkas, M.E.; Nolan, G.P.; Francis, M.B. Synthetically modified viral capsids as versatile carriers for use in antibody-based cell targeting. *Bioconjug. Chem.* **2015**, *26*, 1590–1596. [[CrossRef](#)] [[PubMed](#)]
21. Sutter, M.; Boehringer, D.; Gutmann, S.; Gunther, S.; Prangishvili, D.; Loessner, M.J.; Stetter, K.O.; Weber-Ban, E.; Ban, N. Structural basis of enzyme encapsulation into a bacterial nanocompartment. *Nat. Struct. Mol. Biol.* **2008**, *15*, 939–947. [[CrossRef](#)] [[PubMed](#)]
22. Lai, Y.-T.; Hura, G.L.; Dyer, K.N.; Tang, H.Y.H.; Tainer, J.A.; Yeates, T.O. Designing and defining dynamic protein cage nanoassemblies in solution. *Sci. Adv.* **2016**, *2*. [[CrossRef](#)] [[PubMed](#)]
23. Moon, H.; Kim, W.G.; Lim, S.; Kang, Y.J.; Shin, H.-H.; Ko, H.; Hong, S.Y.; Kang, S. Fabrication of uniform layer-by-layer assemblies with complementary protein cage nanobuilding blocks via simple His-tag/metal recognition. *J. Mater. Chem. B* **2013**, *1*, 4504–4510. [[CrossRef](#)]
24. Fang, P.-Y.; Gómez, R.; Lizzette, M.; Holguin, S.Y.; Hsiao, C.; Bowman, J.C.; Yang, H.-W.; Williams, L.D. Functional RNAs: Combined assembly and packaging in VLPs. *Nucleic Acids Res.* **2017**, *45*, 3519–3527. [[CrossRef](#)] [[PubMed](#)]
25. Rahman, R.; Bugg, T.D. Assembly in vitro of *Rhodococcus jostii* RHA1 encapsulin and peroxidase DypB to form a nanocompartment. *FEBS J.* **2013**, *280*, 2097–2104. [[CrossRef](#)] [[PubMed](#)]
26. Allen, M.; Willits, D.; Mosolf, J.; Young, M.; Douglas, T. Protein cage constrained synthesis of ferrimagnetic iron oxide nanoparticles. *Adv. Mater.* **2002**, *14*, 1562–1565. [[CrossRef](#)]
27. Zhen, Z.; Tang, W.; Guo, C.; Chen, H.; Lin, X.; Liu, G.; Fei, B.; Chen, X.; Xu, B.; Xie, J. Ferritin nanocages to encapsulate and deliver photosensitizers for efficient photodynamic therapy against cancer. *ACS Nano* **2013**, *7*, 6988–6996. [[CrossRef](#)] [[PubMed](#)]
28. Brumfield, S.; Willits, D.; Tang, L.; Johnson, J.E.; Douglas, T.; Young, M. Heterologous expression of the modified coat protein of *Cowpea chlorotic mottle bromovirus* results in the assembly of protein cages with altered architectures and function. *J. Gen. Virol.* **2004**, *85*, 1049–1053. [[CrossRef](#)] [[PubMed](#)]
29. Dalsgaard, K.; Uttenthal, Å.; Jones, T.D.; Xu, F.; Merryweather, A.; Hamilton, W.D.O.; Langeveld, J.P.M.; Boshuizen, R.S.; Kamstrup, S.; Lomonosoff, G.P.; et al. Plant-derived vaccine protects target animals against a viral disease. *Nat. Biotechnol.* **1997**, *15*. [[CrossRef](#)] [[PubMed](#)]
30. Hassani-Mehraban, A.; Creutzburg, S.; Heereveld, L.; Kormelink, R. Feasibility of *Cowpea chlorotic mottle* virus-like particles as scaffold for epitope presentations. *BMC Biotechnol.* **2015**, *15*. [[CrossRef](#)] [[PubMed](#)]

31. Wen, A.M.; Shukla, S.; Saxena, P.; Aljabali, A.A.A.; Yildiz, I.; Dey, S.; Mealy, J.E.; Yang, A.C.; Evans, D.J.; Lomonosoff, G.P.; et al. Interior engineering of a viral nanoparticle and its tumor homing properties. *Biomacromolecules* **2012**, *13*, 3990–4001. [[CrossRef](#)] [[PubMed](#)]
32. Saunders, K.; Sainsbury, F.; Lomonosoff, G.P. Efficient generation of *cowpea mosaicvirus* empty virus-like particles by the proteolytic processing of precursors in insect cells and plants. *Virology* **2009**, *393*, 329–337. [[CrossRef](#)] [[PubMed](#)]
33. Brandenburg, B.; Stockl, L.; Gutzeit, C.; Roos, M.; Lupberger, J.; Schwartlander, R.; Gelderblom, H.; Sauer, I.M.; Hofschneider, P.H.; Hildt, E. A novel system for efficient gene transfer into primary human hepatocytes via cell-permeable hepatitis B virus-like particle. *Hepatology* **2005**, *42*, 1300–1309. [[CrossRef](#)] [[PubMed](#)]
34. Lanford, R.E.; Notvall, L. Expression of hepatitis B virus core and precore antigens in insect cells and characterization of a core-associated kinase activity. *Virology* **1990**, *176*, 222–233. [[CrossRef](#)]
35. Beames, B.; Lanford, R.E. Insertions within the hepatitis B virus capsid protein influence capsid formation and RNA encapsidation. *J. Virol.* **1995**, *69*, 6833–6838. [[PubMed](#)]
36. Li, H.; Onbe, K.; Liu, Q.; Iijima, M.; Tatematsu, K.; Seno, M.; Tada, H.; Kuroda, S.I. Synthesis and assembly of hepatitis B virus envelope protein-derived particles in *Escherichia coli*. *Biochem. Biophys. Res. Commun.* **2017**, *490*, 155–160. [[CrossRef](#)] [[PubMed](#)]
37. Peyret, H.; Gehin, A.; Thuenemann, E.C.; Blond, D.; El Turabi, A.; Beales, L.; Clarke, D.; Gilbert, R.J.; Fry, E.E.; Stuart, D.I.; et al. Tandem fusion of hepatitis B core antigen allows assembly of virus-like particles in bacteria and plants with enhanced capacity to accommodate foreign proteins. *PLoS ONE* **2015**, *10*, e0120751. [[CrossRef](#)] [[PubMed](#)]
38. Ludgate, L.; Liu, K.; Luckenbaugh, L.; Streck, N.; Eng, S.; Voitenleitner, C.; Delaney, W.E.T.; Hu, J. Cell-free hepatitis B virus capsid assembly dependent on the core protein C-terminal domain and regulated by phosphorylation. *J. Virol.* **2016**, *90*, 5830–5844. [[CrossRef](#)] [[PubMed](#)]
39. Fu, Y.; Li, J. A novel delivery platform based on bacteriophage MS2 virus-like particles. *Virus Res.* **2016**, *211*, 9–16. [[CrossRef](#)] [[PubMed](#)]
40. Legendre, D.; Fastrez, J. Production in *Saccharomyces cerevisiae* of MS2 virus-like particles packaging functional heterologous mRNAs. *J. Biotechnol.* **2005**, *117*, 183–194. [[CrossRef](#)] [[PubMed](#)]
41. Bundy, B.C.; Franciszkowicz, M.J.; Swartz, J.R. *Escherichia coli*-based cell-free synthesis of virus-like particles. *Biotechnol. Bioeng.* **2008**, *100*, 28–37. [[CrossRef](#)] [[PubMed](#)]
42. Patterson, D.P.; Prevelige, P.E.; Douglas, T. Nanoreactors by programmed enzyme encapsulation inside the capsid of the bacteriophage P22. *ACS Nano* **2012**, *6*, 5000–5009. [[CrossRef](#)] [[PubMed](#)]
43. Freivalds, J.; Dislers, A.; Ose, V.; Skrastina, D.; Cielens, I.; Pumpens, P.; Sasnauskas, K.; Kazaks, A. Assembly of bacteriophage Q β virus-like particles in yeast *Saccharomyces cerevisiae* and *Pichia pastoris*. *J. Biotechnol.* **2006**, *123*, 297–303. [[CrossRef](#)] [[PubMed](#)]
44. Cielens, I.; Ose, V.; Petrovskis, I.; Strelnikova, A.; Renhofa, R.; Kozlovskas, T.; Pumpens, P. Mutilation of RNA phage Q β virus-like particles: From icosahedrons to rods. *FEBS Lett.* **2000**, *482*, 261–264. [[CrossRef](#)]
45. Smith, M.T.; Varner, C.T.; Bush, D.B.; Bundy, B.C. The incorporation of the A2 protein to produce novel Q β virus-like particles using cell-free protein synthesis. *Biotechnol. Prog.* **2012**, *28*, 549–555. [[CrossRef](#)] [[PubMed](#)]
46. Haikarainen, T.; Papageorgiou, A.C. Dps-like proteins: Structural and functional insights into a versatile protein family. *Cell. Mol. Life Sci.* **2010**, *67*, 341–351. [[CrossRef](#)] [[PubMed](#)]
47. Ilari, A.; Stefanini, S.; Chiancone, E.; Tsernoglou, D. The dodecameric ferritin from *Listeria innocua* contains a novel intersubunit iron-binding site. *Nat. Struct. Biol.* **2000**, *7*, 38–43. [[PubMed](#)]
48. Dalmau, M.; Lim, S.; Chen, H.C.; Ruiz, C.; Wang, S.W. Thermostability and molecular encapsulation within an engineered caged protein scaffold. *Biotechnol. Bioeng.* **2008**, *101*, 654–664. [[CrossRef](#)] [[PubMed](#)]
49. Tamura, A.; Fukutani, Y.; Takami, T.; Fujii, M.; Nakaguchi, Y.; Murakami, Y.; Noguchi, K.; Yohda, M.; Odaka, M. Packaging guest proteins into the encapsulin nanocompartment from *Rhodococcus erythropolis* N771. *Biotechnol. Bioeng.* **2015**, *112*, 13–20. [[CrossRef](#)] [[PubMed](#)]
50. Cassidy-Amstutz, C.; Oltrogge, L.; Going, C.C.; Lee, A.; Teng, P.; Quintanilla, D.; East-Seletsky, A.; Williams, E.R.; Savage, D.F. Identification of a minimal peptide tag for in vivo and in vitro loading of encapsulin. *Biochemistry* **2016**, *55*, 3461–3468. [[CrossRef](#)] [[PubMed](#)]
51. Lau, Y.H.; Giessen, T.W.; Altenburg, W.J.; Silver, P.A. Prokaryotic nanocompartments form synthetic organelles in a eukaryote. *Nat. Commun.* **2018**, *9*. [[CrossRef](#)] [[PubMed](#)]

52. Sigmund, F.; Massner, C.; Erdmann, P.; Stelzl, A.; Rolbieski, H.; Desai, M.; Bricault, S.; Wörner, T.P.; Snijder, J.; Geerlof, A.; et al. Bacterial encapsulins as orthogonal compartments for mammalian cell engineering. *Nat. Commun.* **2018**, *9*. [[CrossRef](#)] [[PubMed](#)]
53. Wang, Z.; Gao, H.; Zhang, Y.; Liu, G.; Niu, G.; Chen, X. Functional ferritin nanoparticles for biomedical applications. *Front. Chem. Sci. Eng.* **2017**, *11*, 633–646. [[CrossRef](#)] [[PubMed](#)]
54. Biswas, P.; Trozado, C.; Lee, J.; Schwartz, R.M. Development of a mammalian cell culture process for rapid Clinical-Scale production of novel influenza nanoparticle vaccines. *BMC Proc.* **2015**, *9*. [[CrossRef](#)]
55. Hong, S.M.; Mon, H.; Lee, J.M.; Kusakabe, T. Characterization and recombinant protein expression of ferritin light chain homologue in the silkworm, *Bombyx mori*. *Insect Sci.* **2014**, *21*, 135–146. [[CrossRef](#)] [[PubMed](#)]
56. Lee, J.L.; Park, C.S.; Kim, H.Y. Functional assembly of recombinant human ferritin subunits in *Pichia pastoris*. *J. Microbiol. Biotechnol.* **2007**, *17*, 1695–1699. [[PubMed](#)]
57. De Llanos, R.; Martínez-Garay, C.A.; Fita-Torró, J.; Romero, A.M.; Martínez-Pastor, M.T.; Puig, S. Soybean ferritin expression in *Saccharomyces cerevisiae* modulates iron accumulation and resistance to elevated iron concentrations. *Appl. Environ. Microbiol.* **2016**, *82*, 3052–3060. [[CrossRef](#)] [[PubMed](#)]
58. Chen, H.; Zhang, S.; Xu, C.; Zhao, G. Engineering protein interfaces yields ferritin disassembly and reassembly under benign experimental conditions. *Chem. Commun.* **2016**, *52*, 7402–7405. [[CrossRef](#)] [[PubMed](#)]
59. Varpness, Z.; Peters, J.W.; Young, M.; Douglas, T. Biomimetic synthesis of a H₂ catalyst using a protein cage architecture. *Nano Lett.* **2005**, *5*, 2306–2309. [[CrossRef](#)] [[PubMed](#)]
60. Kim, R.; Lai, L.; Lee, H.-H.; Cheong, G.-W.; Kim, K.K.; Wu, Z.; Yokota, H.; Marqusee, S.; Kim, S.-H. On the mechanism of chaperone activity of the small heat-shock protein of *Methanococcus jannaschii*. *Proc. Natl. Acad. Sci. USA* **2003**, *100*, 8151–8155. [[CrossRef](#)] [[PubMed](#)]
61. Rudolf, L.; Markus, F.; Adelbert, B. The lumazine synthase/riboflavin synthase complex: Shapes and functions of a highly variable enzyme system. *FEBS J.* **2013**, *280*, 2537–2563.
62. Ra, J.S.; Shin, H.H.; Kang, S.; Do, Y. Lumazine synthase protein cage nanoparticles as antigen delivery nanoplatforams for dendritic cell-based vaccine development. *Clin. Exp. Vaccine Res.* **2014**, *3*, 227–234. [[CrossRef](#)] [[PubMed](#)]
63. Yu, K.; Yau, Y.H.; Sinha, A.; Tan, T.; Kickhoefer, V.A.; Rome, L.H.; Lee, H.; Shochat, S.G.; Lim, S. Modulation of the vault protein-protein interaction for tuning of molecular release. *Sci. Rep.* **2017**, *7*. [[CrossRef](#)] [[PubMed](#)]
64. Ryu, S.J.; An, H.J.; Oh, Y.S.; Choi, H.R.; Ha, M.K.; Park, S.C. On the role of major vault protein in the resistance of senescent human diploid fibroblasts to apoptosis. *Cell Death Differ.* **2008**, *15*. [[CrossRef](#)] [[PubMed](#)]
65. Stephen, A.G.; Raval-Fernandes, S.; Huynh, T.; Torres, M.; Kickhoefer, V.A.; Rome, L.H. Assembly of vault-like particles in insect cells expressing only the major vault protein. *J. Biol. Chem.* **2001**, *276*, 23217–23220. [[CrossRef](#)] [[PubMed](#)]
66. Mrazek, J. Cell-Free Methods of Producing Vault Particles and Vault Particles Resulting Therefrom. WO Patent Application WO2016049122A1, 31 March 2016.
67. Howorka, S. Rationally engineering natural protein assemblies in nanobiotechnology. *Curr. Opin. Biotechnol.* **2011**, *22*, 485–491. [[CrossRef](#)] [[PubMed](#)]
68. Jeon, J.O.; Kim, S. Designed nanocage displaying ligand-specific Peptide bunches for high affinity and biological activity. *ACS Nano* **2013**, *7*, 7462–7471. [[CrossRef](#)] [[PubMed](#)]
69. Lee, N.K.; Lee, E.J. Ferritin nanocage with intrinsically disordered proteins and affibody: A platform for tumor targeting with extended pharmacokinetics. *J. Control. Release* **2017**, *267*, 172–180. [[CrossRef](#)] [[PubMed](#)]
70. Ardejani, M.S.; Li, N.X. Stabilization of a Protein Nanocage through the Plugging of a Protein–Protein Interfacial Water Pocket. *Biochemistry* **2011**, *50*, 4029–4037. [[CrossRef](#)] [[PubMed](#)]
71. Kilic, M.A.; Spiro, S.; Moore, G.R. Stability of a 24-meric homopolymer: Comparative studies of assembly-defective mutants of *Rhodobacter capsulatus* bacterioferritin and the native protein. *Protein Sci.* **2003**, *12*, 1663–1674. [[CrossRef](#)] [[PubMed](#)]
72. Huang, P.-S.; Boyken, S.E.; Baker, D. The coming of age of de novo protein design. *Nature* **2016**, *537*. [[CrossRef](#)] [[PubMed](#)]
73. Norn, C.H.; André, I. Computational design of protein self-assembly. *Curr. Opin. Struct. Biol.* **2016**, *39*, 39–45. [[CrossRef](#)] [[PubMed](#)]

74. Kobayashi, N.; Arai, R. Design and construction of self-assembling supramolecular protein complexes using artificial and fusion proteins as nanoscale building blocks. *Curr. Opin. Biotechnol.* **2017**, *46*, 57–65. [[CrossRef](#)] [[PubMed](#)]
75. Lai, Y.-T.; Tsai, K.-L.; Sawaya, M.R.; Asturias, F.J.; Yeates, T.O. Structure and flexibility of nanoscale protein cages designed by symmetric self-assembly. *J. Am. Chem. Soc.* **2013**, *135*, 7738–7743. [[CrossRef](#)] [[PubMed](#)]
76. Miyamoto, T.; Kuribayashi, M.; Nagao, S.; Shomura, Y.; Higuchi, Y.; Hirota, S. Domain-swapped cytochrome *cb562* dimer and its nanocage encapsulating a Zn–SO₄ cluster in the internal cavity. *Chem. Sci.* **2015**, *6*, 7336–7342. [[CrossRef](#)] [[PubMed](#)]
77. Song, W.J.; Tezcan, F.A. A designed supramolecular protein assembly with in vivo enzymatic activity. *Science* **2014**, *346*, 1525–1528. [[CrossRef](#)] [[PubMed](#)]
78. Fletcher, J.M.; Harniman, R.L.; Barnes, F.R.H.; Boyle, A.L.; Collins, A.; Mantell, J.; Sharp, T.H.; Antognozzi, M.; Booth, P.J.; Linden, N.; et al. Self-assembling cages from coiled-coil peptide modules. *Science* **2013**. [[CrossRef](#)] [[PubMed](#)]
79. Adolf-Bryfogle, J.; Dunbrack, R.L., Jr. The PyRosetta Toolkit: A graphical user interface for the Rosetta software suite. *PLoS ONE* **2013**, *8*, e66856. [[CrossRef](#)] [[PubMed](#)]
80. Bale, J.B.; Gonen, S.; Liu, Y.; Sheffler, W.; Ellis, D.; Thomas, C.; Cascio, D.; Yeates, T.O.; Gonen, T.; King, N.P.; et al. Accurate design of megadalton-scale two-component icosahedral protein complexes. *Science* **2016**, *353*, 389–394. [[CrossRef](#)] [[PubMed](#)]
81. Butterfield, G.L.; Lajoie, M.J.; Gustafson, H.H.; Sellers, D.L.; Nattermann, U.; Ellis, D.; Bale, J.B.; Ke, S.; Lenz, G.H.; Yehdego, A.; et al. Evolution of a designed protein assembly encapsulating its own RNA genome. *Nature* **2017**, *552*. [[CrossRef](#)] [[PubMed](#)]
82. Chen, Q.; Sun, Q.; Molino, N.M.; Wang, S.-W.; Boder, E.T.; Chen, W. Sortase A-mediated multi-functionalization of protein nanoparticles. *Chem. Commun.* **2015**, *51*, 12107–12110. [[CrossRef](#)] [[PubMed](#)]
83. Kostianinen, M.A.; Hiekkataipale, P.; de la Torre, J.A.; Nolte, R.J.M.; Cornelissen, J.J.L.M. Electrostatic self-assembly of virus-polymer complexes. *J. Mater. Chem. B* **2011**, *21*, 2112–2117. [[CrossRef](#)]
84. Liébana, S.; Drago Guido, A. Bioconjugation and stabilisation of biomolecules in biosensors. *Essays Biochem.* **2016**, *60*, 59–68. [[CrossRef](#)] [[PubMed](#)]
85. Cortajarena, A.L.; Grove, T.Z. *Protein-Based Engineered Nanostructures*; Springer: New York, NY, USA, 2016; Volume 940.
86. Falvo, E.; Tremante, E.; Fraioli, R.; Leonetti, C.; Zamparelli, C.; Boffi, A.; Morea, V.; Ceci, P.; Giacomini, P. Antibody-drug conjugates: Targeting melanoma with cisplatin encapsulated in protein-cage nanoparticles based on human ferritin. *Nanoscale* **2013**, *5*, 12278–12285. [[CrossRef](#)] [[PubMed](#)]
87. Flenniken, M.L.; Willits, D.A.; Harmsen, A.L.; Liepold, L.O.; Harmsen, A.G.; Young, M.J.; Douglas, T. Melanoma and lymphocyte cell-specific targeting incorporated into a heat shock protein cage architecture. *Chem. Biol.* **2006**, *13*, 161–170. [[CrossRef](#)] [[PubMed](#)]
88. Terashima, M.; Uchida, M.; Kosuge, H.; Tsao, P.S.; Young, M.J.; Conolly, S.M.; Douglas, T.; McConnell, M.V. Human ferritin cages for imaging vascular macrophages. *Biomaterials* **2011**, *32*, 1430–1437. [[CrossRef](#)] [[PubMed](#)]
89. Destito, G.; Yeh, R.; Rae, C.S.; Finn, M.G.; Manchester, M. Folic acid-mediated targeting of cowpea mosaic virus particles to tumor cells. *Chem. Biol.* **2007**, *14*, 1152–1162. [[CrossRef](#)] [[PubMed](#)]
90. Pan, Y.; Zhang, Y.; Jia, T.; Zhang, K.; Li, J.; Wang, L. Development of a microRNA delivery system based on bacteriophage MS2 virus-like particles. *FEBS J.* **2012**, *279*, 1198–1208. [[CrossRef](#)] [[PubMed](#)]
91. Aljabali, A.A.; Shukla, S.; Lomonosoff, G.P.; Steinmetz, N.F.; Evans, D.J. CPMV-DOX delivers. *Mol. Pharm.* **2013**, *10*, 3–10. [[CrossRef](#)] [[PubMed](#)]
92. Wang, G.; Jia, T.; Xu, X.; Chang, L.; Zhang, R.; Fu, Y.; Li, Y.; Yang, X.; Zhang, K.; Lin, G.; et al. Novel miR-122 delivery system based on MS2 virus like particle surface displaying cell-penetrating peptide TAT for hepatocellular carcinoma. *Oncotarget* **2016**, *7*, 59402–59416. [[CrossRef](#)] [[PubMed](#)]
93. Hein, C.D.; Liu, X.-M.; Wang, D. Click chemistry, a powerful tool for pharmaceutical sciences. *Pharm. Res.* **2008**, *25*, 2216–2230. [[CrossRef](#)] [[PubMed](#)]
94. Smith, M.T.; Hawes, A.K.; Bundy, B.C. Reengineering viruses and virus-like particles through chemical functionalization strategies. *Curr. Opin. Biotechnol.* **2013**, *24*, 620–626. [[CrossRef](#)] [[PubMed](#)]

95. Rhee, J.-K.; Hovlid, M.; Fiedler, J.D.; Brown, S.D.; Manzenrieder, F.; Kitagishi, H.; Nycholat, C.; Paulson, J.C.; Finn, M.G. Colorful virus-like particles: Fluorescent protein packaging by the Q β capsid. *Biomacromolecules* **2011**, *12*, 3977–3981. [[CrossRef](#)] [[PubMed](#)]
96. Pokorski, J.K.; Hovlid, M.L.; Finn, M.G. Cell targeting with hybrid Q β virus-like particles displaying epidermal growth factor. *ChemBioChem* **2011**, *12*, 2441–2447. [[CrossRef](#)] [[PubMed](#)]
97. Hovlid, M.L.; Lau, J.L.; Breitenkamp, K.; Higginson, C.J.; Laufer, B.; Manchester, M.; Finn, M.G. Encapsidated atom-transfer radical polymerization in Q β virus-like nanoparticles. *ACS Nano* **2014**, *8*, 8003–8014. [[CrossRef](#)] [[PubMed](#)]
98. Laplagne, D.A.; Zylberman, V.; Ainciart, N.; Steward, M.W.; Sciutto, E.; Fossati, C.A.; Goldbaum, F.A. Engineering of a polymeric bacterial protein as a scaffold for the multiple display of peptides. *Proteins Struct. Funct. Bioinform.* **2004**, *57*, 820–828. [[CrossRef](#)] [[PubMed](#)]
99. Sano, K.I.; Ajima, K.; Iwahori, K.; Yudasaka, M.; Iijima, S.; Yamashita, I.; Shiba, K. Endowing a ferritin-like cage protein with high affinity and selectivity for certain inorganic materials. *Small* **2005**, *1*, 826–832. [[CrossRef](#)] [[PubMed](#)]
100. Belval, L.; Hemmer, C.; Sauter, C.; Reinbold, C.; Fauny, J.D.; Berthold, F.; Ackerer, L.; Schmitt-Keichinger, C.; Lemaire, O.; Demangeat, G.; et al. Display of whole proteins on inner and outer surfaces of grapevine fanleaf virus-like particles. *Plant Biotechnol. J.* **2016**, *14*, 2288–2299. [[CrossRef](#)] [[PubMed](#)]
101. Phippen, S.W.; Stevens, C.A.; Vance, T.D.R.; King, N.P.; Baker, D.; Davies, P.L. Multivalent display of antifreeze proteins by fusion to self-assembling protein cages enhances ice-binding activities. *Biochemistry* **2016**, *55*, 6811–6820. [[CrossRef](#)] [[PubMed](#)]
102. Kang, H.J.; Kang, Y.J.; Lee, Y.-M.; Shin, H.-H.; Chung, S.J.; Kang, S. Developing an antibody-binding protein cage as a molecular recognition drug modular nanoplatfrom. *Biomaterials* **2012**, *33*, 5423–5430. [[CrossRef](#)] [[PubMed](#)]
103. Shuvaev, V.V.; Dziubla, T.; Wiewrodt, R.; Muzykantov, V.R. Streptavidin-Biotin Crosslinking of Therapeutic Enzymes with Carrier Antibodies. In *Bioconjugation Protocols: Strategies and Methods*; Niemeyer, C.M., Ed.; Humana Press: Totowa, NJ, USA, 2004; pp. 3–19.
104. Suci, P.A.; Kang, S.; Young, M.; Douglas, T. A Streptavidin-protein cage janus particle for polarized targeting and modular functionalization. *J. Am. Chem. Soc.* **2009**, *131*, 9164–9165. [[CrossRef](#)] [[PubMed](#)]
105. Theile, C.S.; Witte, M.D.; Blom, A.E.M.; Kundrat, L.; Ploegh, H.L.; Guimaraes, C.P. Site-specific N-terminal labeling of proteins using sortase-mediated reactions. *Nat. Protoc.* **2013**, *8*. [[CrossRef](#)] [[PubMed](#)]
106. Guimaraes, C.P.; Witte, M.D.; Theile, C.S.; Bozkurt, G.; Kundrat, L.; Blom, A.E.M.; Ploegh, H.L. Site-specific C-terminal and internal loop labeling of proteins using sortase-mediated reactions. *Nat. Protoc.* **2013**, *8*. [[CrossRef](#)] [[PubMed](#)]
107. Patterson, D.; Schwarz, B.; Avera, J.; Western, B.; Hicks, M.; Krugler, P.; Terra, M.; Uchida, M.; McCoy, K.; Douglas, T. Sortase-mediated ligation as a modular approach for the covalent attachment of proteins to the exterior of the bacteriophage P22 virus-like particle. *Bioconjug. Chem.* **2017**, *28*, 2114–2124. [[CrossRef](#)] [[PubMed](#)]
108. Schoonen, L.; Pille, J.; Borrmann, A.; Nolte, R.J.M.; van Hest, J.C.M. Sortase A-mediated N-terminal modification of cowpea chlorotic mottle virus for highly efficient cargo loading. *Bioconjug. Chem.* **2015**, *26*, 2429–2434. [[CrossRef](#)] [[PubMed](#)]
109. Wang, Q.; Lin, T.; Johnson, J.E.; Finn, M.G. Natural supramolecular building blocks: Cysteine-added mutants of cowpea mosaic virus. *Chem. Biol.* **2002**, *9*, 813–819. [[CrossRef](#)]
110. Beatty, K.E.; Tirrell, D.A. Noncanonical Amino Acids in Protein Science and Engineering. In *Protein Engineering*; Köhrer, C., RajBhandary, U.L., Eds.; Springer: Berlin/Heidelberg, Germany, 2009; pp. 127–153.
111. Link, A.J.; Mock, M.L.; Tirrell, D.A. Non-canonical amino acids in protein engineering. *Curr. Opin. Biotechnol.* **2003**, *14*, 603–609. [[CrossRef](#)] [[PubMed](#)]
112. Wals, K.; Ovaa, H. Unnatural amino acid incorporation in *E. coli*: Current and future applications in the design of therapeutic proteins. *Front. Chem.* **2014**, *2*. [[CrossRef](#)] [[PubMed](#)]
113. Capehart, S.L.; Coyle, M.P.; Glasgow, J.E.; Francis, M.B. Controlled integration of gold nanoparticles and organic fluorophores using synthetically modified MS2 viral capsids. *J. Am. Chem. Soc.* **2013**, *135*, 3011–3016. [[CrossRef](#)] [[PubMed](#)]
114. Stephanopoulos, N.; Tong, G.J.; Hsiao, S.C.; Francis, M.B. Dual-surface modified virus capsids for targeted delivery of photodynamic agents to cancer cells. *ACS Nano* **2010**, *4*, 6014–6020. [[CrossRef](#)] [[PubMed](#)]

115. Patterson, D.P.; Schwarz, B.; El-Boubbou, K.; van der Oost, J.; Prevelige, P.E.; Douglas, T. Virus-like particle nanoreactors: Programmed encapsulation of the thermostable CelB glycosidase inside the P22 capsid. *Soft Matter* **2012**, *8*, 10158–10166. [[CrossRef](#)]
116. Ren, Y.; Wong, S.M.; Lim, L.-Y. Folic acid-conjugated protein cages of a plant virus: A novel delivery platform for doxorubicin. *Bioconjug. Chem.* **2007**, *18*, 836–843. [[CrossRef](#)] [[PubMed](#)]
117. Garmann, R.F.; Comas-Garcia, M.; Gopal, A.; Knobler, C.M.; Gelbart, W.M. The assembly pathway of an icosahedral single-stranded RNA virus depends on the strength of inter-subunit attractions. *J. Mol. Biol.* **2014**, *426*, 1050–1060. [[CrossRef](#)] [[PubMed](#)]
118. Comellas-Aragonès, M.; Engelkamp, H.; Claessen, V.I.; Sommerdijk, N.A.J.M.; Rowan, A.E.; Christianen, P.C.M.; Maan, J.C.; Verduin, B.J.M.; Cornelissen, J.J.L.M.; Nolte, R.J.M. A virus-based single-enzyme nanoreactor. *Nat. Nanotechnol.* **2007**, *2*. [[CrossRef](#)] [[PubMed](#)]
119. Sanchez-Sanchez, L.; Cadena-Nava, R.D.; Palomares, L.A.; Ruiz-Garcia, J.; Koay, M.S.; Cornelissen, J.J.; Vazquez-Duhalt, R. Chemotherapy pro-drug activation by biocatalytic virus-like nanoparticles containing cytochrome P450. *Enzym. Microb. Technol.* **2014**, *60*, 24–31. [[CrossRef](#)] [[PubMed](#)]
120. Brasch, M.; Putri, R.M.; de Ruiter, M.V.; Luque, D.; Koay, M.S.T.; Castón, J.R.; Cornelissen, J.J.L.M. Assembling enzymatic cascade pathways inside virus-based nanocages using dual-tasking nucleic acid tags. *J. Am. Chem. Soc.* **2017**, *139*, 1512–1519. [[CrossRef](#)] [[PubMed](#)]
121. Cadena-Nava, R.D.; Comas-Garcia, M.; Garmann, R.F.; Rao, A.L.; Knobler, C.M.; Gelbart, W.M. Self-assembly of viral capsid protein and RNA molecules of different sizes: Requirement for a specific high protein/RNA mass ratio. *J. Virol.* **2012**, *86*, 3318–3326. [[CrossRef](#)] [[PubMed](#)]
122. Rurup, W.F.; Verbij, F.; Koay, M.S.T.; Blum, C.; Subramaniam, V.; Cornelissen, J.J.L.M. Predicting the loading of virus-like particles with fluorescent proteins. *Biomacromolecules* **2014**, *15*, 558–563. [[CrossRef](#)] [[PubMed](#)]
123. Michel, J.P.; Ivanovska, I.L.; Gibbons, M.M.; Klug, W.S.; Knobler, C.M.; Wuite, G.J.L.; Schmidt, C.F. Nanoindentation studies of full and empty viral capsids and the effects of capsid protein mutations on elasticity and strength. *Proc. Natl. Acad. Sci. USA* **2006**, *103*, 6184–6189. [[CrossRef](#)] [[PubMed](#)]
124. Millán, J.G.; Brasch, M.; Anaya-Plaza, E.; de la Escosura, A.; Velders, A.H.; Reinhoudt, D.N.; Torres, T.; Koay, M.S.T.; Cornelissen, J.J.L.M. Self-assembly triggered by self-assembly: Optically active, paramagnetic micelles encapsulated in protein cage nanoparticles. *J. Inorg. Biochem.* **2014**, *136*, 140–146. [[CrossRef](#)] [[PubMed](#)]
125. Fontana, J.; Dressick, W.J.; Phelps, J.; Johnson, J.E.; Rendell, R.W.; Sampson, T.; Ratna, B.R.; Soto, C.M. Virus-templated plasmonic nanoclusters with icosahedral symmetry via directed self-assembly. *Small* **2014**, *10*, 3058–3063. [[CrossRef](#)] [[PubMed](#)]
126. Aljabali, A.A.; Sainsbury, F.; Lomonossoff, G.P.; Evans, D.J. Cowpea mosaic virus unmodified empty viruslike particles loaded with metal and metal oxide. *Small* **2010**, *6*, 818–821. [[CrossRef](#)] [[PubMed](#)]
127. Sainsbury, F.; Saunders, K.; Aljabali, A.A.; Evans, D.J.; Lomonossoff, G.P. Peptide-controlled access to the interior surface of empty virus nanoparticles. *ChemBioChem* **2011**, *12*, 2435–2440. [[CrossRef](#)] [[PubMed](#)]
128. Steinmetz, N.F.; Ablack, A.L.; Hickey, J.L.; Ablack, J.; Manocha, B.; Mymryk, J.S.; Luyt, L.G.; Lewis, J.D. Intravital imaging of human prostate cancer using viral nanoparticles targeted to gastrin-releasing peptide receptors. *Small* **2011**, *7*, 1664–1672. [[CrossRef](#)] [[PubMed](#)]
129. Marc-André, D.A.; Couture, M.M.; Nathalie, C.; Sonia, T.; Nathalie, L.; Frédéric, O.; Louis, P.V. The production of hemagglutinin-based virus-like particles in plants: A rapid, efficient and safe response to pandemic influenza. *Plant Biotechnol. J.* **2010**, *8*, 607–619.
130. Shen, L.; Zhou, J.; Wang, Y.; Kang, N.; Ke, X.; Bi, S.; Ren, L. Efficient Encapsulation of Fe₃O₄ Nanoparticles into genetically engineered hepatitis B core virus-like particles through a specific interaction for potential bioapplications. *Small* **2015**, *11*, 1190–1196. [[CrossRef](#)] [[PubMed](#)]
131. Dishlers, A.; Skrastina, D.; Renhofa, R.; Petrovskis, I.; Ose, V.; Lieknina, I.; Jansons, J.; Pumpens, P.; Sominskaya, I. The hepatitis B virus core variants that expose foreign C-terminal insertions on the outer surface of virus-like particles. *Mol. Biotechnol.* **2015**, *57*, 1038–1049. [[CrossRef](#)] [[PubMed](#)]
132. Strable, E.; Prasuhn, D.E.; Udit, A.K.; Brown, S.; Link, A.J.; Ngo, J.T.; Lander, G.; Quispe, J.; Potter, C.S.; Carragher, B.; et al. Unnatural amino acid incorporation into virus-like particles. *Bioconjug. Chem.* **2008**, *19*, 866–875. [[CrossRef](#)] [[PubMed](#)]

133. Tang, S.; Xuan, B.; Ye, X.; Huang, Z.; Qian, Z. A modular vaccine development platform based on sortase-mediated site-specific tagging of antigens onto virus-like particles. *Sci. Rep.* **2016**, *6*. [[CrossRef](#)] [[PubMed](#)]
134. Shan, W.; Zhang, D.; Wu, Y.; Lv, X.; Hu, B.; Zhou, X.; Ye, S.; Bi, S.; Ren, L.; Zhang, X. Modularized peptides modified HBc virus-like particles for encapsulation and tumor-targeted delivery of doxorubicin. *Nanomed. Nanotechnol. Biol. Med.* **2018**, *14*, 725–734. [[CrossRef](#)] [[PubMed](#)]
135. Choi, K.-M.; Kim, K.; Kwon, I.C.; Kim, I.-S.; Ahn, H.J. Systemic Delivery of siRNA by chimeric capsid protein: Tumor targeting and RNAi activity in vivo. *Mol. Pharm.* **2013**, *10*, 18–25. [[CrossRef](#)] [[PubMed](#)]
136. Galaway, F.A.; Stockley, P.G. MS2 Viruslike particles: A robust, semisynthetic targeted drug delivery platform. *Mol. Pharm.* **2013**, *10*, 59–68. [[CrossRef](#)] [[PubMed](#)]
137. Ashley, C.E.; Carnes, E.C.; Phillips, G.K.; Durfee, P.N.; Buley, M.D.; Lino, C.A.; Padilla, D.P.; Phillips, B.; Carter, M.B.; Willman, C.L.; et al. Cell-specific delivery of diverse cargos by bacteriophage MS2 virus-like particles. *ACS Nano* **2011**, *5*, 5729–5745. [[CrossRef](#)] [[PubMed](#)]
138. Pan, Y.; Jia, T.; Zhang, Y.; Zhang, K.; Zhang, R.; Li, J.; Wang, L. MS2 VLP-based delivery of microRNA-146a inhibits autoantibody production in lupus-prone mice. *Int. J. Nanomed.* **2012**, *7*, 5957–5967. [[CrossRef](#)] [[PubMed](#)]
139. Giessen, T.W.; Silver, P.A. A catalytic nanoreactor based on in vivo encapsulation of multiple enzymes in an engineered protein nanocompartment. *ChemBioChem* **2016**, *17*, 1931–1935. [[CrossRef](#)] [[PubMed](#)]
140. Lagoutte, P.; Mignon, C.; Donnat, S.; Stadthagen, G.; Mast, J.; Sodoyer, R.; Lugari, A.; Werle, B. Scalable chromatography-based purification of virus-like particle carrier for epitope based influenza A vaccine produced in *Escherichia coli*. *J. Virol. Methods* **2016**, *232*, 8–11. [[CrossRef](#)] [[PubMed](#)]
141. Patterson, D.P.; LaFrance, B.; Douglas, T. Rescuing recombinant proteins by sequestration into the P22 VLP. *Chem. Commun.* **2013**, *49*, 10412–10414. [[CrossRef](#)] [[PubMed](#)]
142. Uchida, M.; Morris, D.S.; Kang, S.; Jolley, C.C.; Lucon, J.; Liepold, L.O.; LaFrance, B.; Prevelige, P.E.; Douglas, T. Site-directed coordination chemistry with P22 virus-like particles. *Langmuir* **2012**, *28*, 1998–2006. [[CrossRef](#)] [[PubMed](#)]
143. Patterson, D.P.; Schwarz, B.; Waters, R.S.; Gedeon, T.; Douglas, T. Encapsulation of an enzyme cascade within the bacteriophage P22 virus-like particle. *ACS Chem. Biol.* **2014**, *9*, 359–365. [[CrossRef](#)] [[PubMed](#)]
144. Patterson, D.P.; Rynda-Apelle, A.; Harmsen, A.L.; Harmsen, A.G.; Douglas, T. Biomimetic antigenic nanoparticles elicit controlled protective immune response to influenza. *ACS Nano* **2013**, *7*, 3036–3044. [[CrossRef](#)] [[PubMed](#)]
145. Patterson, D.; Edwards, E.; Douglas, T. Hybrid nanoreactors: Coupling enzymes and small-molecule catalysts within virus-like particles. *Isr. J. Chem.* **2015**, *55*, 96–101. [[CrossRef](#)]
146. Qazi, S.; Miettinen, H.M.; Wilkinson, R.A.; McCoy, K.; Douglas, T.; Wiedenheft, B. Programmed self-assembly of an active P22-Cas9 nanocarrier system. *Mol. Pharm.* **2016**, *13*, 1191–1196. [[CrossRef](#)] [[PubMed](#)]
147. Fiedler, J.D.; Brown, S.D.; Lau, J.L.; Finn, M.G. RNA-directed packaging of enzymes within virus-like particles. *Angew. Chem. Int. Ed.* **2010**, *49*, 9648–9651. [[CrossRef](#)] [[PubMed](#)]
148. Jegerlehner, A.; Zabel, F.; Langer, A.; Dietmeier, K.; Jennings, G.T.; Saudan, P.; Bachmann, M.F. Bacterially produced recombinant influenza vaccines based on virus-like particles. *PLOS ONE* **2013**, *8*. [[CrossRef](#)] [[PubMed](#)]
149. Pierpaolo, C.; Emilia, C.; Oksana, K.; Giuliano, B.; Lisa, C.; Maria, F.; Dante, G.; Claudia, I.; Claudio, S. Synthesis of iron oxide nanoparticles in *Listeria innocua* Dps (DNA-binding protein from starved cells): A study with the wild-type protein and a catalytic centre mutant. *Chemistry* **2010**, *16*, 709–717.
150. Yamashita, I. Biosupramolecules for nano-devices: Biomineralization of nanoparticles and their applications. *J. Mater. Chem.* **2008**, *18*, 3813–3820. [[CrossRef](#)]
151. Dalmau, M.; Lim, S.; Wang, S.W. Design of a pH-dependent molecular switch in a caged protein platform. *Nano Lett.* **2009**, *9*, 160–166. [[CrossRef](#)] [[PubMed](#)]
152. Caivano, A.; Doria-Rose, N.A.; Buelow, B.; Sartorius, R.; Trovato, M.; D'Apice, L.; Domingo, G.J.; Sutton, W.F.; Haigwood, N.L.; De Berardinis, P. HIV-1 Gag p17 presented as virus-like particles on the E2 scaffold from *Geobacillus stearothermophilus* induces sustained humoral and cellular immune responses in the absence of IFN γ production by CD4⁺ T cells. *Virology* **2010**, *407*, 296–305. [[CrossRef](#)] [[PubMed](#)]
153. Ren, D.; Kratz, F.; Wang, S.-W. Protein nanocapsules containing doxorubicin as a pH-responsive delivery system. *Small* **2011**, *7*, 1051–1060. [[CrossRef](#)] [[PubMed](#)]

154. Jaworski, J.P.; Krebs, S.J.; Trovato, M.; Kovarik, D.N.; Brower, Z.; Sutton, W.F.; Waagmeester, G.; Sartorius, R.; D'Apice, L.; Caivano, A.; et al. Co-immunization with multimeric scaffolds and DNA rapidly induces potent autologous HIV-1 neutralizing antibodies and CD8⁺ T cells. *PLOS ONE* **2012**, *7*. [[CrossRef](#)] [[PubMed](#)]
155. Molino, N.M.; Anderson, A.K.L.; Nelson, E.L.; Wang, S.-W. Biomimetic protein nanoparticles facilitate enhanced dendritic cell activation and cross-presentation. *ACS Nano* **2013**, *7*, 9743–9752. [[CrossRef](#)] [[PubMed](#)]
156. Swartz, A.R.; Xu, X.; Traylor, S.J.; Li, Z.J.; Chen, W. One-step affinity capture and precipitation for improved purification of an industrial monoclonal antibody using Z-ELP functionalized nanocages. *Biotechnol. Bioeng.* **2018**, *115*, 423–432. [[CrossRef](#)] [[PubMed](#)]
157. Moon, H.; Lee, J.; Kim, H.; Heo, S.; Min, J.; Kang, S. Genetically engineering encapsulin protein cage nanoparticle as a SCC-7 cell targeting optical nanoprobe. *Biomater. Res.* **2014**, *18*. [[CrossRef](#)] [[PubMed](#)]
158. Giessen, T.W.; Silver, P.A. Converting a natural protein compartment into a nanofactory for the size-constrained synthesis of antimicrobial silver nanoparticles. *ACS Synth. Biol.* **2016**. [[CrossRef](#)] [[PubMed](#)]
159. Choi, B.; Moon, H.; Hong, S.J.; Shin, C.; Do, Y.; Ryu, S.; Kang, S. Effective delivery of antigen-encapsulin nanoparticle fusions to dendritic cells leads to antigen-specific cytotoxic T cell activation and tumor rejection. *ACS Nano* **2016**, *10*, 7339–7350. [[CrossRef](#)] [[PubMed](#)]
160. Chen, L.; Bai, G.; Yang, R.; Zang, J.; Zhou, T.; Zhao, G. Encapsulation of β -carotene within ferritin nanocages greatly increases its water-solubility and thermal stability. *Food Chem.* **2014**, *149*, 307–312. [[CrossRef](#)] [[PubMed](#)]
161. Zhen, Z.; Tang, W.; Chen, H.; Lin, X.; Todd, T.; Wang, G.; Cowger, T.; Chen, X.; Xie, J. RGD-modified apoferritin nanoparticles for efficient drug delivery to tumors. *ACS Nano* **2013**, *7*, 4830–4837. [[CrossRef](#)] [[PubMed](#)]
162. Kanekiyo, M.; Wei, C.-J.; Yassine, H.M.; McTamney, P.M.; Boyington, J.C.; Whittle, J.R.R.; Rao, S.S.; Kong, W.-P.; Wang, L.; Nabel, G.J. Self-assembling influenza nanoparticle vaccines elicit broadly neutralizing H1N1 antibodies. *Nature* **2013**, *499*. [[CrossRef](#)] [[PubMed](#)]
163. Yassine, H.M.; Boyington, J.C.; McTamney, P.M.; Wei, C.-J.; Kanekiyo, M.; Kong, W.-P.; Gallagher, J.R.; Wang, L.; Zhang, Y.; Joyce, M.G.; et al. Hemagglutinin-stem nanoparticles generate heterosubtypic influenza protection. *Nat. Med.* **2015**, *21*. [[CrossRef](#)] [[PubMed](#)]
164. Nandwana, V.; Ryoo, S.R.; Kanthala, S.; Kumar, A.; Sharma, A.; Castro, F.C.; Li, Y.; Hoffman, B.; Lim, S.; Dravid, V.P. Engineered ferritin nanocages as natural contrast agents in magnetic resonance imaging. *RSC Adv.* **2017**, *7*, 34892–34900. [[CrossRef](#)]
165. Khoshnejad, M.; Greineder, C.F.; Pulsipher, K.W.; Villa, C.H.; Altun, B.; Pan, D.C.; Tsourkas, A.; Dmochowski, I.J.; Muzykantov, V.R. Ferritin nanocages with biologically orthogonal conjugation for vascular targeting and imaging. *Bioconjug. Chem.* **2018**, *29*, 1209–1218. [[CrossRef](#)] [[PubMed](#)]
166. Ensign, D.; Young, M.; Douglas, T. Photocatalytic synthesis of copper colloids from Cu(II) by the ferrihydrite core of ferritin. *Inorg. Chem.* **2004**, *43*, 3441–3446. [[CrossRef](#)] [[PubMed](#)]
167. Chiarpotto, M.; Ciasca, G.; Vassalli, M.; Rossi, C.; Campi, G.; Ricci, A.; Bocca, B.; Pino, A.; Alimonti, A.; Sole, P.D.; et al. Mechanism of aluminium bio-mineralization in the apoferritin cavity. *Appl. Phys. Lett.* **2013**, *103*. [[CrossRef](#)]
168. Han, J.-A.; Kang, Y.J.; Shin, C.; Ra, J.-S.; Shin, H.-H.; Hong, S.Y.; Do, Y.; Kang, S. Ferritin protein cage nanoparticles as versatile antigen delivery nanoplatforms for dendritic cell (DC)-based vaccine development. *Nanomed. Nanotechnol. Biol. Med.* **2014**, *10*, 561–569. [[CrossRef](#)] [[PubMed](#)]
169. Pontillo, N.; Pane, F.; Messori, L.; Amoresano, A.; Merlino, A. Cisplatin encapsulation within a ferritin nanocage: A high-resolution crystallographic study. *Chem. Commun.* **2016**, *52*, 4136–4139. [[CrossRef](#)] [[PubMed](#)]
170. Murata, M.; Narahara, S.; Kawano, T.; Hamano, N.; Piao, J.S.; Kang, J.-H.; Ohuchida, K.; Murakami, T.; Hashizume, M. Design and function of engineered protein nanocages as a drug delivery system for targeting pancreatic cancer cells via neuropilin-1. *Mol. Pharm.* **2015**, *12*, 1422–1430. [[CrossRef](#)] [[PubMed](#)]
171. Flenniken, M.L.; Willits, D.A.; Brumfield, S.; Young, M.J.; Douglas, T. The small heat shock protein cage from *Methanococcus jannaschii* is a versatile nanoscale platform for genetic and chemical modification. *Nano Lett.* **2003**, *3*, 1573–1576. [[CrossRef](#)]
172. Bova, M.P.; Huang, Q.; Ding, L.; Horwitz, J. Subunit exchange, conformational stability, and chaperone-like function of the small heat shock protein 16.5 from *Methanococcus jannaschii*. *J. Biol. Chem.* **2002**, *277*, 38468–38475. [[CrossRef](#)] [[PubMed](#)]

173. Hiriart, Y.; Rossi, A.H.; Biedma, M.E.; Errea, A.J.; Moreno, G.; Cayet, D.; Rinaldi, J.; Blanca, B.; Sirard, J.C.; Goldbaum, F.; et al. Characterization of structural and immunological properties of a fusion protein between flagellin from *Salmonella* and lumazine synthase from *Brucella*. *Protein Sci.* **2017**, *26*, 1049–1059. [[CrossRef](#)] [[PubMed](#)]
174. Yusuke, A.; Reinhard, Z.; Matthias, T.; Donald, H. Quantitative packaging of active enzymes into a protein cage. *Angew. Chem. Int. Ed.* **2016**, *55*, 1531–1534.
175. Song, Y.; Kang, Y.J.; Jung, H.; Kim, H.; Kang, S.; Cho, H. Lumazine synthase protein nanoparticle-Gd(III)-DOTA conjugate as a T1 contrast agent for high-field MRI. *Sci. Rep.* **2015**, *5*. [[CrossRef](#)] [[PubMed](#)]
176. Min, J.; Kim, S.; Lee, J.; Kang, S. Lumazine synthase protein cage nanoparticles as modular delivery platforms for targeted drug delivery. *RSC Adv.* **2014**, *4*, 48596–48600. [[CrossRef](#)]
177. Kim, H.; Kang, Y.J.; Min, J.; Choi, H.; Kang, S. Development of an antibody-binding modular nanopatform for antibody-guided targeted cell imaging and delivery. *RSC Adv.* **2016**, *6*, 19208–19213. [[CrossRef](#)]
178. Poderycki, M.J.; Kickhoefer, V.A.; Kaddis, C.S.; Raval-Fernandes, S.; Johansson, E.; Zink, J.I.; Loo, J.A.; Rome, L.H. The vault exterior shell is a dynamic structure that allows incorporation of vault-associated proteins into its interior. *Biochemistry* **2006**, *45*, 12184–12193. [[CrossRef](#)] [[PubMed](#)]
179. Kickhoefer, V.A.; Garcia, Y.; Mikyas, Y.; Johansson, E.; Zhou, J.C.; Raval-Fernandes, S.; Minoofar, P.; Zink, J.I.; Dunn, B.; Stewart, P.L.; et al. Engineering of vault nanocapsules with enzymatic and fluorescent properties. *Proc. Natl. Acad. Sci. USA* **2005**, *102*, 4348–4352. [[CrossRef](#)] [[PubMed](#)]
180. Zhu, Y.; Jiang, J.; Said-Sadier, N.; Boxx, G.; Champion, C.; Tetlow, A.; Kickhoefer, V.A.; Rome, L.H.; Ojcius, D.M.; Kelly, K.A. Activation of the NLRP3 inflammasome by vault nanoparticles expressing a chlamydial epitope. *Vaccine* **2015**, *33*, 298–306. [[CrossRef](#)] [[PubMed](#)]
181. Kar, U.K.; Srivastava, M.K.; Andersson, A.; Baratelli, F.; Huang, M.; Kickhoefer, V.A.; Dubinett, S.M.; Rome, L.H.; Sharma, S. Novel CCL21-vault nanocapsule intratumoral delivery inhibits lung cancer growth. *PLoS ONE* **2011**, *6*. [[CrossRef](#)] [[PubMed](#)]
182. Kar, U.K.; Jiang, J.; Champion, C.I.; Salehi, S.; Srivastava, M.; Sharma, S.; Rabizadeh, S.; Niazi, K.; Kickhoefer, V.; Rome, L.H.; et al. Vault nanocapsules as adjuvants favor cell-mediated over antibody-mediated immune responses following immunization of mice. *PLOS ONE* **2012**, *7*. [[CrossRef](#)] [[PubMed](#)]
183. Goldsmith, L.E.; Pupols, M.; Kickhoefer, V.A.; Rome, L.H.; Monbouquette, H.G. Utilization of a protein “shuttle” to load vault nanocapsules with gold probes and proteins. *ACS Nano* **2009**, *3*, 3175–3183. [[CrossRef](#)] [[PubMed](#)]
184. Buehler, D.C.; Marsden, M.D.; Shen, S.; Toso, D.B.; Wu, X.; Loo, J.A.; Zhou, Z.H.; Kickhoefer, V.A.; Wender, P.A.; Zack, J.A.; et al. Bioengineered vaults: Self-assembling protein shell-lipophilic core nanoparticles for drug delivery. *ACS Nano* **2014**, *8*, 7723–7732. [[CrossRef](#)] [[PubMed](#)]
185. Matsumoto, N.M.; Prabhakaran, P.; Rome, L.H.; Maynard, H.D. Smart vaults: Thermally-responsive protein nanocapsules. *ACS Nano* **2013**, *7*, 867–874. [[CrossRef](#)] [[PubMed](#)]
186. Kickhoefer, V.A.; Han, M.; Raval-Fernandes, S.; Poderycki, M.J.; Moniz, R.J.; Vaccari, D.; Silvestry, M.; Stewart, P.L.; Kelly, K.A.; Rome, L.H. Targeting vault nanoparticles to specific cell surface receptors. *ACS Nano* **2009**, *3*, 27–36. [[CrossRef](#)] [[PubMed](#)]
187. Wang, M.; Abad, D.; Kickhoefer, V.A.; Rome, L.H.; Mahendra, S. Vault nanoparticles packaged with enzymes as an efficient pollutant biodegradation technology. *ACS Nano* **2015**, *9*, 10931–10940. [[CrossRef](#)] [[PubMed](#)]
188. Putri, R.M.; Allende-Ballester, C.; Luque, D.; Klem, R.; Rousou, K.A.; Liu, A.; Traulsen, C.H.; Rurup, W.F.; Koay, M.S.T.; Caston, J.R.; et al. Structural characterization of native and modified encapsulins as nanoplatfoms for in vitro catalysis and cellular uptake. *ACS Nano* **2017**, *11*, 12796–12804. [[CrossRef](#)] [[PubMed](#)]
189. Champion, C.I.; Kickhoefer, V.A.; Liu, G.; Moniz, R.J.; Freed, A.S.; Bergmann, L.L.; Vaccari, D.; Raval-Fernandes, S.; Chan, A.M.; Rome, L.H.; et al. A vault nanoparticle vaccine induces protective mucosal immunity. *PLoS ONE* **2009**, *4*. [[CrossRef](#)] [[PubMed](#)]
190. Aumiller, W.M.; Uchida, M. Stimuli Responsive Hierarchical Assembly of P22 Virus-like Particles. *Chem. Mater.* **2018**, *30*, 2262–2273. [[CrossRef](#)]
191. Sánchez-Sánchez, L.; Tapia-Moreno, A. Design of a VLP-nanovehicle for CYP450 enzymatic activity delivery. *J. Nanobiotechnol.* **2015**, *13*, 66. [[CrossRef](#)] [[PubMed](#)]

192. Seebeck, F.P.; Woycechowsky, K.J.; Zhuang, W.; Rabe, J.P.; Hilvert, D. A simple tagging system for protein encapsulation. *J. Am. Chem. Soc.* **2006**, *128*, 4516–4517. [[CrossRef](#)] [[PubMed](#)]
193. Zakeri, B.; Fierer, J.O.; Celik, E.; Chittock, E.C.; Schwarz-Linek, U.; Moy, V.T.; Howarth, M. Peptide tag forming a rapid covalent bond to a protein, through engineering a bacterial adhesin. *Proc. Natl. Acad. Sci. USA* **2012**, *109*, E690–E697. [[CrossRef](#)] [[PubMed](#)]
194. Minten, I.J.; Hendriks, L.J.A.; Nolte, R.J.M.; Cornelissen, J.J.L.M. Controlled encapsulation of multiple proteins in virus capsids. *J. Am. Chem. Soc.* **2009**, *131*, 17771–17773. [[CrossRef](#)] [[PubMed](#)]
195. Seidel, S.R.; Stang, P.J. High-symmetry coordination cages via self-assembly. *Acc. Chem. Res.* **2002**, *35*, 972–983. [[CrossRef](#)] [[PubMed](#)]
196. Zhang, Y.; Orner, B.P. Self-assembly in the ferritin nano-cage protein superfamily. *Int. J. Mol. Sci.* **2011**, *12*, 5406–5421. [[CrossRef](#)] [[PubMed](#)]
197. Doyle, C.M.; Rumfeldt, J.A.; Broom, H.R.; Broom, A.; Stathopoulos, P.B.; Vassall, K.A.; Almey, J.J.; Meiering, E.M. Energetics of oligomeric protein folding and association. *Arch. Biochem. Biophys.* **2013**, *531*, 44–64. [[CrossRef](#)] [[PubMed](#)]
198. Kim, M.; Rho, Y.; Jin, K.S.; Ahn, B.; Jung, S.; Kim, H.; Ree, M. pH-dependent structures of ferritin and apoferritin in solution: Disassembly and reassembly. *Biomacromolecules* **2011**, *12*, 1629–1640. [[CrossRef](#)] [[PubMed](#)]
199. Sana, B.; Johnson, E.; Lim, S. The unique self-assembly/disassembly property of *Archaeoglobus fulgidus* ferritin and its implications on molecular release from the protein cage. *Biochim. Biophys. Acta* **2015**, *1850*, 2544–2551. [[CrossRef](#)] [[PubMed](#)]
200. Peng, T.; Lee, H.; Lim, S. Design of a reversible inversed pH-responsive caged protein. *Biomater. Sci.* **2015**, *3*, 627–635. [[CrossRef](#)] [[PubMed](#)]
201. Manchester, M.; Singh, P. Virus-based nanoparticles (VNPs): Platform technologies for diagnostic imaging. *Adv. Drug Deliv. Rev.* **2006**, *58*, 1505–1522. [[CrossRef](#)] [[PubMed](#)]
202. Kasper, R.; Patric, B.; Karolina, L.; Ozana, O.; Nico, B.; Wolfgang, M. Selective and responsive nanoreactors. *Adv. Funct. Mater.* **2011**, *21*, 1241–1259.
203. Yeates, T.O.; Padilla, J.E. Designing supramolecular protein assemblies. *Curr. Opin. Struct. Biol.* **2002**, *12*, 464–470. [[CrossRef](#)]
204. Heddle, J.G.; Chakraborti, S.; Iwasaki, K. Natural and artificial protein cages: Design, structure and therapeutic applications. *Curr. Opin. Struct. Biol.* **2017**, *43*, 148–155. [[CrossRef](#)] [[PubMed](#)]
205. Iglesias, E.; Garcia, D.; Aguilar, J.C. Parenteral delivery of the vaccine candidate TERA-VAC-HIV-1 bypasses pre-existing immune response to the hepatitis B virus antigens in mice. *Biotechnol. Appl.* **2015**, *32*, 2241–2244.
206. Oliveira, G.A.; Wetzel, K.; Calvo-Calle, J.M.; Nussenzweig, R.; Schmidt, A.; Birkett, A.; Dubovsky, F.; Tierney, E.; Gleiter, C.H.; Boehmer, G.; et al. Safety and enhanced immunogenicity of a hepatitis B core particle *Plasmodium falciparum* malaria vaccine formulated in adjuvant Montanide ISA 720 in a phase I trial. *Infect. Immun.* **2005**, *73*, 3587–3597. [[CrossRef](#)] [[PubMed](#)]
207. Yin, Y.; Li, H.; Wu, S.; Dong, D.; Zhang, J.; Fu, L.; Xu, J.; Chen, W. Hepatitis B virus core particles displaying *Mycobacterium tuberculosis* antigen ESAT-6 enhance ESAT-6-specific immune responses. *Vaccine* **2011**, *29*, 5645–5651. [[CrossRef](#)] [[PubMed](#)]
208. Chu, X.; Li, Y.; Long, Q.; Xia, Y.; Yao, Y.; Sun, W.; Huang, W.; Yang, X.; Liu, C.; Ma, Y. Chimeric HBcAg virus-like particles presenting a HPV 16 E7 epitope significantly suppressed tumor progression through preventive or therapeutic immunization in a TC-1-grafted mouse model. *Int. J. Nanomed.* **2016**, *11*, 2417–2429.
209. Arora, U.; Tyagi, P.; Swaminathan, S.; Khanna, N. Chimeric hepatitis B core antigen virus-like particles displaying the envelope domain III of dengue virus type 2. *J. Nanobiotechnol.* **2012**, *10*. [[CrossRef](#)] [[PubMed](#)]
210. Huang, X.; Wang, X.; Zhang, J.; Xia, N.; Zhao, Q. *Escherichia coli*-derived virus-like particles in vaccine development. *NPJ Vaccines* **2017**, *2*. [[CrossRef](#)] [[PubMed](#)]
211. Bae, Y.H.; Park, K. Targeted drug delivery to tumors: Myths, reality and possibility. *J. Control. Release* **2011**, *153*, 198–205. [[CrossRef](#)] [[PubMed](#)]
212. Sahandi Zangabad, P.; Karimi, M.; Mehdizadeh, F.; Malekzad, H.; Ghasemi, A.; Bahrami, S.; Zare, H.; Moghooei, M.; Hekmatmanesh, A.; Hamblin, M.R. Nanocaged platforms: Modification, drug delivery and nanotoxicity. Opening synthetic cages to release the tiger. *Nanoscale* **2017**, *9*, 1356–1392. [[CrossRef](#)] [[PubMed](#)]
213. Singh, R.; Lillard, J.W. Nanoparticle-based targeted drug delivery. *Exp. Mol. Pathol.* **2009**, *86*, 215–223. [[CrossRef](#)] [[PubMed](#)]

214. Bertrand, N.; Wu, J.; Xu, X.; Kamaly, N.; Farokhzad, O.C. Cancer nanotechnology: The impact of passive and active targeting in the era of modern cancer biology. *Adv. Drug Deliv. Rev.* **2014**, *66*, 2–25. [[CrossRef](#)] [[PubMed](#)]
215. Van Kan-Davelaar, H.E.; van Hest, J.C.M.; Cornelissen, J.J.L.M.; Koay, M.S.T. Using viruses as nanomedicines. *Br. J. Pharmacol.* **2014**, *171*, 4001–4009. [[CrossRef](#)] [[PubMed](#)]
216. Rupaimoole, R.; Calin, G.A.; Lopez-Berestein, G.; Sood, A.K. miRNA deregulation in cancer cells and the tumor microenvironment. *Cancer Discov* **2016**, *6*, 235–246. [[CrossRef](#)] [[PubMed](#)]
217. Yao, Y.; Jia, T.; Pan, Y.; Gou, H.; Li, Y.; Sun, Y.; Zhang, R.; Zhang, K.; Lin, G.; Xie, J.; et al. Using a novel microRNA delivery system to inhibit osteoclastogenesis. *Int. J. Mol. Sci.* **2015**, *16*, 8337–8350. [[CrossRef](#)] [[PubMed](#)]
218. Vuralhan, Z.; Luttkik, M.A.; Tai, S.L.; Boer, V.M.; Morais, M.A.; Schipper, D.; Almering, M.J.; Kötter, P.; Dickinson, J.R.; Daran, J.-M. Physiological characterization of the ARO10-dependent, broad-substrate-specificity 2-oxo acid decarboxylase activity of *Saccharomyces cerevisiae*. *Appl. Environ. Microbiol.* **2005**, *71*, 3276–3284. [[CrossRef](#)] [[PubMed](#)]
219. Liscombe, D.K.; Macleod, B.P.; Loukanina, N.; Nandi, O.I.; Facchini, P.J. Evidence for the monophyletic evolution of benzyloquinoline alkaloid biosynthesis in angiosperms. *Phytochemistry* **2005**, *66*, 1374–1393. [[CrossRef](#)] [[PubMed](#)]
220. Hagel, J.M.; Facchini, P.J. Benzyloquinoline alkaloid metabolism: A century of discovery and a brave new world. *Plant Cell Physiol.* **2013**, *54*, 647–672. [[CrossRef](#)] [[PubMed](#)]
221. Aranda, A.; del Olmo, M.-L. Exposure of *Saccharomyces cerevisiae* to acetaldehyde induces sulfur amino acid metabolism and polyamine transporter genes, which depend on Met4p and Haa1p transcription factors, respectively. *Appl. Environ. Microbiol.* **2004**, *70*, 1913–1922. [[CrossRef](#)] [[PubMed](#)]
222. Kunjapur, A.M.; Prather, K.L.J. Microbial engineering for aldehyde synthesis. *Appl. Environ. Microbiol.* **2015**, *81*, 1892–1901. [[CrossRef](#)] [[PubMed](#)]
223. Hartley, A.; Glynn, S.E.; Barynin, V.; Baker, P.J.; Sedelnikova, S.E.; Verhees, C.; de Geus, D.; van der Oost, J.; Timson, D.J.; Reece, R.J.; et al. Substrate specificity and mechanism from the structure of *Pyrococcus furiosus* galactokinase. *J. Mol. Biol.* **2004**, *337*, 387–398. [[CrossRef](#)] [[PubMed](#)]
224. Kengen, S.W.; Tuininga, J.E.; de Bok, F.A.; Stams, A.J.; de Vos, W.M. Purification and characterization of a novel ADP-dependent glucokinase from the hyperthermophilic archaeon *Pyrococcus furiosus*. *J. Biol. Chem.* **1995**, *270*, 30453–30457. [[CrossRef](#)] [[PubMed](#)]
225. Kuznetsova, I.M.; Turoverov, K.K.; Uversky, V.N. What macromolecular crowding can do to a protein. *Int. J. Mol. Sci.* **2014**, *15*, 23090–23140. [[CrossRef](#)] [[PubMed](#)]
226. Royo, J.L.; Moreno-Ruiz, E.; Cebolla, A.; Santero, E. Stable long-term indigo production by overexpression of dioxygenase genes using a chromosomal integrated cascade expression circuit. *J. Biotechnol.* **2005**, *116*, 113–124. [[CrossRef](#)] [[PubMed](#)]
227. Choi, H.S.; Kim, J.K.; Cho, E.H.; Kim, Y.C.; Kim, J.I.; Kim, S.W. A novel flavin-containing monooxygenase from *Methylophaga* sp. strain SK1 and its indigo synthesis in *Escherichia coli*. *Biochem. Biophys. Res. Commun.* **2003**, *306*, 930–936. [[CrossRef](#)]



© 2018 by the authors. Licensee MDPI, Basel, Switzerland. This article is an open access article distributed under the terms and conditions of the Creative Commons Attribution (CC BY) license (<http://creativecommons.org/licenses/by/4.0/>).

2

**Reprogramming encapsulin into
a light-activatable nanoreactor
for the “on demand” generation
of reactive oxygen species**

Introduction

In Chapter 1, I highlighted and discussed the engineerability of self-assembling protein-based nanoparticles, including encapsulin nanocompartments. In recent years, encapsulins have attracted the attention of synthetic biologists due to their high modularity and programmability. In Chapter 2, I aimed to take advantage of encapsulin's unique protein encapsulation system to bioengineer a light-activatable nanoreactor that generates reactive oxygen species (ROS) that can trigger photosensitizations reactions.

The results reported in this chapter have been prepared as a manuscript for submission to *Nature Communications*.

Contributions to manuscript 1

The concept of this publication was developed in partnership with my supervisors Anwar Sunna and Andrew Care. They were also involved in designing experiments and troubleshooting. I performed all the experimental work and data analysis. Febrina Sandra supported tissue culture experiments. Xavier Vidal constructed the laser set-up and supported laser irradiation experiments. The initial draft of the manuscript was prepared by me.

Table 2-1 Author contribution summary for Manuscript 1.

	Dennis Diaz	Febrina Sandra	Xavier Vidal	Anwar Sunna	Andrew Care
Experiment Design	•			•	•
Data Collection	•	•	•		
Data Analysis	•				
Manuscript	•			•	•

Reprogramming encapsulin into a light-activatable nanoreactor for the “on demand” generation of reactive oxygen species

Dennis Diaz¹, Febrina Sandra¹, Xavier Vidal², Anwar Sunna^{1,3} & Andrew Care^{1,3}*

¹Department of Molecular Sciences, Macquarie University, NSW 2109, Australia

²Department of Physics and Astronomy, Macquarie University, NSW 2109, Australia

³Australian Research Council Centre of Excellence for Nanoscale BioPhotonics, Macquarie University, NSW 2109, Australia.

* Corresponding author: Andrew Care
Department of Molecular Sciences
Macquarie University
Sydney, NSW 2109
Australia

Phone: +61 2 9850 4220
Fax: +61 2 9850 8313
Email: andrew.care@mq.edu.au

Abstract

Encapsulins are a novel class of protein nanocompartments found in prokaryotes. There is a growing interest in reprogramming encapsulins to function as customizable ‘nanoreactors’ for the enhancement or creation of biological reactions. Herein, we reprogrammed encapsulins into light-activatable nanoreactors for the ‘on demand’ production of reactive oxygen species (ROS). To achieve this, two variants of the green fluorescent flavoprotein mini-Single Oxygen Generator (mSOG), mSOG1 and mSOG2 were loaded into *Thermotoga maritima* encapsulin nanocompartments. mSOG is a biological photosensitizer that generates ROS, primarily singlet oxygen ($^1\text{O}_2$), upon blue light irradiation. mSOG-loaded encapsulins permitted the “on demand” production of $^1\text{O}_2$ upon light-activation. Subsequently, these ROS-generating nanoreactors were shown to trigger photosensitized oxidation reactions that exerted a phototoxic effect against lung cancer cells. Thus, we anticipate that these light-activatable nanoreactors can be utilized to precisely initiate and/or modulate ROS-sensitive processes that have technological, biological and therapeutic relevance.

Keywords

Nanocompartment, Encapsulin, miniSOG, Synthetic biology, Photodynamic therapy, Biocatalysis, Nanoreactors, Protein-based organelle, Synthetic organelles

Introduction

Compartmentalization is a key structural feature inside living cells that permits the spatial organization and optimization of metabolic and physiological processes ¹. While eukaryotes mainly use membrane-bound organelles to realize subcellular organization, prokaryotes instead employ organelle-like compartments composed entirely of proteins ². These protein compartments encase enzymes within a selectively permeable protein shell that self-assembles from multiple protein subunits ^{3, 4}. This design isolates and promotes specialized reactions by placing enzymes, their substrates and cofactors within close proximity of each other; regulating the influx and efflux of molecules; preventing the escape of volatile or toxic reaction intermediates; and creating distinct microenvironments that can improve enzyme function ⁵. Well-known examples include bacterial microcompartments like carboxysomes, which package carbonic anhydrase and Ribulose-1,5-bisphosphate carboxylase/oxygenase (RuBisCo) enhance carbon dioxide fixation in cyanobacteria ⁶⁻⁸.

Encapsulins are a newly established class of prokaryotic protein nanocompartments ⁹. A recent bioinformatics study identified over 900 encapsulin systems in known archaeal and bacterial genomes ¹⁰. Giessen et al. defines an encapsulin system as a core operon that encodes both an encapsulin shell protein and a core cargo protein ⁹. These core cargo protein-types include ferritin-like proteins (FLPs), iron-mineralizing encapsulin-associated Firmicute cargo, Dye-decolorizing peroxidases DyP-type peroxidases, hemerythrins, and the fusion protein nitrite reductase like-hydroxylamine oxidoreductase. Based on the function of these cargoes, encapsulin systems are thought to act as protein-based organelles that help their microbial hosts to maintain iron homeostasis, cope with oxidative and nitrosative stress, and safely derive energy from ammonium ⁹⁻¹¹.

In the era of synthetic biology, encapsulins represent a set of highly modular tools that can be readily engineered to have immense utility. Encapsulins precisely self-assemble from identical subunit proteins into robust icosahedral protein shells with a triangulation number (T) $T = 1$ (60 subunits, 20–24 nm), $T = 3$ (180 subunits, 30–32 nm) or $T = 4$ (240 subunits, 43 nm) ¹²⁻¹⁵. Surface pores (3–10 Å in diameter) control the channelling of small molecules in and out of the protein shell, allowing interactions with any encapsulated cargo ^{12, 15-17}. A distinctive aspect of encapsulins,

is their ability to selectively package cargo proteins that display a short encapsulation signal peptide (ESig) on either terminus ^{9, 12, 18}.

There is consequently an increasing interest in reprogramming encapsulins to serve as customizable ‘nanoreactors’, which augment or enhance existing biological reactions, or enable the creation of new synthetic reactions^{15, 19, 20}. Efforts to realize these objectives have used ESig-tagged proteins with non-native functions to produce synthetic nanoreactors and organelles. For instance, encapsulin has been modified to protect and stabilize the production of a precursor for opioids and has been transformed to mimic the function of a melanosome^{19, 20}. Here in, we utilized encapsulin’s unique encapsulation and substrate channelling mechanisms along with their high genetic adaptability, to reprogram encapsulin from a natural oxidative stress protector to a reactive oxygen species (ROS)-producing protein nanocompartment.

The green fluorescent flavin-binding protein mini Singlet Oxygen Generator (mSOG) is a biological photosensitizer, which produces singlet oxygen ($^1\text{O}_2$) and ROS upon excitation with blue light in a process called photosensitization ²¹. miniSOG1 (mSOG1) was originally developed from the blue-light responsive light-oxygen-voltage (LOV2) domain of *Arabidopsis* phototropin ²². Further protein engineering yielded a mSOG1 variant called miniSOG2 (mSOG2), which is about four times more effective at generating ROS than mSOG1 ²³. These photosensitizing proteins initiate two light induced reaction types to generate ROS. Type I, wherein the photosensitizer donates its electron to molecular oxygen (O_2), driving the generation of superoxide-anion (O_2^-) and other radical species; and Type II, wherein the photosensitizer transfers energy to O_2 , triggering the transition from its stable triplet state to its reactive singlet state ($^1\text{O}_2$) ^{24, 25}. mSOGs mainly produce $^1\text{O}_2$ via the Type II photoreaction, which transfers energy from their bound flavin mononucleotide (FMN) chromophore to O_2 .

$^1\text{O}_2$ is a highly reactive compound that readily oxidizes molecules near its site of production. Consequently, the ability of light-activated mSOG to generate $^1\text{O}_2$ has been exploited in a diverse range of applications ²⁶. Examples include the photooxidation of contrast agents in bioimaging (e.g. diaminobenzidine, DAB), photoredox activation of metal-based prodrugs, photomodulation of ROS-activated

pathways, chromophore-assisted light inactivation of proteins in optogenetics, and photoinduced ablation of cells and tissue in photodynamic therapy (PDT) ^{23, 27-32}.

In this communication, we show for the first time the encapsulation of ESig-tagged mSOG variants inside encapsulin nanocompartments, reprogramming them to serve as light-activatable nanoreactors for the “on demand” generation of ROS. The effect of encapsulation on mSOG function and the impact of ROS generation on the nanocompartments’ structure and stability was examined. Using an *in vitro* model of lung cancer, the ROS produced by a light-activated nanoreactor was shown to be sufficient to trigger photosensitized oxidation reactions that exert a phototoxic effect on cancer cells. While preliminary, our results show that the ROS-producing encapsulin nanoreactors could be further developed as a nanoplatform for PDT of cancer.

Materials and methods

Materials

All chemicals and reagents used in this study were purchased from Sigma-Aldrich unless stated otherwise.

Molecular biology and cloning

All inserts were codon optimized for expression in *Escherichia coli* and custom synthesized as gBlock Gene Fragments (Integrated DNA Technologies). A surface-exposed loop region between residues 138 and 139 of the encapsulin from *Thermotoga maritima* (Uniprot: Q9WZP3) was modified with a hexahistidine tag (GGGGGGHHHHHHGGGGGG) as previously described ³³. To selectively encapsulate the mSOG1 ²² or mSOG2 ²³ cargo within his-tagged encapsulin (Enc), both photosensitizing proteins were C-terminally tagged with either a native full-length encapsulation signal (LFTDKPITEIEEETSGGSENTGGDLGIRKL) (ESig) or a previously reported functional truncated form (GGSENTGGDLGIRKL) (ESig_T) ³⁴. To generate expression vectors, Enc was ligated into pETDuet-1 (Merck) via NcoI/BamHI restriction sites, while all mSOG constructions were inserted into pACYC-Duet-1 (Merck) via NdeI/BglII restriction sites. *E. coli* α -Select (Bioline) was used as a host for general gene cloning. Gene insertion was verified by performing

PCR using the primers pairs pETUpstream/DuetDOWN or DuetUP2/T7 Terminator (Merck) with Enc or mSOG-containing plasmid constructions, respectively. All gene constructions used in this study are summarized in Table S1. *E. coli* BL21 (DE3) cells (New England Biolabs) were used for recombinant protein expression. For the co-expression of Enc and its intended cargo protein, cells were co-transformed with the appropriate expression plasmids, and the resulting transformants were selected on Luria–Bertani (LB) agar supplemented with carbenicillin (100 µg/ml) and chloramphenicol (50 µg/ml) (see Table S2).

Protein expression and purification

Protein expression (or co-expression) experiments were carried out in LB medium supplemented with carbenicillin (100 µg/ml), chloramphenicol (50 µg/ml) or both. Briefly, 500 ml LB (1:100) was inoculated with an overnight culture of cells harboring the expression plasmid(s) of interest, grown aerobically at 37 °C to an optical density at 600 nm (OD_{600}) of 0.5-0.8 and induced by the addition of isopropyl- β -D-thiogalactopyranoside (IPTG). The optimized conditions for the recombinant expression of all proteins in this study are outlined in Table S2. Finally, cells were harvested by centrifugation (10,000 x *g* 15 min, 4 °C) and stored at -30 °C.

For the purification of Enc and mSOG-loaded Enc (Enc-mSOG) variants, the pellet from a 500 mL culture was resuspended in 50 mL lysis buffer (20 mM NaH_2PO_4 , 300 mM NaCl, 40 mM imidazole, 1 U/mL Benzonase® nuclease, pH 7.4). Cells were lysed with three rounds of French press and subsequently centrifuged at 10,000 x *g* for 15 min. The lysate was purified by nickel-immobilized metal affinity chromatography (IMAC) using a HisPrep™ Fast Flow 16/10 column (GE Healthcare, USA) in equilibration buffer (20 mM NaH_2PO_4 , 300 mM NaCl, 40 mM imidazole, pH 7.4). Enc eluted at 400 mM imidazole while Enc-mSOG variants eluted at 260 mM imidazole. Next, the eluted fractions were concentrated using Amicon® Ultra-15 centrifugal filter units (Merck, USA) with a 100 KDa cut-off, followed by dilution in 7 mL of 50 mM HEPES buffer pH 7.4 (Chem-Supply Pty, Australia). A second purification step by size exclusion chromatography (SEC) was subsequently performed using a HiPrep™ 26/60 Sephacryl® S-500 HR column (GE Healthcare, USA) in 100 mM HEPES Buffer. All purifications were carried out on an Äkta™ start or Äkta™ pure chromatography system (GE Healthcare, USA).

For the purification of free mSOG1-ESig_T, the unbound fraction obtained during the IMAC purification of Enc-mSOG1-ESig_T was used. Herein, a saturated solution of ammonium sulphate was added to a final concentration of 30% (v/v), incubated on ice for 30 min and spun down at 10,000 x *g* for 15 min. Next, ammonium sulphate was added to the supernatant to a final concentration of 50% (v/v) and precipitation occurred under the conditions detailed above. The precipitated protein was resuspended in 100 mM HEPES buffer (pH 7.4) and subjected to SEC using a HiPrep™ 16/60 Sephacryl® S-400 column (GE Healthcare, USA). The fractions containing free mSOG1-ESig_T were pooled and concentrated using Amicon Ultra-15 centrifugal filter units with a 10 KDa cut-off. The final protein concentration concentrations were determined by measuring absorbance at 280 nm. Examples of purification chromatographs are provided in Supplementary Fig. 1.

Polyacrylamide gel electrophoresis (PAGE)

The Bio-Rad mini-protean system (Bio-Rad laboratories) was used for all SDS-PAGE and Native-PAGE analysis. For SDS-PAGE, samples were diluted in 2X Laemmli sample buffer with 50 mM 1,4-dithiothreitol, heated at 95 °C for 5 min, loaded into pre-cast Bio-Rad Mini-PROTEAN® TGX™ gels (4-15 %) and run at 200V for 30 min. For Native-PAGE, samples were diluted in 4X native sample buffer (200 mM Tris-HCl pH 6.8, 40% glycerol, and 0.08% bromophenol blue), loaded into pre-cast Bio-Rad Mini-PROTEAN® TGX™ gels (4-20%) and run at 200 V for a minimum of 2 h. In-gel fluorescence of proteins was observed with a gel documentation imager (Bio-Rad laboratories). All gels were stained following the Coomassie G-250 safe stain protocol ³⁵. The densitometric intensity of protein bands was quantified using ImageJ software (NIH) ³⁶.

Transmission electron microscopy (TEM)

10 µL of Enc or Enc-mSOG variant (~100 µg/ml) was adsorbed onto formvar-carbon coated copper grids for 2 min and negatively stained with uranyl acetate replacement stain (UAR-EMS) for 1 hour. Grids were then washed with ultrapure water and allowed to dry for 15 min. Finally, the grids were observed under a Philips CM10 TEM operated at 100 kV accelerating voltage.

Dynamic light scattering (DLS)

DLS data was collected on a Malvern Nano ZS90 Zetasizer. Measurements were performed at room temperature using standard cuvettes containing 1 ml of Enc or Enc-mSOG variants were diluted in 100 mM HEPES (pH 7.4) to a final concentration 0.2-0.4 mg/ml. The signal was averaged over 13 readings each lasting 30 s.

Absorbance and fluorescence spectrometry

The fluorescence excitation and emission spectra (480/520nm) of free and encapsulated mSOG were obtained on a Cary Eclipse Fluorescence Spectrophotometer (Agilent Technologies) or Fluorolog® (Horiba) using quartz cuvettes. The 280 nm absorbance for protein concentration measurements was acquired on a SPECTROstar® Nano Plate Reader (BMG Labtech) using UV transparent 96-well plates.

Singlet oxygen detection

Singlet oxygen generation from free mSOG1-ESig_T, Enc-mSOG variants, and unloaded Enc was detected in solution with the fluorescent probe Singlet Oxygen Sensor Green (SOSG) according to the manufacturer's protocol (Invitrogen). The reaction mixture contained: ~40 µg/ml of protein samples (in 100 mM HEPES buffer pH 7.5), 1 µM SOSG, and 50% deuterium oxide (D₂O). Reaction mixtures were irradiated with a Chameleon-Ultra II laser (Coherent) set at 450 nm (for mSOG1 variants) or 420 nm (for mSOG2 variants) with a power density of 55 mW/cm² for 5 min. For further characterization of the variant with the highest ¹O₂ production other irradiation times were evaluated (0, 10, 15 and 20 min). Fluorescence signals from the oxidized SOSG (excitation/emission = 485/520 nm) were measured on a PHERAstart FS (BMG Labtech) microplate reader.

In vitro cytotoxicity and phototoxicity studies

In phototoxicity studies, 5.0 x10³ A549 cells per well were seeded into 96-well microplates and cultured at 37 °C for 24h. First, the effect of laser irradiation on cell viability was investigated by exposing cells to a 450 nm blue laser at a power density of 55 mW/cm² for different time periods (0, 5, 10 and 15 min). To evaluate the cytotoxicity of free and encapsulated mSOG1-ESig_T in the absence of light activation, cells were incubated with 500 nM of free mSOG1-ESig_T or Enc-mSOG1-

ESig_T (normalized to mSOG-ESig_T content) at 37 °C in the dark for 2, 4, 8 and 12 h. After being subjected to either treatment, cells were washed once with PBS to remove non-internalized protein and fresh growth medium added. Next cell were cultivated for a further 48 h and cell viability was then determined using the 3-(4,5-dimethylthiazol-2-yl)-2,5-diphenyltetrazolium bromide (MTT) cell viability assay (Invitrogen) according to the manufacturer's protocol³⁷. In phototoxicity studies, the same protocol described for cytotoxicity was performed with minor changes. Briefly, after A549 cells were treated with free or encapsulated mSOG-ESig_T for different times (2, 4, 8 and 12 h) and medium was replaced with PBS, cells were irradiated with a 450 nm blue laser at 55 mW/cm² for 10 min. Next, fresh media was added to the cells, followed by cultivation for another 48 h in the dark. Cell viability was subsequently measured by MTT assay. For each experiment at least three technical replicates were performed.

Results

Reprogramming an encapsulin nanocompartment into a light-activatable nanoreactor

With the aim of bioengineering a light-activatable nanoreactor for the production of reactive oxygen species (ROS), we elected to reprogram the encapsulin (Enc) from *Thermotoga maritima* (*Tm*) by encapsulating the mini-Singlet Oxygen Generating proteins, mSOG1 and mSOG2. To direct their selective encapsulation inside encapsulin, mSOG1 and mSOG2 were each C-terminally tagged with the *Tm* encapsulation signal (ESig)³⁴. The *Tm* ESig is 30 amino acids (aa) long and can be minimized to a 15 aa truncated form (ESig_T) without loss of its packaging function³⁴. Thus, to assess the effect *Tm* ESig length has on cargo loading, ESig and ESig_T were appended to mSOG1 and mSOG2, yielding four different mSOG variants for packaging inside Enc (Fig 1a). The resulting mSOG-loaded encapsulins (Enc-mSOGs) will be referred to in this manuscript as: Enc-mSOG1-ESig_T; Enc-mSOG1-ESig; Enc-mSOG2-ESig_T; and Enc-mSOG2-ESig.

For the heterologous production of Enc-mSOGs in *E. coli*, each mSOG variant cargo was co-expressed with a His-tagged Enc (Fig. 1b). Following their purification by IMAC and SEC, all Enc-mSOGs underwent biophysical characterization (Fig 1c-e).

SDS-PAGE confirmed the co-purification of Enc (Enc_{subunit}; 31.9 kDa) and mSOG cargo tagged with ESig (mSOG1-ESig or mSOG2-ESig; ~15.9 kDa) or ESig_T (mSOG1-ESig_T or mSOG2-ESig_T; ~14.4 kDa) (Fig. 1c, upper panel). Under native-PAGE conditions, high molecular weight bands were observed, consistent with the self-assembly of encapsulin nanocompartments. Enc-mSOGs showed bands at similar positions to the empty Enc (Fig. 1c, middle panel). The blue-light excitation of mSOG proteins inside Enc-mSOGs was detected via fluorescence imaging of the native-PAGE, with no fluorescence observed from empty Enc (Fig. 1c, lower panel). In order to confirm the correct self-assembly, morphology and size of the mSOG-loaded nanocompartments, TEM observations and DLS measurements were performed. TEM images of negatively stained samples showed the correct formation of Enc-mSOGs and empty Enc into spherical nanocompartments (Fig. 1d and Supplementary Fig. 2). DLS measurement of empty Enc revealed a mean hydrodynamic diameter of 30.5 ± 10.8 nm (Supplementary Fig. 2), which was expected to be ~24 nm based on the crystal structure of *Tm* encapsulin (Protein database ID: 3DKT)³⁴. This observed enlargement is likely due to the insertion and display of his-tags on the Enc's external surface. This would align with research by Moon et al, who observed an enlargement of *Tm* encapsulin to 29.1 nm after introducing cancer-targeting peptides into the same 138-139 loop region³³. Moreover, DLS determined that all Enc-mSOGs were intact and monodisperse with mean diameters between 22-34 nm (Fig. 1d), lying within the measured size distribution of empty Enc. Additionally, the fluorescence emission spectra of Enc-mSOGs were examined by spectroscopy, with mSOG1 variants (free and encapsulated) exhibiting emission maxima (Em_{max}) at ~495 with a shoulder at ~525 nm, while mSOG2 variants (free and encapsulated) displayed Em_{max} at ~491 nm only (Supplementary Fig. 3).

The cargo loading capacity (LC%) and the number of cargo molecules per nanocompartment was estimated by protein gel densitometric analysis (Fig. 1e). ESig truncation showed no observable effect on its cargo loading function. However, despite having almost identical molecular sizes and protein sequences, the mSOG1 and mSOG2 cargo showed significantly different loading efficiencies. The estimated LC% for nanocompartments loaded with mSOG1 variants was 7-9 (mSOG1-ESig: 12 ± 7 molecules; mSOG1-ESig_T: 7 ± 2 molecules); while the LC% for those loaded

with mSOG2 variants were 24-34 (mSOG2-ESig: 40 ± 3 molecules; mSOG2-ESig_T: 71 ± 15 molecules). This represents a ~30% variation between the Enc-mSOGs with the lowest (Enc-mSOG1-ESig_T) and highest (Enc-mSOG2-ESig_T) LC%, which also equates to a ~10-fold difference in the number of cargo molecules per nanocompartment.

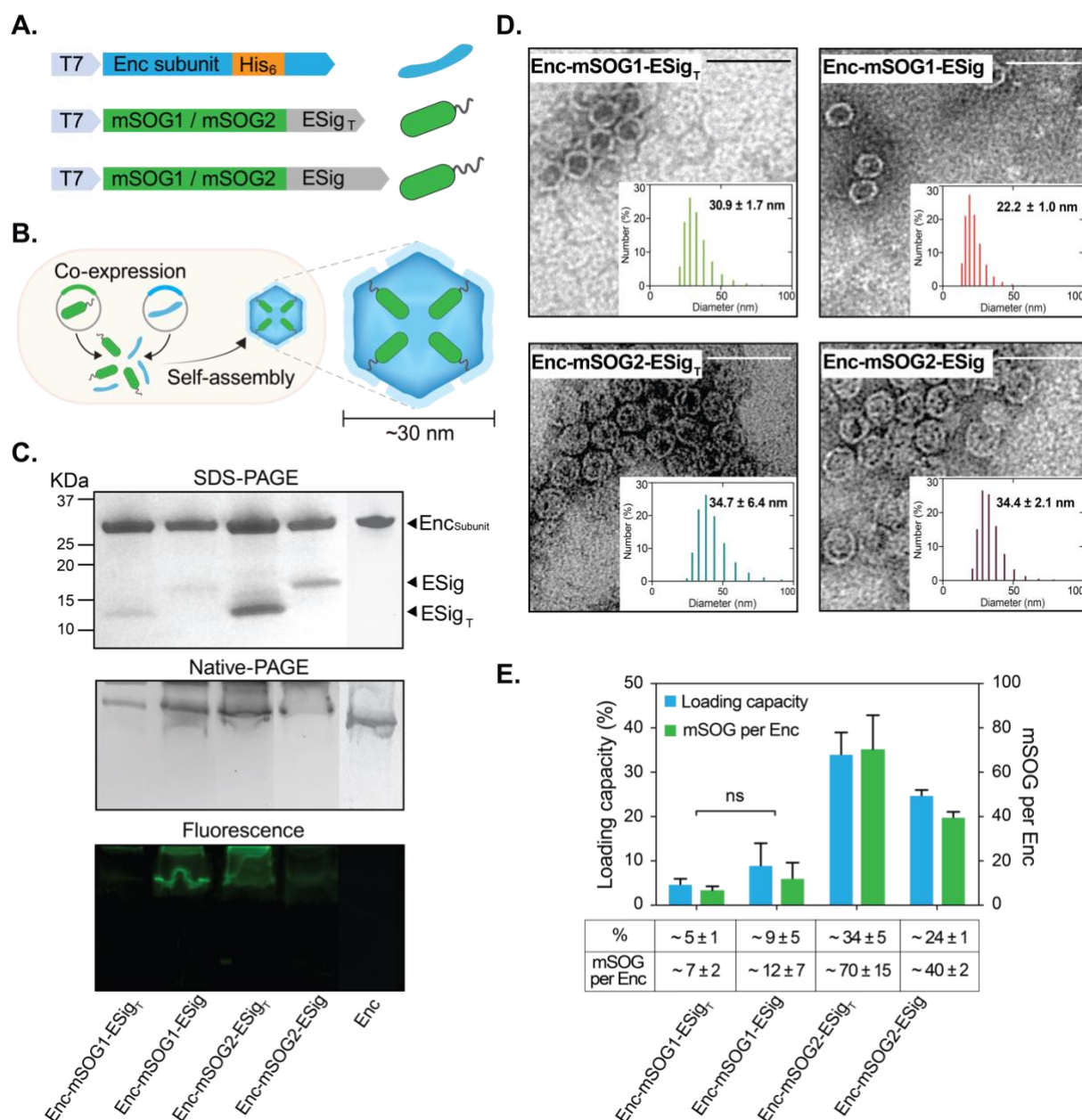


Fig. 1. Design, production and biophysical characterization of mSOG-loaded encapsulins (Enc-mSOGs). **A.** Genetic constructions encoding the Enc subunit from *Thermotoga maritima* (blue) displaying a His-tag within a surface-exposed loop region (yellow); and mSOG1 and mSOG2 cargo proteins (green) C-terminally tagged with a truncated (ESig_T) or native full-length (ESig) encapsulation signal (grey). **B.** Heterologous co-expression of encapsulin subunits and ESig-tagged cargo proteins in *E. coli* leads to the *in vivo* self-assembly of cargo-loaded *T. maritima* encapsulin T=1 nanocompartments. **C.** Gel analysis of Enc-mSOGs purified by sequential IMAC and SEC.

(Upper panel) Coomassie-stained SDS-PAGE showing the co-purification of the Enc subunit (31.9 KDa) and mSOG cargo proteins (tagged with ESig: 15.9 KDa or ESig τ : 14.4 KDa). **(Middle panel)** Coomassie-stained Native-PAGE verifying the self-assembly of Enc-mSOGs into cargo-loaded nanocompartments. **(Lower panel)** The in-gel fluorescence of the same Native-PAGE confirming the encapsulation of fluorescent mSOG variant cargo. **D.** TEM images of Enc-mSOGs show their self-assembly into spherical nanocompartments (Scale bars = 50 nm), while their respective size distributions measured by DLS (inset) indicate that their diameters range between ~22 and 34 nm. **E.** The average number of mSOG cargo molecules loaded each Enc (mSOG per Enc) and the corresponding loading capacity (%) was calculated for each of the Enc-mSOGs by performing densitometric analysis on SDS-PAGE gels. Error bars represent the mean \pm standard deviation, $n \geq 3$. ($p \leq 0.03$), one-way ANOVA, Tukey, $n \geq 3$. All sample comparisons showed significant differences except for those highlighted as 'ns' (non-significant).

“On demand” generation of singlet oxygen by light-activated Enc-mSOG nanoreactors

Encapsulin nanocompartments are naturally occurring catalytic nanoreactors, which package enzymes and use 3 – 10 Å sized surface pores to regulate the flow of small molecule substrates and products in and out of their internal cavities^{15, 18}. As depicted in Figure 2a, we hypothesized that molecular oxygen (O_2) can be channeled through the open surface pores of Enc-mSOGs, enabling its interaction with the mSOG cargo within. Enc-mSOGs can then be activated “on demand” with blue light to photoconvert O_2 into 1O_2 . The resulting 1O_2 subsequently exits Enc-mSOGs via their surface pores, allowing it to react with nearby molecules in a process called ‘photosensitization’.

To test this hypothesis, the capacity for light-activated Enc-mSOGs to generate 1O_2 in solution was measured using a Singlet Oxygen Sensor Green (SOSG) reagent. SOSG is selectively oxidized by 1O_2 to emit green fluorescence at 525 nm, the intensity of which is relative to the quantity of 1O_2 produced. Enc-mSOGs were mixed with SOSG (in deuterated-HEPES buffer), irradiated each sample with a blue laser for 5 min (mSOG1 450 nm; mSOG2 420 nm), and their fluorescence intensity measured at 525 nm. Figure 2b shows that the relative amount of 1O_2 generated by mSOG1-loaded nanocompartments was significantly greater than the background levels produced by empty Enc. In contrast, the 1O_2 production levels of mSOG2-loaded nanocompartments were only slightly higher than empty Enc. This result was unexpected because the mSOG2-loaded nanocompartments possessed the highest cargo loading capacities (Fig. 1e) and mSOG2 is also known to generate 1O_2 more efficiently than its mSOG1 counterpart. Of all the Enc-mSOGs tested, Enc-

mSOG1-ESig τ was found to be the most effective $^1\text{O}_2$ generator. Its $^1\text{O}_2$ production levels were 1.7-fold greater than the other mSOG1-loaded nanocompartment (Enc-mSOG1-ESig), up to 2.5-fold better than the mSOG2-loaded nanocompartments and almost 5-fold higher than empty Enc. Surprisingly, Enc-mSOG1-ESig τ was the best $^1\text{O}_2$ producer despite having the lowest cargo loading capacity (Fig. 1e). This superior functionality may be the result of minimal molecular crowding inside the nanocompartment, which enhances substrate diffusion and conversion.

To better understand Enc-mSOG1-ESig τ 's ability to efficiently generate $^1\text{O}_2$, the effect encapsulation had on the properties and functions of its mSOG1-ESig τ cargo was investigated. mSOG-ESig τ 's fluorescence excitation/emission spectra became weaker and noisier upon encapsulation (Supplementary Fig. 4), which also coincided with an 87% reduction in its fluorescence intensity (Fig 2c). Next, the $^1\text{O}_2$ generated by free mSOG-ESig τ and Enc-mSOG1-ESig τ were compared after different irradiation time periods (0, 5, 10, 15, 20 min) (Fig. 2d). Following 20 min laser irradiation, the free and encapsulated forms of mSOG1-ESig τ produced similar amounts of $^1\text{O}_2$ (Fig. 2d), indicating that the encapsulation of mSOG1-ESig τ and its subsequent loss of fluorescence intensity (Fig. 2c) had no significant adverse effect on its $^1\text{O}_2$ -generating function. Enc-mSOG1-ESig τ generated $^1\text{O}_2$ more efficiently than free mSOG1-ESig τ when it was exposed to laser irradiation for 5-15 min durations. After 10 min of laser excitation, Enc-mSOG1-ESig τ was shown to photoconvert O_2 to $^1\text{O}_2$ at a significantly faster rate (0.617 NFU/min) than free mSOG1-ESig τ (0.396 NFU/min), showcasing a 56% enhancement in mSOG1-ESig τ 's $^1\text{O}_2$ -generating efficiency. This outcome suggests that the confinement of mSOG1-ESig τ within the encapsulin nanocompartment may enhance its functionality at shorter irradiation times. Encapsulin protein shells are considered robust nanostructures, exhibiting resilience against extreme pH, high temperatures and proteolytic degradation^{19, 33, 34}. To assess the physical effect of laser irradiation and $^1\text{O}_2$ generation on the nanocompartments, we monitored changes to the structure and stability of empty Enc and Enc-mSOG-ESig τ after exposure to a blue laser (55 mW/cm², 10 min). Following the irradiation of empty Enc, DLS measurements indicated a ~27% increase in its hydrodynamic diameter from 30.5 to 38.7 nm, while TEM images revealed the presence of relatively normal spherical nanocompartments and a small proportion of large amorphous structures

(Supplementary Fig. 5 and 6). Thus, laser irradiation alone had a minimal effect on the protein shell's physical properties. In contrast, DLS measurements showed that irradiated Enc-mSOG-ESigT enlarged ~385% from 29.1 to 111.6 nm (Fig. 2e) and lost its monodispersity. Under TEM, a highly heterogeneous population was observed, consisting of enlarged nanocompartments and numerous bulky amorphous structures (Supplementary Fig. 6). The loss of Enc-mSOG-ESigT's structural integrity and stability can be attributed to the light-induced activation of its mSOG cargo, which generates $^1\text{O}_2$ that could severely damage its surrounding protein shell ³⁸. This is consistent with research by Zhen et al., in which ferritin protein nanocages were loaded with the potent chemical photosensitizer ZnF₁₆Pc, and subsequently destroyed by $^1\text{O}_2$ generated from the light-activated ZnF₁₆Pc cargo ³⁹. Furthermore, the $^1\text{O}_2$ -mediated damage to Enc-mSOG-ESigT's macrostructure could explain why its photoconversion rate begins to somewhat plateau after exposure to more than 10 min laser irradiation (Fig 2d).

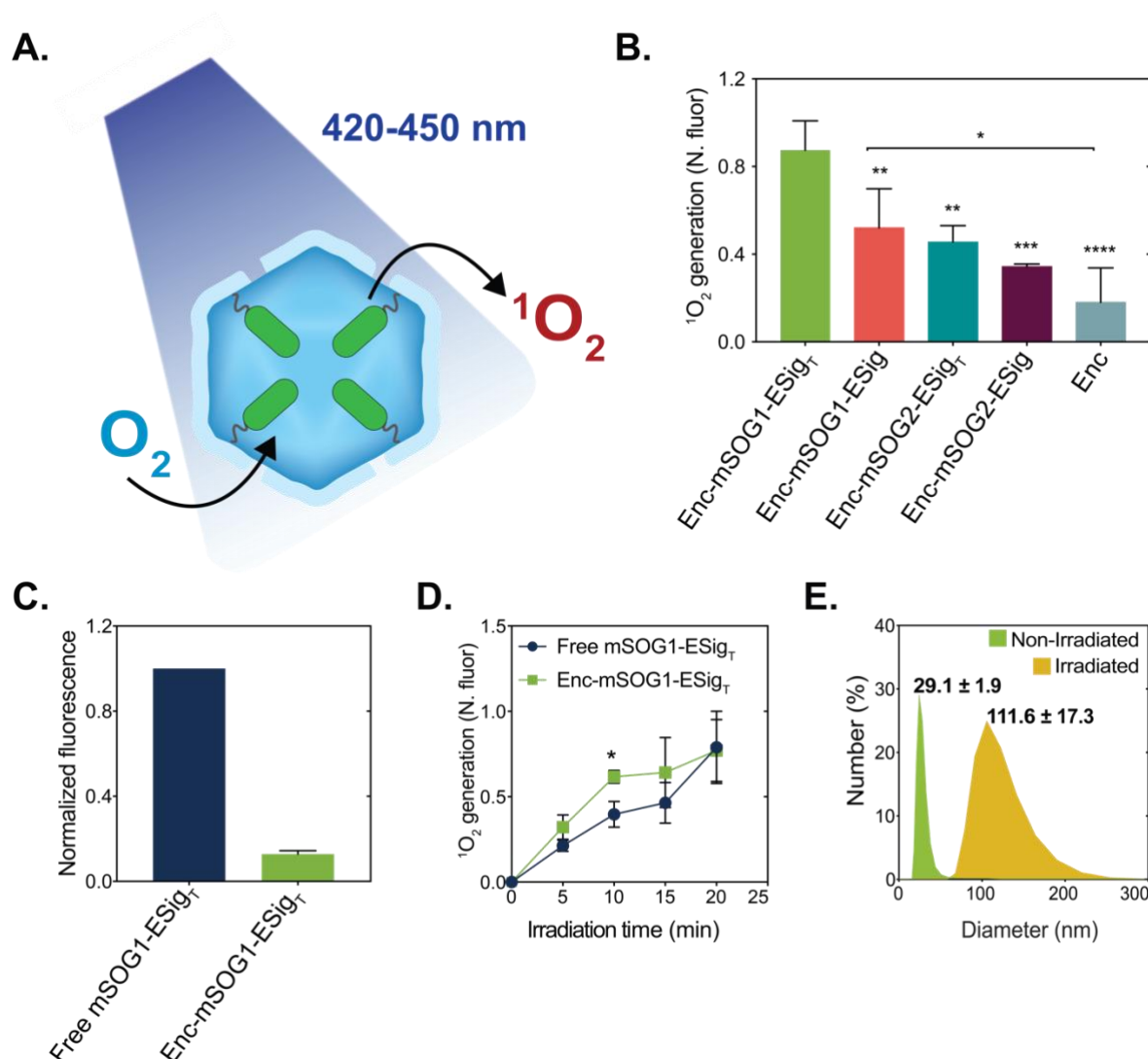


Fig. 2. The “on demand” generation of singlet oxygen by light-activated mSOG-loaded encapsulins (Enc-mSOGs). **A.** Illustration showing the production of singlet oxygen (1O_2) by a light-activated Enc-mSOG nanocompartment. In this process, molecular oxygen (O_2) enters the internal cavity of the nanocompartment via open surface pores where it interacts with encapsulated mSOG. Upon activation with blue laser light, the mSOG cargo converts O_2 (substrate) into 1O_2 (product), which subsequently diffuses out of the same open surface pores. **B.** 1O_2 generation from Enc-mSOGs and unloaded Enc upon irradiation with a blue laser (mSOG1 = 450 nm; mSOG2 = 420 nm) at 55 mW/cm² for 5 min. 1O_2 production was determined by the accumulated fluorescence intensity of oxidized SOSG, with the fluorescence intensity of each reaction normalized to nanocompartment concentration (Normalized Fluorescent Units, NFU). Error bars represent the mean \pm standard deviation (* $p \leq 0.05$, ** $p \leq 0.01$, *** $p \leq 0.001$, **** $p \leq 0.0001$), one-way ANOVA, Tukey, $n \geq 3$, from two independent experiments. **C.** The fluorescence emission intensity (ex/em = 485/520 nm) of free and encapsulated mSOG1-ESig_T. Each sample contained 500 nM mSOG1-Eig_T equivalent. Error bars represent the mean \pm standard deviation, $n=3$ from three independent experiments. **D.** 1O_2 production by free and encapsulated mSOG1-ESig_T after laser irradiation at 450 nm (55 mW/cm²) for 0, 5, 10, 15 and 20 min. 1O_2 generation was measured using SOSG. Error bars represent the mean \pm standard deviation (* $p \leq 0.05$), multiple t-test, $n=3$. **E.** DLS-measured size distributions of Enc-mSOG1-ESig_T before (Non-Irradiated) and after (Irradiated) laser excitation at 450 nm (55 mW/cm²) for 10 min.

Evaluating the photosensitizing function of Enc-mSOG1-ESigT in an in vitro model of photodynamic therapy

The $^1\text{O}_2$ and other ROS generated by light-activated mSOGs readily reacts with nearby molecules in a process called ‘photosensitization’. As a result, mSOG has been effectively employed as a biological photosensitizer in photodynamic therapy (PDT) ^{45, 46}. PDT is a highly selective and minimally invasiveness cancer treatment. To eliminate cancer cells, PDT relies on light-induced photosensitizers that convert intracellular oxygen into ROS, which damage cellular componentry and cause cell death ⁴⁰. As a proof-of-concept (Fig. 3a), we evaluated whether ROS produced by the light-activated Enc-mSOG1-ESigT nanoreactor is sufficient to trigger cellular photodynamic responses in an *in vitro* model of human lung cancer.

First, the cytotoxicity of free and encapsulated mSOG1-ESigT were assessed in dark conditions. Previous work by Deyev, demonstrated that a mSOG1 variant tagged with a cancer-specific antibody mediated targeted PDT *in vitro*, exerting its maximal phototoxic effect against cancer cells at a concentration of 500 nmol ⁴¹. Accordingly, A549 human lung cancer cells were incubated with 500 nmol of mSOG1-ESigT (free or encapsulated) for various time periods (2, 4, 8 and 12 h) in the dark and then measured their viability by standard MTT assay (see “Materials and Methods”). As shown in Figure 3b, free mSOG1-ESigT had variable effects on cell viability but showed no significant cytotoxicity when compared to untreated cells. Alternatively, Enc-mSOG1-ESigT exhibited minimal or no effect on cell viability, even after the longest incubation time of 12 h. These results indicate that both samples have low cytotoxicity in the absence of light activation, but also suggest that the encapsulation of mSOG1-ESigT within the nanocompartment may help to mitigate any of its variable and unwanted interactions with cells.

Next, we sought to evaluate the cytotoxicity of free and encapsulated mSOG1-ESigT in conjunction with blue-light irradiation i.e. phototoxicity. Initially, the effect of laser irradiation on live cells was assessed by exposing A549 cells to a blue laser (55 mW/cm²). An irradiation time of up to 10 min had no significant effect on cell viability (Supplementary Fig. 7) and was therefore used to study *in vitro* phototoxicity. Herein, A549 cells were exposed to 500 nmol mSOG1-ESigT (free or encapsulated)

for different periods of time (2, 4, 8 and 12 h) in the dark, followed by 10 min blue-light irradiation, with cell viability then determined via MTT assay (see “Materials and Methods”). As seen in Figure 3c, after incubation with free mSOG1-ESig_T and blue-light irradiation, A549 cells showed no significant changes in viability. This is consistent with reports in which unmodified free mSOG1 was unable to efficiently enter cancer cells and exert its phototoxic effect ⁴¹. In contrast, cells exposed to Enc-mSOG1-ESig_T and light activation, exhibited a decrease in viability for all incubation times tested. For instance, the viability of cells incubated with Enc-mSOG1-ESig_T for 8 -12 hours was significantly reduced by ~34%. These results show that encapsulin nanocompartments can act as a viable nanocarrier for mSOG1-ESig_T, facilitating its intracellular delivery. They also confirm that light-activated Enc-mSOG1-ESig_T is able to trigger photosensitized oxidation reactions that exert a phototoxic effect on cancer cells.

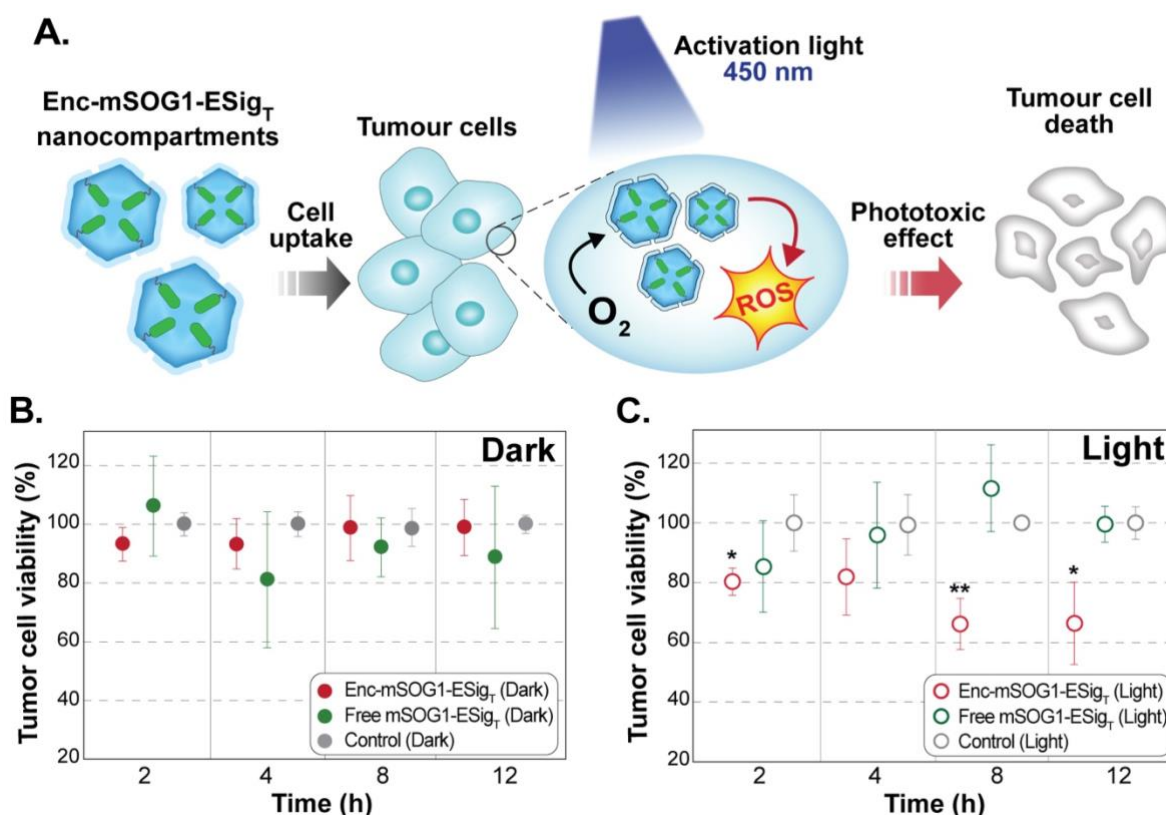


Figure 3. Proof-of-concept: Testing the capacity of light-activated Enc-mSOG1-ESig_T to induce photodynamic responses in an *in vitro* cancer model. **A.** A schematic diagram showing the proposed delivery, activation and phototoxic effect of Enc-mSOG1-ESig_T nanocompartments. Photosensitizing Enc-mSOG1-ESig_T enters tumour cells via endocytosis. Upon photoexcitation with blue light, Enc-mSOG1-ESig_T converts intracellular oxygen into cytotoxic reactive oxygen species (ROS) (e.g. 1O_2) that induces tumour cell death. **B.** Cytotoxicity of free and encapsulated mSOG-ESig_T: Viability of A549 cells after incubation without (control) or with mSOG-ESig_T and Enc-mSOG-ESig_T for different times (2, 4, 8, and 12 h) in the dark. Cell viability was subsequently determined by standard MTT assay. Error bars represent the mean \pm standard deviation ($p \leq 0.05$), one-way ANOVA, Dunnett, $n=6$ from two independent experiments (Enc-mSOG1-ESig_T and control) and $n=3$ from one experiment (free mSOG1-ESig_T). **C.** Phototoxicity of free and encapsulated mSOG-ESig_T: Viability of A549 cells incubated without (control) or with mSOG-ESig_T Enc-mSOG-ESig_T for different times (2, 4, 8, and 12 h) in the dark, followed by blue laser irradiation at 450 nm (55 mW/cm²) for 10 min. Cell viability was finally quantified via MTT assay. Error bars represent the mean \pm standard deviation (* $p \leq 0.05$, ** $p \leq 0.01$), one-way ANOVA, Dunnett, $n=6$ from two independent experiments.

Discussion

In nature, the *Tm* encapsulin encases a ferritin-like protein (FLP) with ferroxidase activity, enabling the nanocompartment to oxidize soluble ferrous iron (Fe_{2+}) into insoluble ferric iron (Fe_{3+})₁₂. FLP-loaded encapsulins have therefore been implicated in the removal and storage of excess Fe_{2+} inside microbial cells. In aerobes, this prevents redox-active Fe_{2+} reacting with intracellular oxygen to produce lethal ROS₁₂. In anaerobes, where iron-induced toxicity is not a significant

issue, this provides a protective response mechanism to unwanted oxygen exposure¹². In this work, we successfully reversed the native antioxidant functions of *Tm* encapsulin, programming it to instead serve as a light-activatable ROS-generating nanoreactor. In this work, we successfully reversed the native antioxidant functions of *Tm* encapsulin, programming it to instead serve as a light-activatable ROS-generating nanoreactor with the capacity to trigger photosensitization reactions.

To achieve this outcome, the light-inducible ROS generators mSOG1 and mSOG2 were packaged inside *Tm* encapsulin via full or truncated versions of the *Tm* ESig. ESig direct cargo encapsulation via specific non-covalent interactions with a binding pocket located on the inner surface of the nanocompartment's protein shell¹. While truncation of the ESig appeared to have no effect on mSOG loading, modifying residues within its sequence could augment its docking interactions with encapsulin, providing a means to manipulate cargo loading¹⁹. The loading stoichiometry of cargo inside encapsulins and its effect on their storage capacity is poorly understood. In this study, mSOG1 and mSOG2 cargo exhibited vastly different loading efficiencies, in spite of their nearly identical protein structures. In previous studies, efficient cargo loading was attained by modulating the rate and ratio of recombinant protein expression (cargo:encapsulin) via a combination of constitutive and inducible promoters¹⁹. Thus, the observed variation in mSOG cargo loading is likely due to the poorly controlled simultaneous co-expression of cargo and encapsulin under the inducible IPTG promoter.

The fluorescence properties and $^1\text{O}_2$ -generating functions of mSOG1 (and variants thereof) is attributed to its chromophore flavin mononucleotide (FMN), a recognized photosensitizer, which is bound within the core of mSOG1's structure⁴³. mSOG2 is a genetically engineered variant of mSOG1 that exhibits approximately 7-fold less fluorescence intensity but generates $^1\text{O}_2$ 4-fold more efficiently²³. Contrary to expectations, both mSOG2-loaded nanocompartments contained the most cargo molecules but generated the lowest quantities of $^1\text{O}_2$ under blue-light irradiation. A possible explanation for these observations is the presence of an overcrowded environment inside the mSOG2-loaded nanocompartments. Previous reports suggest that cargo crowding in encapsulins limits cargo function. For example,

molecular crowding of the fluorescent calcium indicator GCaMP inside *Tm* encapsulin prevented key conformation changes in GCaMP that occur upon Ca^{2+} -binding, limiting its capacity to fluorescently detect Ca^{2+} ⁴⁴. Hence, the dense packing of mSOG2 cargo inside the nanocompartments make it prone to unwanted conformational states, which can both limit FMN's access to O_2 substrate and induce adverse quenching interactions between the triplet state of FMN and electron-rich residues near mSOG2's chromophore that together inhibit its photosensitizing function ⁴⁵.

From the Enc-mSOGs developed in this study, light-activated Enc-mSOG1-ESig_T was the most proficient “on demand” $^1\text{O}_2$ generator. Surprisingly, the concentration of photosensitizing cargo inside Enc-mSOG1-ESig_T (0.06 g/mL) was 6- to 11-fold less than the mSOG2-loaded nanocompartments (0.40-0.66 g/mL). Therefore, we propose that Enc-mSOG1-ESig_T's exceptional functionality is in part due to the absence of molecular crowding within its internal cavity, which allows O_2 to move freely and interact easily with the mSOG1-ESig_T cargo. Enc-mSOG1-ESig_T also showed a 56% faster photoconversion rate than free mSOG1-ESig_T upon exposure to blue-light for 10 min, indicating that packaging mSOG1-ESig_T inside nanocompartments may improve its function. Together, these findings suggest that encapsulin nanocompartments provide a beneficial microenvironment that favors the production of $^1\text{O}_2$ by mSOG1-ESig_T.

The photoconversion rate of Enc-mSOG1-ESig_T began to plateau at irradiation times longer than 10 min, which also coincided with a loss in Enc-mSOG-ESig_T's structural stability. These structural changes can be attributed to the rapid generation and accumulation of reactive $^1\text{O}_2$ inside Enc-mSOG1-ESig_T that damages its protein shell⁴⁶. Re-engineering the protein shell may provide an avenue to dampen the destructive effects and prolong the stability of Enc-mSOG1-ESig_T. For instance, amino acids within the Enc_{Subunit} that are prone to oxidation by $^1\text{O}_2$ (e.g. tryptophan, histidine and cysteine) can be substituted with $^1\text{O}_2$ -insensitive residues (i.e. leucine and alanine) ⁴⁷, making the assembled protein shell more resilient to ROS produced by the photosensitizing cargo. Additionally, to minimize unwanted $^1\text{O}_2$ accumulation, the external pores of the protein shell can be re-engineered to allow the selective and continuous flow of O_2 into and $^1\text{O}_2$ out of Enc-

mSOG1-ESigT's internal cavity. Williams et al. explored this strategy by substituting specific residues located within pore-forming loop regions of *Tm* encapsulin's structure ⁴⁴. This action enlarged the diameter of the nanocompartment's 5-fold pore from 3 Å to 11Å and enhanced the diffusion rate of metal ions into the nanocompartment by almost 700% ⁴⁴.

The distance travelled by $^1\text{O}_2$ is dependent upon its lifetime, rate of diffusion and the presence of quenching molecules. The lifetime of $^1\text{O}_2$ is ~4 μs in H₂O and ~68 μs in D₂O, while the distance $^1\text{O}_2$ diffuses from its site of inception over one lifetime is 100-150 nm in H₂O and 500-600 nm in D₂O ⁴⁸. Using an *in vitro* model of PDT, we demonstrated that the light-activated Enc-mSOG1-ESigT nanoreactor generates sufficient quantities of $^1\text{O}_2$ that diffused through the viscous intracellular milieu and triggered photosensitized oxidation reactions that reduce cancer cell viability. Under these conditions, Enc-mSOG1-ESigT's reactive range may be expanded by intracellular biological reductants that react with $^1\text{O}_2$ to form longer lived cytotoxic ROS, including hydrogen peroxide (H₂O₂) ²⁴.

In an effort to stabilize, protect and target the delivery of therapeutic proteins their encapsulation in synthetic nanoparticles (e.g. polymeric, liposomal and ceramics) have been widely used ⁴⁸. While some of these nanoparticle-based drug delivery systems have shown potential, significant problems still exist, including, physicochemical heterogeneity, problematic functionalization, inactivation and destruction of therapeutic proteins caused by harsh synthesis conditions, instability and toxicity *in vivo* ⁴⁹⁻⁵¹. In contrast, encapsulin nanocompartments are monodisperse, biocompatible and biodegradable ⁵². Additionally, they possess the inherent ability to encapsulate proteins in a stable non-destructive manner and their external surfaces can be genetically and/or chemically modified to enhance their functionalities ⁵². Nevertheless, despite this features the utility of encapsulins as delivery vehicles for therapeutic proteins has remained unexplored until now ³³. This is likely owing to the fact that proteins typically enter cells and become trapped inside lysosomes, leading to their degradation and a loss of therapeutic efficacy. In this work, light-activated Enc-mSOG1-ESigT exhibited phototoxicity in a cellular model of human lung cancer, reducing cellular viability by up to ~34%. In contrast, free mSOG1-ESigT elicited no phototoxic effect on cells, indicating that the

encapsulin nanocompartment serves as a nanocarrier for the intracellular delivery of mSOG1-ESigT. These findings infer that Enc-mSOG1-ESigT, to some degree, escapes lysosomal degradation, entering the cell cytosol to elicit its therapeutic effect. This process may be driven by polyhistidine-tags on the nanocompartment's surface that allow its purification but can also trigger endo/lysosomal escape via the "proton sponge" effect⁴⁹. However, further studies aimed at understanding the intracellular trafficking of encapsulins is critical to their application as therapeutic delivery vehicles.

To realise the delivery of mSOG1 for *in vitro* PDT, Deyev et al. genetically fused an anti-HER2 antibody fragment to its N-terminus ⁴¹. Following this modification, mSOG1 selectively entered HER2-positive breast cancer cells where it reduced cell viability by ~80% upon photoactivation ⁴¹. While light-activated Enc-mSOG1-ESigT reduces cancer cell viability, higher intracellular doses will be required to reach a therapeutic threshold of cytotoxic $^1\text{O}_2$ (i.e. $\geq 50\%$ loss in cell viability) in PDT applications. This can be accomplished by engineering Enc-mSOG1-ESigT's external surface to present targeting ligands (e.g. peptides and antibodies) that enhance cancer cell uptake. In an example of this approach, *Tm* encapsulin was modified to display a hepatocellular carcinoma (HCC)-targeting peptide and the anticancer prodrug aldoxorubicin, resulting in a platform that delivered and released drugs into HCC cells, inducing a $\geq 50\%$ loss in viability ³³.

In summary, the light-activatable Enc-mSOG1-ESigT nanoreactor bioengineered in this study, represents a versatile platform for the "on demand" generation of ROS. As demonstrated, light-activated Enc-mSOG1-ESigT can trigger photosensitized oxidation reactions. Thus, in conjunction with the exquisite spatial and temporal resolution offered by light, we anticipate that Enc-mSOG1-ESigT can be utilized to precisely initiate and/or modulate ROS-sensitive processes that have technological, biological and therapeutic relevance. Moreover, this work showcases the remarkable modularity and programmability of encapsulin nanocompartments, paving the way for their wider application.

References

1. Cornejo, E.; Abreu, N.; Komeili, A., Compartmentalization and organelle formation in bacteria. *Current Opinion in Cell Biology* **2014**, *26*, 132-138.
2. Diekmann, Y.; Pereira-Leal, J. B., Evolution of intracellular compartmentalization. *The Biochemical journal* **2013**, *449* (2), 319-31.
3. Rother, M.; Nussbaumer, M. G.; Renggli, K.; Bruns, N., Protein cages and synthetic polymers: a fruitful symbiosis for drug delivery applications, bionanotechnology and materials science. *Chem Soc Rev* **2016**, *45* (22), 6213-6249.
4. Mosayebi, M.; Shoemark, D. K.; Fletcher, J. M.; Sessions, R. B.; Linden, N.; Woolfson, D. N.; Liverpool, T. B., Beyond icosahedral symmetry in packings of proteins in spherical shells. *Proceedings of the National Academy of Sciences* **2017**, *114* (34), 9014-9019.
5. Chen, A. H.; Silver, P. A., Designing biological compartmentalization. *Trends in Cell Biology* **2012**, *22* (12), 662-670.
6. Plegaria, J. S.; Kerfeld, C. A., Engineering nanoreactors using bacterial microcompartment architectures. *Current Opinion in Biotechnology* **2018**, *51*, 1-7.
7. Frank, S.; Lawrence, A. D.; Prentice, M. B.; Warren, M. J., Bacterial microcompartments moving into a synthetic biological world. *Journal of biotechnology* **2013**, *163* (2), 273-279.
8. Thompson, M. C.; Crowley, C. S.; Kopstein, J.; Bobik, T. A.; Yeates, T. O., Structure of a bacterial microcompartment shell protein bound to a cobalamin cofactor. *Acta Crystallographica Section F Structural Biology Communications* **2014**, *70* (Pt 12), 1584-1590.
9. Giessen, T. W.; Silver, P. A., Widespread distribution of encapsulin nanocompartments reveals functional diversity. *Nature microbiology* **2017**, *2*, 17029.
10. Contreras, H.; Joens, M. S.; McMath, L. M.; Le, V. P.; Tullius, M. V.; Kimmey, J. M.; Bionghi, N.; Horwitz, M. A.; Fitzpatrick, J. A.; Goulding, C. W., Characterization of a *Mycobacterium tuberculosis* nanocompartment and its potential cargo proteins. *The Journal of Biological Chemistry* **2014**, *289* (26), 18279-89.
11. He, D.; Hughes, S.; Vanden-Hehir, S.; Georgiev, A.; Altenbach, K.; Tarrant, E.; Mackay, C. L.; Waldron, K. J.; Clarke, D. J.; Marles-Wright, J., Structural characterization of encapsulated ferritin provides insight into iron storage in bacterial nanocompartments. *eLife* **2016**, *5*.
12. Sutter, M.; Boehringer, D.; Gutmann, S.; Gunther, S.; Prangishvili, D.; Loessner, M. J.; Stetter, K. O.; Weber-Ban, E.; Ban, N., Structural basis of enzyme encapsulation into a bacterial nanocompartment. *Nature structural & molecular biology* **2008**, *15* (9), 939-47.
13. McHugh, C. A.; Fontana, J.; Nemecek, D.; Cheng, N.; Aksyuk, A. A.; Heymann, J. B.; Winkler, D. C.; Lam, A. S.; Wall, J. S.; Steven, A. C.; Hoiczky, E., A virus capsid-like nanocompartment that stores iron and protects bacteria from oxidative stress. *Embo Journal* **2014**, *33* (17), 1896-911.
14. Giessen, T. W.; Orlando, B. J.; Verdegaal, A. A.; Chambers, M. G.; Gardener, J.; Bell, D. C.; Birrane, G.; Liao, M.; Silver, P. A., Large protein organelles form a new iron sequestration system with high storage capacity. *eLife* **2019**, *8*, e46070.

15. Sigmund, F.; Pettinger, S.; Kube, M.; Schneider, F.; Schifferer, M.; Schneider, S.; Efremova, M. V.; Pujol-Martí, J.; Aichler, M.; Walch, A.; Misgeld, T.; Dietz, H.; Westmeyer, G. G., Iron-Sequestering Nanocompartments as Multiplexed Electron Microscopy Gene Reporters. *ACS Nano* **2019**, *13* (7), 8114-8123.
16. Rahmanpour, R.; Bugg, T. D. H., Assembly in vitro of *Rhodococcus jostii* RHA1 encapsulin and peroxidase DypB to form a nanocompartment. *The FEBS Journal* **2013**, *280* (9), 2097-2104.
17. He, D.; Hughes, S.; Vanden-Hehir, S.; Georgiev, A.; Altenbach, K.; Tarrant, E.; Mackay, C. L.; Waldron, K. J.; Clarke, D. J.; Marles-Wright, J., Structural characterization of encapsulated ferritin provides insight into iron storage in bacterial nanocompartments. *eLife* **2016**, *5*, e18972.
18. Nichols, R. J.; Cassidy-Amstutz, C.; Chaijarasphong, T.; Savage, D. F., Encapsulins: molecular biology of the shell. *Critical Reviews in Biochemistry and Molecular Biology* **2017**, *52* (5), 583-594.
19. Lau, Y. H.; Giessen, T. W.; Altenburg, W. J.; Silver, P. A., Prokaryotic nanocompartments form synthetic organelles in a eukaryote. *Nature Communications* **2018**, *9* (1), 1311.
20. Sigmund, F.; Massner, C.; Erdmann, P.; Stelzl, A.; Rolbieski, H.; Desai, M.; Bricault, S.; Worner, T. P.; Snijder, J.; Geerlof, A.; Fuchs, H.; Hrabe de Angelis, M.; Heck, A. J. R.; Jasanoff, A.; Ntziachristos, V.; Plitzko, J.; Westmeyer, G. G., Bacterial encapsulins as orthogonal compartments for mammalian cell engineering. *Nature Communications* **2018**, *9* (1), 1990.
21. Barnett, M. E.; Baran, T. M.; Foster, T. H.; Wojtovich, A. P., Quantification of light-induced miniSOG superoxide production using the selective marker, 2-hydroxyethidium. *Free Radical Biology & Medicine* **2018**, *116*, 134-140.
22. Shu, X.; Lev-Ram, V.; Deerinck, T. J.; Qi, Y.; Ramko, E. B.; Davidson, M. W.; Jin, Y.; Ellisman, M. H.; Tsien, R. Y., A genetically encoded tag for correlated light and electron microscopy of intact cells, tissues, and organisms. *PLoS biology* **2011**, *9* (4), e1001041.
23. Makhijani, K.; To, T. L.; Ruiz-Gonzalez, R.; Lafaye, C.; Royant, A.; Shu, X., Precision Optogenetic Tool for Selective Single- and Multiple-Cell Ablation in a Live Animal Model System. *Cell chemical biology* **2017**, *24* (1), 110-119.
24. Souslova, E. A.; Mironova, K. E.; Deyev, S. M., Applications of genetically encoded photosensitizer miniSOG: from correlative light electron microscopy to immunophotosensitizing. *Journal of Biophotonics* **2017**, *10* (3), 338-352.
25. DeRosa, M. C.; Crutchley, R. J., Photosensitized singlet oxygen and its applications. *Coordination Chemistry Reviews* **2002**, *233-234*, 351-371.
26. Ogilby, P. R., Singlet oxygen: there is indeed something new under the sun. *Chemical Society Reviews* **2010**, *39* (8), 3181-209.
27. Chen, X.; Winters, C.; Crocker, V.; Lazarou, M.; Sousa, A. A.; Leapman, R. D.; Reese, T. S., Identification of PSD-95 in the Postsynaptic Density Using MiniSOG and EM Tomography. *Frontiers in Neuroanatomy* **2018**, *12*, 107-107.
28. Alonso-de Castro, S.; Cortajarena, A. L.; López-Gallego, F.; Salassa, L., Bioorthogonal Catalytic Activation of Platinum and Ruthenium Anticancer Complexes by FAD and Flavoproteins. *Angewandte Chemie* **2018**, *130* (12), 3197-3201.

29. Jiang, H. N.; Li, Y.; Jiang, W. Y.; Cui, Z. J., Cholecystokinin 1 Receptor - A Unique G Protein-Coupled Receptor Activated by Singlet Oxygen (GPCR-ABSO). *Frontiers in Physiology* **2018**, *9*, 497.
30. Burgers, P. P.; Ma, Y.; Margarucci, L.; Mackey, M.; van der Heyden, M. A.; Ellisman, M.; Scholten, A.; Taylor, S. S.; Heck, A. J., A small novel A-kinase anchoring protein (AKAP) that localizes specifically protein kinase A-regulatory subunit I (PKA-RI) to the plasma membrane. *The Journal of Biological Chemistry* **2012**, *287* (52), 43789-97.
31. Lin, J. Y.; Sann, S. B.; Zhou, K.; Nabavi, S.; Proulx, C. D.; Malinow, R.; Jin, Y.; Tsien, R. Y., Optogenetic inhibition of synaptic release with chromophore-assisted light inactivation (CALI). *Neuron* **2013**, *79* (2), 241-253.
32. Proshkina, G. M.; Shramova, E. I.; Shilova, O. N.; Ryabova, A. V.; Deyev, S. M., Phototoxicity of flavoprotein miniSOG induced by bioluminescence resonance energy transfer in genetically encoded system NanoLuc-miniSOG is comparable with its LED-excited phototoxicity. *Journal of Photochemistry and Photobiology B* **2018**, *188*, 107-115.
33. Moon, H.; Lee, J.; Min, J.; Kang, S., Developing genetically engineered encapsulin protein cage nanoparticles as a targeted delivery nanoplatfrom. *Biomacromolecules* **2014**, *15* (10), 3794-801.
34. Cassidy-Amstutz, C.; Oltrogge, L.; Going, C. C.; Lee, A.; Teng, P.; Quintanilla, D.; East-Seletsky, A.; Williams, E. R.; Savage, D. F., Identification of a Minimal Peptide Tag for in Vivo and in Vitro Loading of Encapsulin. *Biochemistry* **2016**, *55* (24), 3461-8.
35. Lawrence, A.-M.; Besir, H. U. S., Staining of proteins in gels with Coomassie G-250 without organic solvent and acetic acid. *Journal of visualized experiments* **2009**, (30), 1350.
36. Schneider, C. A.; Rasband, W. S.; Eliceiri, K. W., NIH Image to ImageJ: 25 years of image analysis. *Nature Methods* **2012**, *9* (7), 671-5.
37. Iselt, M.; Holtei, W.; Hilgard, P., The tetrazolium dye assay for rapid in vitro assessment of cytotoxicity. *Arzneimittel-Forschung* **1989**, *39* (7), 747-9.
38. Michaeli, A.; Feitelson, J., Reactivity of singlet oxygen toward proteins: the effect of structure in basic pancreatic trypsin inhibitor and in ribonuclease A. *Photochemistry and Photobiology* **1997**, *65* (2), 309-15.
39. Zhen, Z.; Tang, W.; Guo, C.; Chen, H.; Lin, X.; Liu, G.; Fei, B.; Chen, X.; Xu, B.; Xie, J., Ferritin nanocages to encapsulate and deliver photosensitizers for efficient photodynamic therapy against cancer. *ACS Nano* **2013**, *7* (8), 6988-96.
40. Serebrovskaya, E. O.; Edelweiss, E. F.; Stremovskiy, O. A.; Lukyanov, K. A.; Chudakov, D. M.; Deyev, S. M., Targeting cancer cells by using an antireceptor antibody-photosensitizer fusion protein. *Proceedings of the National Academy of Sciences* **2009** *106* (23), 9221-9225.
41. Mironova, K. E.; Proshkina, G. M.; Ryabova, A. V.; Stremovskiy, O. A.; Lukyanov, S. A.; Petrov, R. V.; Deyev, S. M., Genetically encoded immunophotosensitizer 4D5scFv-miniSOG is a highly selective agent for targeted photokilling of tumor cells in vitro. *Theranostics* **2013**, *3* (11), 831-40.
42. Pimenta, F. M.; Jensen, R. L.; Breitenbach, T.; Etzerodt, M.; Ogilby, P. R., Oxygen-dependent photochemistry and photophysics of "miniSOG," a protein-encased flavin. *Photochemistry and Photobiology* **2013**, *89* (5), 1116-26.

43. Williams, E. M.; Jung, S. M.; Coffman, J. L.; Lutz, S., Pore Engineering for Enhanced Mass Transport in Encapsulin Nanocompartments. *ACS Synthetic Biology* **2018**, 7 (11), 2514-2517.
44. Kuznetsova, I. M.; Turoverov, K. K.; Uversky, V. N., What macromolecular crowding can do to a protein. *International journal of molecular sciences* **2014**, 15 (12), 23090-23140.
45. Gracanin, M.; Hawkins, C. L.; Pattison, D. I.; Davies, M. J., Singlet-oxygen-mediated amino acid and protein oxidation: formation of tryptophan peroxides and decomposition products. *Free Radical Biology & Medicine* **2009**, 47 (1), 92-102.
46. Dogra, V.; Li, M.; Singh, S.; Li, M.; Kim, C., Oxidative post-translational modification of EXECUTER1 is required for singlet oxygen sensing in plastids. *Nature Communications* **2019**, 10 (1), 2834.
47. Skovsen, E.; Snyder, J. W.; Lambert, J. D. C.; Ogilby, P. R., Lifetime and Diffusion of Singlet Oxygen in a Cell. *The Journal of Physical Chemistry B* **2005**, 109 (18), 8570-8573.
48. Barry, J. N.; Vertegel, A. A., Nanomaterials for Protein Mediated Therapy and Delivery. *Nano Life* **2013**, 3 (4), 1343001.
49. De Jong, W. H.; Borm, P. J. A., Drug delivery and nanoparticles: applications and hazards. *International journal of nanomedicine* **2008**, 3 (2), 133-149.
50. Hua, S.; de Matos, M. B. C.; Metselaar, J. M.; Storm, G., Current Trends and Challenges in the Clinical Translation of Nanoparticulate Nanomedicines: Pathways for Translational Development and Commercialization. *Frontiers in Pharmacology* **2018**, 9 (790).
51. Yu, M.; Wu, J.; Shi, J.; Farokhzad, O. C., Nanotechnology for protein delivery: Overview and perspectives. *Journal of controlled release : official journal of the Controlled Release Society* **2016**, 240, 24-37.
52. Giessen, T. W., Encapsulins: microbial nanocompartments with applications in biomedicine, nanobiotechnology and materials science. *Current Opinion in Chemical Biology* **2016**, 34, 1-10.
53. Meng, Z.; Luan, L.; Kang, Z.; Feng, S.; Meng, Q.; Liu, K., Histidine-enriched multifunctional peptide vectors with enhanced cellular uptake and endosomal escape for gene delivery. *Journal of Materials Chemistry B* **2017**, 5 (1), 74-84.

Acknowledgments

D.D. is supported by an international Macquarie University Research Excellence Scholarship (iMQRES), Sydney Vital Research Scholar Award and the Commonwealth Scientific and Industrial Research Organisation (CSIRO) PhD Scholarship Program in Synthetic Biology. A.C. is supported by a Cancer Institute New South Wales Early Career Fellowship (Project Number: ECF171114) and the Australian Research Council (CE140100003).

Author contributions

D.D co-designed the research, generated all nanocompartment constructs, conducted all physical and functional characterization work, performed data analysis and wrote the manuscript. X.V. Constructed the laser set-up and supported laser irradiation experiments. A.S. Supervised the project and wrote the manuscript. A.C. conceptualized and co-designed the study, supervised the project and wrote the manuscript.

Additional information

Competing interests: The authors declare no competing interests.

Supplementary Information

Reprogramming encapsulin into a light-activatable nanoreactor for the “on demand” generation of reactive oxygen species

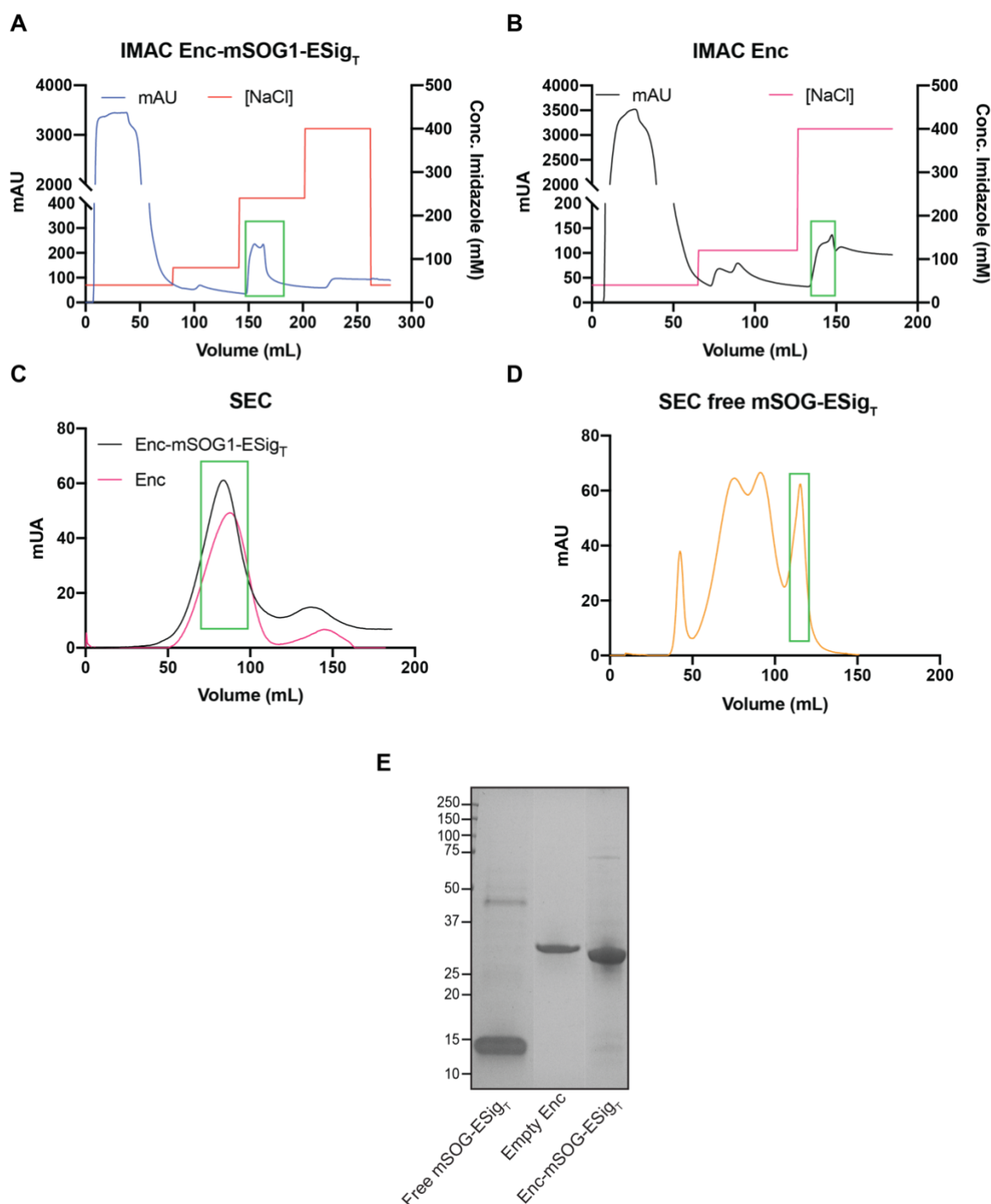
Dennis Diaz, Febrina Sandra, Xavier Vidal, Anwar Sunna, Andrew Care

Supplementary Table 1. Expression plasmids constructed for this study.

Plasmids	Description	Protein ID
pACYC-Duet-1_Enc	Encapsulin from <i>Thermotoga maritima</i> (Tm) 138-GGGGGGHHHHHGGGGGG-139	UniProt: Q9WZP3
-	Tm Encapsulation signal peptide (ESig)	UniProt: R4NZH3
-	mSOG 1 and 2: fluorescent flavoprotein protein engineered from <i>Arabidopsis thaliana</i> phototropin-2.	Phototropin-2 UniProt: P93025
pPETDuet-1_mSOG1-ESig _T	mSOG1-GGSENTGGDLGIRKL	
pPETDuet-1_mSOG1-ESig	mSOG1-LFTDKPITEIEEETSGGSENTG GDLGIRKL	
pPETDuet-1_mSOG2-ESig _T	mSOG2-GGSENTGGDLGIRKL	
pPETDuet-1_mSOG2-ESig	mSOG2-LFTDKPITEIEEETSGGSENTG GDLGIRKL	

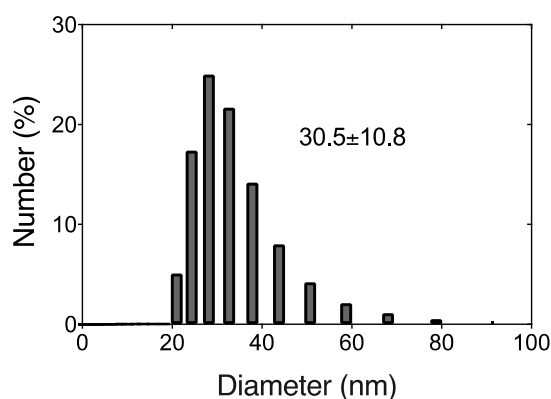
Supplementary Table 2. Optimized conditions for the recombinant production of all proteins in *E. coli*.

Protein(s)	Plasmid(s)	Antibiotic(s)	IPTG (mM)	Induction temperature (°C)	Induction time (h)
Enc	pACYC-Duet-1_Enc	Chloramphenicol	0.1	37	4-6
mSOG1-ESig _T	pPETDuet-1_mSOG1-ESig _T	Carbenicillin			
mSOG1-ESig	pPETDuet-1_mSOG1-ESig	Carbenicillin			
mSOG2-ESig _T	pPETDuet-1_mSOG2-ESig _T	Carbenicillin			
mSOG2-ESig	pPETDuet-1_mSOG2-ESig	Carbenicillin			
Enc-mSOG1-ESig _T	pACYC-Duet-1_Enc pPETDuet-1_mSOG1-ESig _T	Chloramphenicol Carbenicillin	0.05	30	18-20
Enc-mSOG1-ESig	pACYC-Duet-1_Enc pPETDuet-1_mSOG1-ESig	Chloramphenicol Carbenicillin			
Enc-mSOG2-ESig _T	pACYC-Duet-1_Enc pPETDuet-1_mSOG2-ESig _T	Chloramphenicol Carbenicillin	0.05	20	18-20
Enc-mSOG2-ESig	pACYC-Duet-1_Enc pPETDuet-1_mSOG2-ESig	Chloramphenicol Carbenicillin			

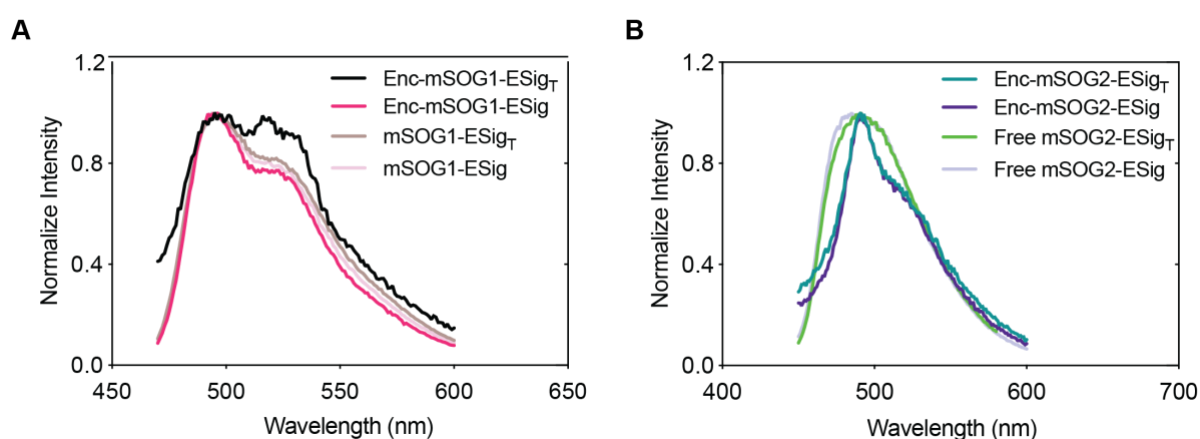


Supplementary Fig. 1. Example chromatograms of recombinant protein purifications. Nickel-immobilized metal-affinity chromatography (IMAC) of **(A)** Enc-mSOG1-ESig_T and **(B)** empty Enc. The green square highlights the peak corresponding to the protein of interest. **C.** Size exclusion chromatography (SEC) of IMAC-purified Enc-mSOG1-ESig_T (pink line) or empty Enc (black line). The protein of interest (green square) elutes between 70-95 mL. **D.** SEC of partially purified free mSOG-ESig_T. The protein of interest (green square) elutes between 106-120 mL.

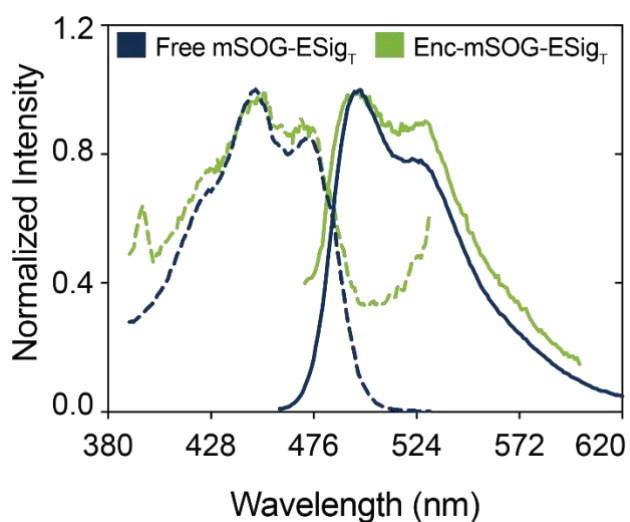
E. Coomassie-stained SDS-PAGE showing the purification and co-purification of the EncSubunit (~31.9 KDa) and mSOG-ESig_T (~14.4 KDa) cargo proteins. The proteins showed a purity of 82% for free mSOG1-ESig_T, 99% for Enc and 93% for Enc-mSOG1-ESig_T.



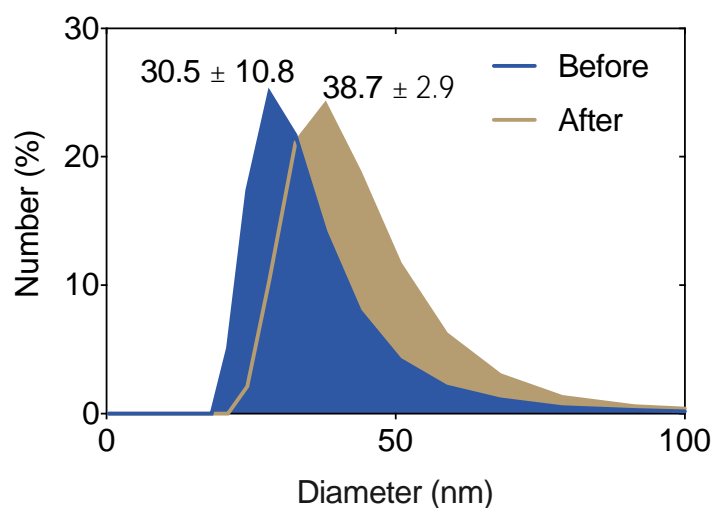
Supplementary Fig. 2. Size distribution of empty Enc. The size distribution of purified empty Enc was measured by dynamic light scattering (DLS).



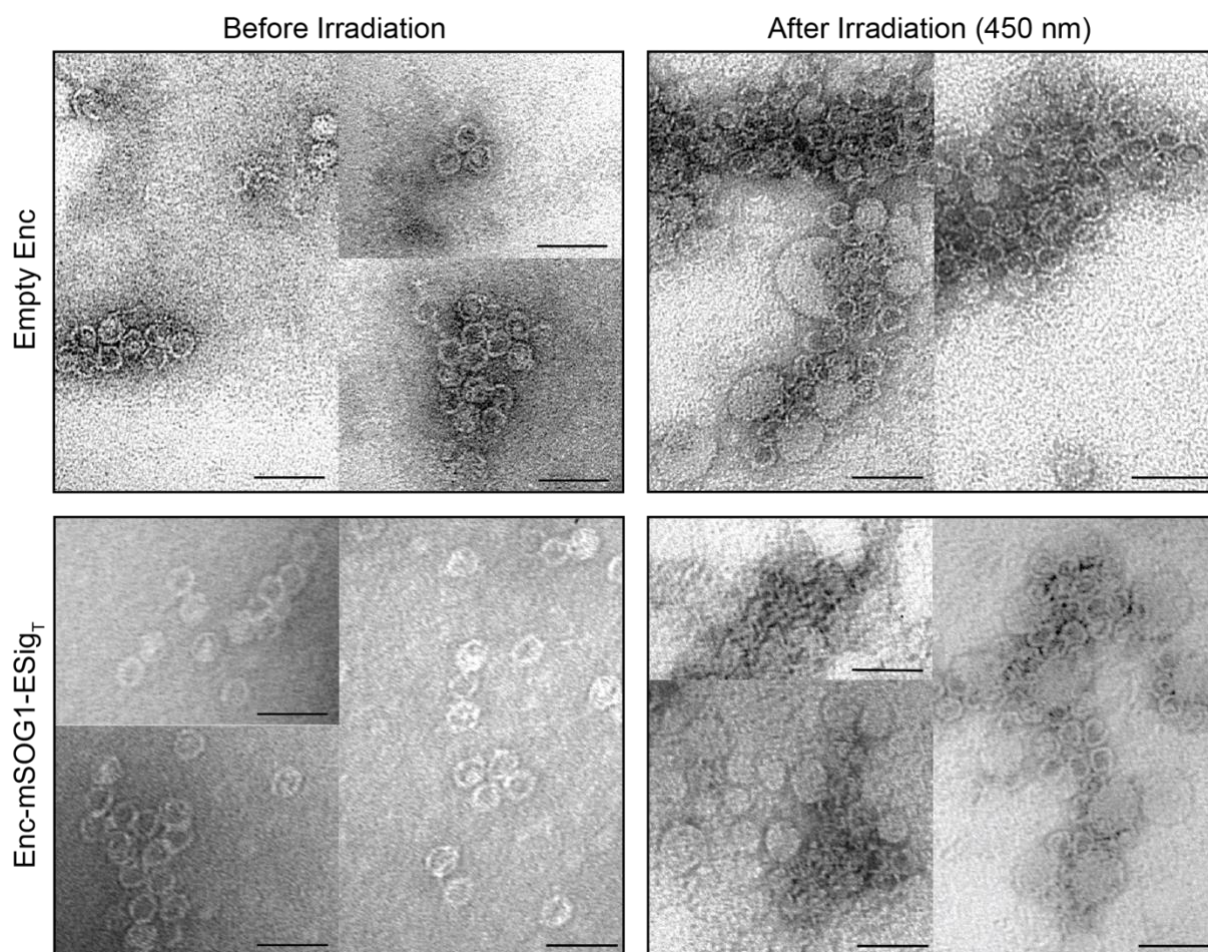
Supplementary Fig. 2. Effect of encapsulation on the fluorescence emission spectra of mSOG variants. Normalized fluorescence emission spectra of free and encapsulated (A) mSOG-1 and (B) mSOG-2 variants under 420 nm (mSOG2) and 450 nm (mSOG1) excitation.



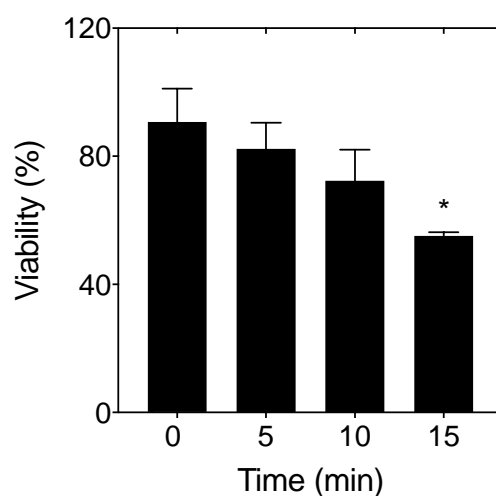
Supplementary Fig. 4. Effect of encapsulation on the fluorescence excitation/emission spectra mSOG-ESig_T. Normalized fluorescence excitation (dashed line) and emission (solid line) spectra of free and encapsulated mSOG-ESig_T.



Supplementary Fig. 5. Effect of laser irradiation on encapsulin size. DLS-measured size distributions of empty Enc before (blue area) and after (gold area) laser irradiation at 450 nm (55 mW/cm²) for 10 min.



Supplementary Fig. 6. Effect of laser irradiation and $^1\text{O}_2$ generation on encapsulin structure. TEM images showing **(Top panel)** empty Enc and **(Bottom panel)** Enc-mSOG1-ESig_T before and after laser irradiation at 450 nm (55 mW/cm²) for 10 min (Scale bars = 50 nm).



Supplementary Fig. 7. Effect of laser irradiation on A549 lung cancer cells. Cell viability of A549 cells after laser irradiation at 450 nm (55 mW/cm²) for different time periods (0-15 min). Error bars represent the mean \pm standard deviation ($p \leq 0.05$), one-way ANOVA, Tukey, $n \geq 3$.

3

Engineering encapsulins as ROS-generating nanocompartments

Introduction

In Chapter 2, I developed a light-triggerable nanoreactor for the “on demand” production of $^1\text{O}_2$ (i.e. Type II photoconversion). In Chapter 3, I aimed to bioengineer a nanoreactor that could instead perform Type I photoconversion, in which superoxide ($\text{O}_2^{\cdot-}$) is the primary ROS product produced.

The results reported in this chapter have been prepared as a manuscript for submission to *ACS Biomaterials Science & Engineering*.

Contribution to manuscript 2

The concept of this publication was developed in partnership with my supervisors Anwar Sunna and Andrew Care. They were also involved in designing experiments and troubleshooting. I performed all the experimental work and data analysis. Xavier Vidal constructed the laser set-up and supported laser irradiation experiments. The initial draft of the manuscript was prepared by me.

Table 3-1 Author contribution summary for Manuscript 2.

	Dennis Diaz	Xavier Vidal	Anwar Sunna	Andrew Care
Experiment Design	•		•	•
Data Collection	•	•		
Data Analysis	•			
Manuscript	•		•	•

Engineering encapsulin as a ROS-generating nanocompartment

Dennis Diaz^a, Xavier Vidal^b, Anwar Sunna^{a,c}, Andrew Care^{a,c}*

^a Department of Molecular Sciences, Macquarie University, NSW 2109, Australia

^b Department of Physics and Astronomy, Macquarie University, NSW 2109, Australia

^c Australian Research Council Centre of Excellence for Nanoscale BioPhotonics, Macquarie University, NSW 2109, Australia.

* Corresponding author: Andrew Care
Department of Molecular Sciences
Macquarie University
Sydney, NSW 2109
Australia

Phone: +61 2 9850 4220
Fax: +61 2 9850 8313
Email: andrew.care@mq.edu.au

ABSTRACT

Encapsulins are self-assembling protein nanocompartments found in prokaryotes. They are known to be highly engineerable and robust, which has made them attractive nanoplatfroms for the construction of synthetic nanoreactors. Herein, the *Thermotoga maritima* encapsulin was reprogrammed to create a light-activated reaction vessel that produces reactive oxygen species (ROS). We evaluated several versions of red fluorescent protein KillerRed (KR) tagged with an encapsulation signal (ESig) to allow its loading inside encapsulin nanocompartments. KR is a biological photosensitizer that can produce ROS upon green light irradiation. N-terminally ESig-tagged KR variants showed good protein expression and fluorescence. Co-expression with encapsulin resulted in the selective encapsulation of ~4 KR, creating nanoreactors that exhibited similar fluorescence and ROS generation abilities as the non-encapsulated KR. In general, further development of this ROS-generation nanoreactors could allow their application in different fields such as protein-based drug delivery, nanomedicine and antimicrobial research.

Keywords: Nanocompartment, Encapsulin, KillerRed, Synthetic biology, Synthetic organelles, Photosensitization, Reactive Oxygen Species (ROS)

Introduction

Historically prokaryotes were thought to be simple microorganisms lacking subcellular compartmentalization. However, in recent years, research has shown that prokaryotes have a wide selection of unique organelles that encase enzymes and isolate complex and/or incompatible metabolic reactions¹. One example of a prokaryotic organelle is the newly established encapsulins, a class of protein-based nanocompartments found in 1-4% of known genomes of prokaryotes². Encapsulin systems are organized as a core operon encoding the encapsulin subunit and the core cargo genes². So far, several core cargo proteins have been described including ferritin-like proteins (Flp) and DyP-type peroxidases which are thought to be involved in oxidative stress response pathways and/or iron mineralization²⁻⁴. Encapsulins self-assemble from identical protein subunits into hollow icosahedral protein shells that are 18-43 nm in diameter and exhibit good colloidal properties and robust stability⁵⁻⁸. Small molecules can interact with the encapsulated cargo via surface pore openings that permit their diffusion in and out the nanocompartment^{4, 5, 9}. Additionally, encapsulins selectively package and protect cargo proteins tagged with an encapsulation signal peptide (ESig) that interacts with a highly conserved hydrophobic pocket located on the inner surface of the encapsulin subunits⁵. In most encapsulin systems, the ESig is found at the C-terminus of the cargo proteins, however, in iron-mineralizing encapsulin-associated Firmicute cargo systems a N-terminal ESig has been reported for the secondary cargo ferredoxin^{2, 5}. Overall, the ESig cargo-loading mechanism represents an interchangeable system for the programmed encapsulation of ESig-tagged cargo.

The modularity of encapsulin systems has caught the interest of the synthetic biology field to develop compartments that can perform specific metabolic processes. Efforts to achieve this have explored the encapsulation of foreign proteins including ESig-tagged enzymes, fluorescent, photoconvertible, photoactivatable and luminescent proteins¹⁰⁻¹³. Some encapsulin systems (e.g. *Myxococcus xanthus*) co-encapsulate multiple cargo, a process that has been mimicked using complementary 'split' fluorescent protein fragments^{6, 13, 14}. Additionally, successful attempts have been reported to reprogram encapsulin into catalytically active nanoreactors. For example, the polymerization of

diaminobenzidine (DAB) for electron microscopy (EM) has been achieved by encapsulation of the engineered peroxidase APEX2¹³. Moreover, an orthogonal encapsulin-based melanosome was constructed via encapsulation of a melanin-generating tyrosinase. These bioengineered melanosomes reduced the melanin cytotoxicity in mammalian cells and showed potential as novel contrast agents in photoacoustic tomography¹³.

Photosensitizers are molecules that upon light activation undergo a photochemical reaction that converts oxygen (O_2) into highly toxic reactive oxygen species (ROS) e.g. superoxide radical ($O_2^{\cdot-}$), hydrogen peroxide (H_2O_2), and singlet oxygen (1O_2)¹⁵. The red fluorescent protein KillerRed (KR) is a biological photosensitizer that can be activated with green and yellow light (520-590 nm) to generate ROS¹⁶. KR was derived by directed evolution of the green fluorescent protein (GFP) homolog hydrozoan chromoprotein anm2CP found in *Anemonia sulcata*¹⁷. The minimal ROS-generating activity of conventional fluorescent proteins has been attributed to the presence of a rigid β -barrels which encases the chromophore, providing a cage-like structure that significantly restricts the generation of ROS¹⁸. In comparison, KR has a water-filled channel that extends along its β -barrel towards its chromophore, which has been proposed to allow oxygen (O_2) and ROS diffusion in and out of the protein¹⁹. In general, KR is believed to act as a Type I photosensitizer, which primarily generates the $O_2^{\cdot-}$. However, KR production of 1O_2 has also been reported^{16, 20}. $O_2^{\cdot-}$ is the product of the one-electron reduction of O_2 , which is not considered to be a good oxidant nor a good reductant, due to its low rate constant values²¹. However, biological consequences of $O_2^{\cdot-}$ are indirect since it can generate highly reactive secondary ROS such as H_2O_2 , hydroxyl radical (OH^{\cdot}), hypochlorous acid (HOCl) and peroxynitrite (ONO_2^-)^{21, 22}. $O_2^{\cdot-}$ (and secondary ROS) generated by light-activated KR can oxidize nearby molecules, in a process known as 'photosensitization'. This photosensitizing function has been employed in different applications including; chromophore-assisted light inactivation (CALI) of proteins²³, spatiotemporal optogenetic ablation of specific cell types (e.g. zebra fish kidney cells)²⁴, photodynamic therapy (PDT) of cancer²⁵ and ROS-activated DNA damage studies²⁶.

In this study, we engineered a light-activated ROS-generating nanocompartment via the encapsulation of an N-terminally ESig-tagged version of KR inside the encapsulin from the bacterium *Thermotoga maritima*. The resulting KR-loaded encapsulin was soluble, monodisperse and fluorescent. Encapsulation of KR did not disturb KR's fluorescence properties or its capacity to generate ROS. Further development of this technology could allow their use as photosensitizing nanoreactors for ROS-activated applications in biotechnology and biomedicine.

Materials and methods

Materials

Most reagents were purchased from Sigma-Aldrich unless stated otherwise. HEPES-free acid was purchased from Chem-Supply Pty. Restriction enzymes and competent *Escherichia coli* cells were purchased from New England Biolabs unless stated otherwise. Chromatography columns were purchased from GE Healthcare, USA unless stated otherwise. Protein purification was performed on Äkta™ start or Äkta™ pure chromatography systems (GE Healthcare, USA).

Molecular biology and cloning

All inserts were codon optimized for expression in *E. coli* and custom synthesized as gBlock Gene Fragments (Integrated DNA Technologies). A surface-exposed loop region between residues 138 and 139 of the *Thermotoga maritima* (Uniprot: Q9WZP3) encapsulin was modified with a hexahistidine tag (GGGGGGHHHHHHGGGGGG) as previously described²⁷. To selectively encapsulate the KillerRed (KR)¹⁷ cargo within his-tagged encapsulin (Enc), the KR was C- or N-terminally tagged with either *T. maritima* cargo encapsulation signal (LFTDKPITEIEEETSGGSENTGGDLGIRKL)¹⁰ (ESig) or a peptide linker (L) (SGLRSRAE) positioned between the cargo protein and the ESig²⁸. To generate expression vectors, Enc was ligated into plasmid pETDuet-1 (Merck) via NcoI/BamHI restriction sites, while all KR constructions were inserted into pACYC-Duet-1 (Merck) via NdeI/BglII restriction sites. *E. coli* α -Select (Bioline) was used as a host for general gene cloning. Gene insertion was verified by performing PCR using the primer pairs pETUpstream/DuetDOWN or DuetUP2/T7 Terminator (Merck) with Enc- or cargo-containing plasmid constructs, respectively. All gene

constructions used in this study are summarized in Supplementary Table 1. *E. coli* T7 Express lysY/lq cells were used for recombinant protein expression of KR variants. For the single expression of Enc and the co-expression of Enc and its intended cargo protein, *E. coli* BL21 (DE3) cells were co-transformed with the appropriate plasmids, and the resulting transformants were selected on Luria–Bertani (LB) agar supplemented with carbenicillin (100 µg/ml) and chloramphenicol (50 µg/ml).

Protein expression and purification

Small-scale protein expression

To pre-evaluate the single expression of KR variants and their co-expression with Enc, 10 ml LB supplemented with carbenicillin (100 µg/ml), chloramphenicol (50 µg/ml) or both (1:100) was inoculated with an overnight culture of cells harboring the expression plasmid(s) of interest. Cells were grown aerobically at 37 °C to an optical density at 600 nm (OD₆₀₀) of 0.4-0.6. Protein synthesis was induced by the addition of 0.05 mM isopropyl-β-D-thiogalactopyranoside (IPTG) and the cultures were then cultivated at 27 °C for 24 h in the dark. Next, cells were harvested by centrifugation (10,000 x g 15 min, 4 °C) and stored at -30 °C until further use. To check the production of the protein of interest, cell pellets were resuspended in 1 mL of 100 mM HEPES buffer pH 7.4 with 1 U/mL of Benzonase® nuclease and then lysed by glass beads using a cell disruptor. Afterwards, glass beads were spun down at 100 x g for 30 sec and the resulting supernatant was transferred to a new tube. The cell lysate was spun down again at 13,000 x g for 5 min, to separate the cell debris (insoluble fraction) from the soluble fraction. Additionally, the encapsulated KR variants were partially purified by nickel-immobilized metal affinity chromatography (IMAC) with the Ni-NTA Fast Start Kit (QIAGEN) following manufacturer's recommendations. The soluble and insoluble fractions and partially purified proteins were subjected to SDS-PAGE analysis. The fluorescence in the fractions was observed in a Safe Imager™ 2.0 Blue Light Transilluminator (ThermoFisher Scientific).

Large-scale protein expression and purification

For the large-scale single expression of Enc and its co-expression with N-terminally ESig-Linker tagged KR (ESig-L-KR), 500 ml of LB (1:100) LB supplemented with carbenicillin (100 µg/ml), chloramphenicol (50 µg/ml) or both was inoculated with an overnight culture of cells harboring the expression plasmid(s) of interest. Cells were grown aerobically at 37 °C to an optical density OD₆₀₀ 0.4-0.6. Protein synthesis was induced by the addition of 0.05 mM IPTG and cultures were grown at 30 °C for 20-24 h. Finally, cells were harvested by centrifugation (10,000 x g 15 min, 4 °C) and stored at -30 °C until further use.

For the purification of Enc and Enc-ESig-L-KR, the pellet from a 500 mL culture was resuspended in 50 mL lysis buffer (20 mM NaH₂PO₄, 300 mM NaCl, 40 mM imidazole, 1 U/mL Benzonase® nuclease, pH 7.4). Cells were lysed via three passages through a of French pressure cell and subsequently centrifuged at 10,000 x g for 15 min. The lysate was purified by (IMAC) using a HisPrep™ Fast Flow 16/10 column in equilibration buffer (20 mM NaH₂PO₄, 300 mM NaCl, 40 mM imidazole, pH 7.4). Enc eluted at 400 mM imidazole while Enc-ESig-L-KR eluted at 260 mM imidazole. Next, the eluted fractions were concentrated using Amicon® Ultra-15 centrifugal filter units (Merck, USA) with a 100 KDa cut-off, followed by dilution in 7 mL of 50 mM HEPES buffer pH 7.4. A second purification step by size exclusion chromatography (SEC) was subsequently performed using a HiPrep™ 26/60 Sephacryl® S-500 HR column in 100 mM HEPES buffer.

For the purification of free ESig-L-KR, the unbound fraction obtained during the IMAC purification of Enc-ESig-L-KR was used. Herein, a saturated solution of ammonium sulphate was added to a final concentration of 30% (v/v), incubated on ice for 30 min and spun down at 10,000 x g for 15 min. Next, ammonium sulphate was added to the supernatant to a final concentration of 50% (v/v) and precipitation occurred under the conditions detailed above. The precipitated protein was resuspended in 20 mM L-histidine buffer (pH 5.7) and subjected to SEC using a HiPrep™ 16/60 Sephacryl® S-400 HR column in 20 mM L-histidine buffer. The fractions containing free ESig-L-KR were pooled and further purified by anion exchange chromatography using a Hitrap Q HP 5 mL column. The protein was eluted with a step method at 250 mM NaCl. The fraction containing free ESig-L-KR

was concentrated and buffer exchange (100 mM HEPES buffer) using Amicon Ultra-15 centrifugal filter units with a 30 KDa cut-off. The final protein concentrations were determined by measuring absorbance at 280 nm. Examples of purification chromatographs are provided in Supplementary Fig. 1.

Polyacrylamide gel electrophoresis (PAGE)

The Bio-Rad mini-protean system (Bio-Rad laboratories) was used for all SDS-PAGE and Native-PAGE analysis. For SDS-PAGE, samples were diluted in 2X Laemmli sample buffer with 50 mM 1,4-dithiothreitol, heated at 95 °C for 5 min, loaded into pre-cast Bio-Rad Mini-PROTEAN® TGX™ gels (4-15%) and run at 200V for 30 min. For Native-PAGE, samples were diluted in 4X native sample buffer (200 mM Tris-HCl pH 6.8, 40% glycerol, and 0.08% bromophenol blue), loaded into pre-cast Bio-Rad Mini-PROTEAN® TGX™ gels (4-20%) and run at 200V for a minimum of 2 h. In-gel fluorescence of proteins was observed on a G-BOX gel documentation system (Syngene). All gels were stained following the Coomassie G-250 safe stain protocol²⁹. The densitometric intensity of protein bands was quantified using ImageJ software (NIH) and was used to calculate protein purity³⁰.

Transmission electron microscopy (TEM)

10 µL of Enc or Enc-ESig-L-KR variant (~100 µg/ml) was adsorbed onto formvar-carbon coated copper grids for 2 min and negatively stained with uranyl acetate replacement stain (UAR-EMS) for 1 h. Grids were then washed with ultrapure water and allowed to dry for 15 min. Finally, the grids were observed under a Philips CM10 TEM operated at 100 kV accelerating voltage.

Dynamic light scattering (DLS)

DLS data was collected on a Malvern Nano ZS90 Zetasizer. Measurements were carried out at room temperature (RT) using standard cuvettes containing 1 ml of Enc or Enc-KR diluted in 100 mM HEPES (pH 7.4) to a final concentration 0.2-0.4 mg/ml. The signal was averaged over 13 readings each lasting 30 s.

Absorbance and fluorescence spectrometry

The fluorescence excitation and emission spectra of encapsulated and free ESig-L-KR were obtained on a Cary Eclipse Fluorescence Spectrophotometer (Agilent

Technologies) or Fluorolog® (Horiba) using quartz cuvettes. The standard curve of free ESig-L-KR fluorescence was measured on a PHERAstart FS (BMG Labtech) microplate reader (excitation/emission= 585/620 nm).

ROS detection

ROS generation by free and encapsulated ESig-L-KR and unloaded Enc was detected in solution with the fluorescent probe 2',7'-dichlorodihydrofluorescein diacetate (DCFH-DA). To measure ROS *in vitro*, DCFH-DA needs to be deacetylated. Accordingly, 2 mM DCFH-DA solution (ethanol), was diluted 1:5 in 10 mM NaOH and incubated at RT for 30 min. The solution was then neutralized by diluting in 100 mM HEPES buffer and used immediately for ROS measurement. The reaction mixture contained: ~353 nM of free ESig-L-KR or corresponding Enc-ESig-L-KR (in 100 mM HEPES buffer pH 7.5). Reaction mixtures were irradiated with a Chameleon-Ultra II laser (Coherent) set at 520 nm with a power density of ~35 mW/cm² for 10 min. Right after irradiation, DCFH-DA was added to the reaction mixture to a final concentration of 5 µM and left to incubate at RT for 15 min. The fluorescence signal from the oxidized DCFH-DA (excitation/emission = 485/520 nm) was measured on a PHERAstart FS (BMG Labtech) microplate reader.

Results

Engineering encapsulin into a light-activatable ROS generator

With the aim of bioengineering a light-activatable nanocompartment to produce reactive oxygen species (ROS), we decided to engineer the encapsulin (Enc) from *Thermotoga maritima* (*Tm*) to contain red fluorescent protein KillerRed (KR)¹⁷. To direct its selective encapsulation inside encapsulin, KR was initially C-terminally tagged with the *Tm* encapsulation signal (ESig)¹⁰ to produce a KR-ESig construct. The small-scale expression KR-ESig showed low expression in BL21 (DE3) *E. coli* cells (Supplementary Fig.2), which may have been the result of protein toxicity or incorrect folding induced by the C-terminal ESig. To address this, we decided to use an alternative *E. coli* strain (pLysY/lq) that tightly regulates the expression of the target protein. To help mitigate any misfolding effects, three additional KR variants with altered ESigs were also designed. Specifically, we first elected to introduce a flexible peptide linker (L) region, between the C-terminus of the KR and

the ESig (KR-L-ESig). This peptide linker (SGLRSRAE) was previously incorporated between KR and a targeting antibody to avoid any steric hindrance between the two proteins²⁵. Secondly, given that KR's C-terminus is near its dimerization domain, we appended an ESig at its N-terminus, with or without a separating linker region (ESig-KR and ESig-L-KR)²⁵ (Fig.1A). This position is opposite to that of the ESig in the native *Tm* encapsulin system, which is located at the C-terminus of its cargo proteins⁵. SDS-PAGE verified the expression of N- or C-terminally ESig-tagged KR with (ESig-L-KR = 30.6 KDa) and without (ESig-KR = 29.7 KDa) the linker (Fig. 1C). However, when observed under blue light, KR-L-ESig showed no fluorescence, KR-ESig displayed minimal fluorescence, while both ESig-KR and ESig-L-KR exhibited the expected red fluorescence (data not shown). Consequently, ESig-KR ESig-L-KR were each co-expressed with Enc in *E. coli* BL21(DE3). This approach was required as *E. coli* pLysY/lq cannot express plasmids carrying a chloramphenicol selection marker (i.e. pACYC-Duet-Enc). SDS-PAGE analysis indicated that the both KR variants were successfully co-expressed with Enc (Enc_{Subunit} = 31.9 kDa) (Fig. 1D). This finding was supported by the fact that protein lysates presented red fluorescence under blue light (data not shown).

To verify the encapsulation of ESig-KR and ESig-L-KR inside Enc, soluble cell lysates from each co-expression were subjected to IMAC purification (Fig. 1E) and the fluorescence of the purified fractions determined (Fig. 1F). As shown in Figure 1E, the purified fraction of Enc-ESig-L-KR exhibited a strong protein band on SDS-PAGE, which most likely contained both the Enc_{Subunit} and ESig-L-KR, due to their almost identical molecular weights (differ by only 1.3 KDa). Additionally, the Enc-ESig-L-KR purified fraction showed the expected red fluorescence (Fig. 1F). In contrast, the purified fraction of Enc-ESig-KR showed a thin protein band on the SDS-PAGE and no observable fluorescence (Fig. 1E and F). These results suggest that the N-terminal ESig allows KR to retain its fluorescent properties, but encapsulation is only achieved when a flexible linker region is positioned between KR and the N-terminal ESig.

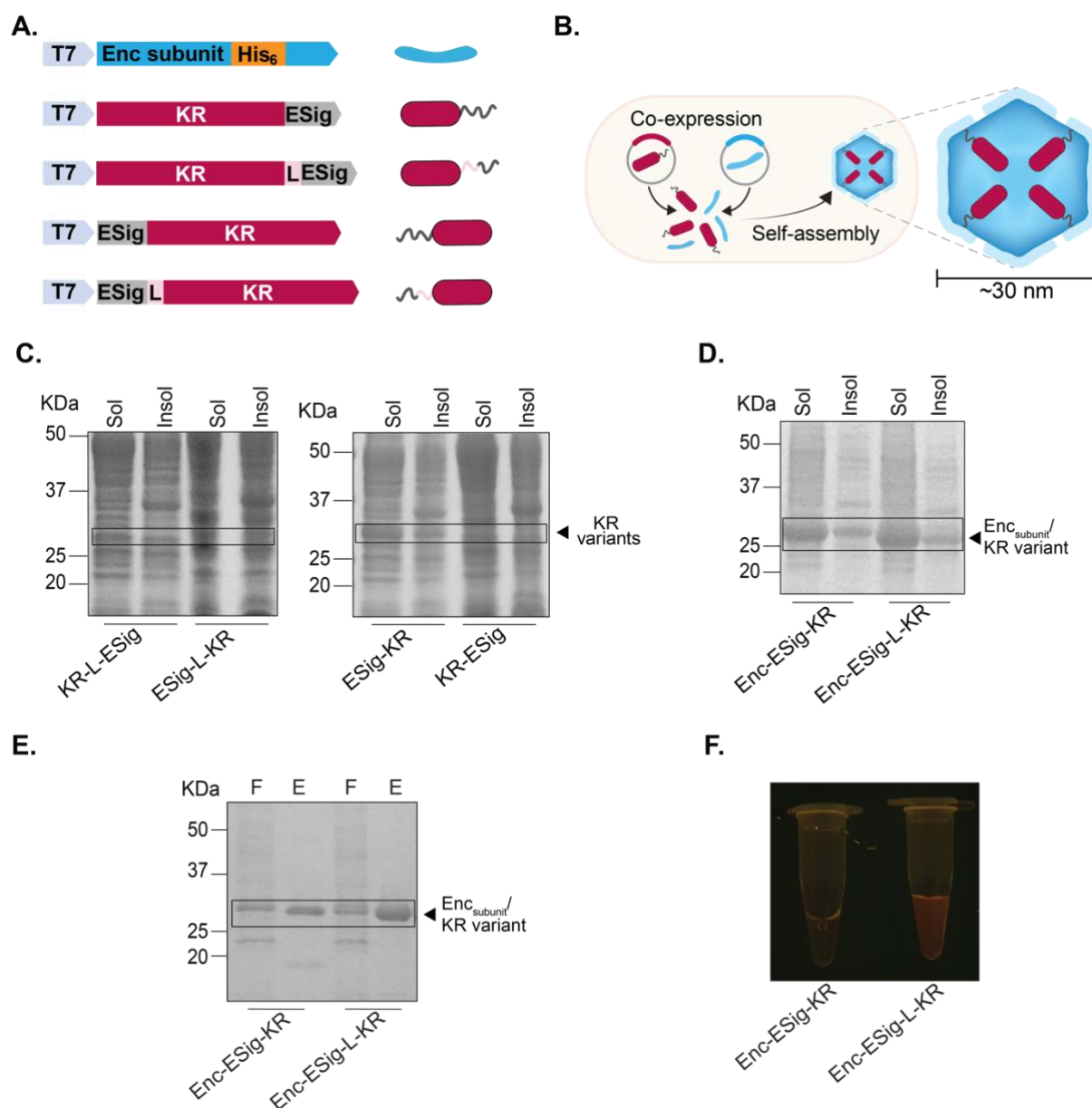


Fig. 1. Design and production of KR-loaded encapsulins (Enc-KRs). **A.** Genetic constructions encoding the Enc_{subunit} from *Thermotoga maritima* (blue) displaying a His-tag within a surface-exposed loop region (yellow); and KR (Red) C- or N-terminally tagged with an encapsulation signal (ESig) (with or without a peptide linker (L)). **B.** Heterologous co-expression of encapsulin subunits and ESig-tagged cargo proteins in *E. coli* leads to the *in vivo* self-assembly of cargo-loaded encapsulin nanocompartments. **C.** SDS-PAGE analysis of KR variants expression in *E. coli* T7 Express lysY/lq cells. **D.** SDS-PAGE analysis of KR-Encs expression in *E. coli* BL21 (DE3). **C.** and **D.** After cell lysis the soluble proteins (Sol) and cell debris (Insol) were observed via Coomassie-stained SDS-PAGE. **E.** SDS-PAGE analysis of encapsulated ESig-KR and ESig-L-KR purified by IMAC. **F.** Fluorescence of IMAC purified Enc-ESig-KR and Enc-ESig-L-KR.

Biophysical characterization of encapsulated KillerRed

Next, we sought to further characterize the self-assembly, fluorescence and cargo loading of Enc-ESig-L-KR. To achieve this, empty Enc and ESig-L-KR (free and encapsulated) were each purified by chromatographic techniques (see “Materials and Methods”), resulting in highly pure proteins (90-99%) as verified by SDS-PAGE (Fig. 2a). Under native-PAGE conditions, empty Enc and Enc-ESig-L-KR presented high molecular weight bands consistent with the self-assembly of encapsulin nanocompartments (Fig. 2B, left panel). The photoactivation of the native-PAGE gel showed in-gel fluorescence corresponding to free and encapsulated ESig-L-KR (Fig. 2B, right panel), which was further supported by fluorescence spectroscopy of the purified samples (Fig. 2D). No fluorescence was observed in unloaded Enc samples. Both free and encapsulated ESig-L-KR exhibited a broad excitation band with a shoulder at ~548 nm and an excitation maximum (Ex_{max}) of ~583 nm, and a narrow emission band with a peak (Em_{max}) at ~610 nm (Fig. 2d). This is in agreement with the reported Ex_{max}/Em_{max} for KR (585 nm/610 nm) ²³. These results suggest that the addition of the ESig-L sequence at the N-terminus of the protein and its subsequent encapsulation does not affect the KR’s fluorescent properties.

The self-assembly, morphology and size of the Enc-ESig-L-KR nanocompartments was validated further by transmission electron microscopy (TEM) observations and dynamic light scattering (DLS) measurements. TEM images of negatively-stained samples presented the correct auto-assembly of Enc-ESig-L-KR and empty Enc into spherical nanocompartments (Fig. 2C). DLS measurements of empty Enc revealed a mean hydrodynamic diameter of 30.5 ± 10.8 nm (Fig. 2c) with a monodisperse size distribution. This coincides with the enlargement observed by Moon et al, who observed a slightly larger size (from ~24 nm to 29.1 nm) for *Tm* encapsulin engineered to externally display cell-targeting peptides within the 138-139 loop region ^{10, 27}. Moreover, DLS measurements revealed that Enc-ESig-L-KR was intact and monodisperse with a diameter of 35.6 ± 5.1 nm (Fig. 2c), lying within the measured size distribution of empty Enc. Next, we used the fluorescence intensity of ESig-L-KR to estimate the cargo loading capacity (LC%) and the number of cargo molecules per nanocompartment. This approach was employed because conventional protein gel densitometric analysis was ineffective due to the close molecular weight presented by Enc_{Subunit} and ESig-L-KR on SDS-PAGE (Fig. 2A).

The standard curve of fluorescence vs protein concentration of free ESig-L-KR shown in Figure 2E allowed to estimate a LC% of 5% which translates into ~4 molecules of ESig-L-KR per nanocompartment. The loading of KR is slightly lower than the that reported for a structurally similar fluorescent protein (superfolder GFP) which was found to encapsulate $\sim 7 \pm 2$ molecules per encapsulin nanocompartment

10.

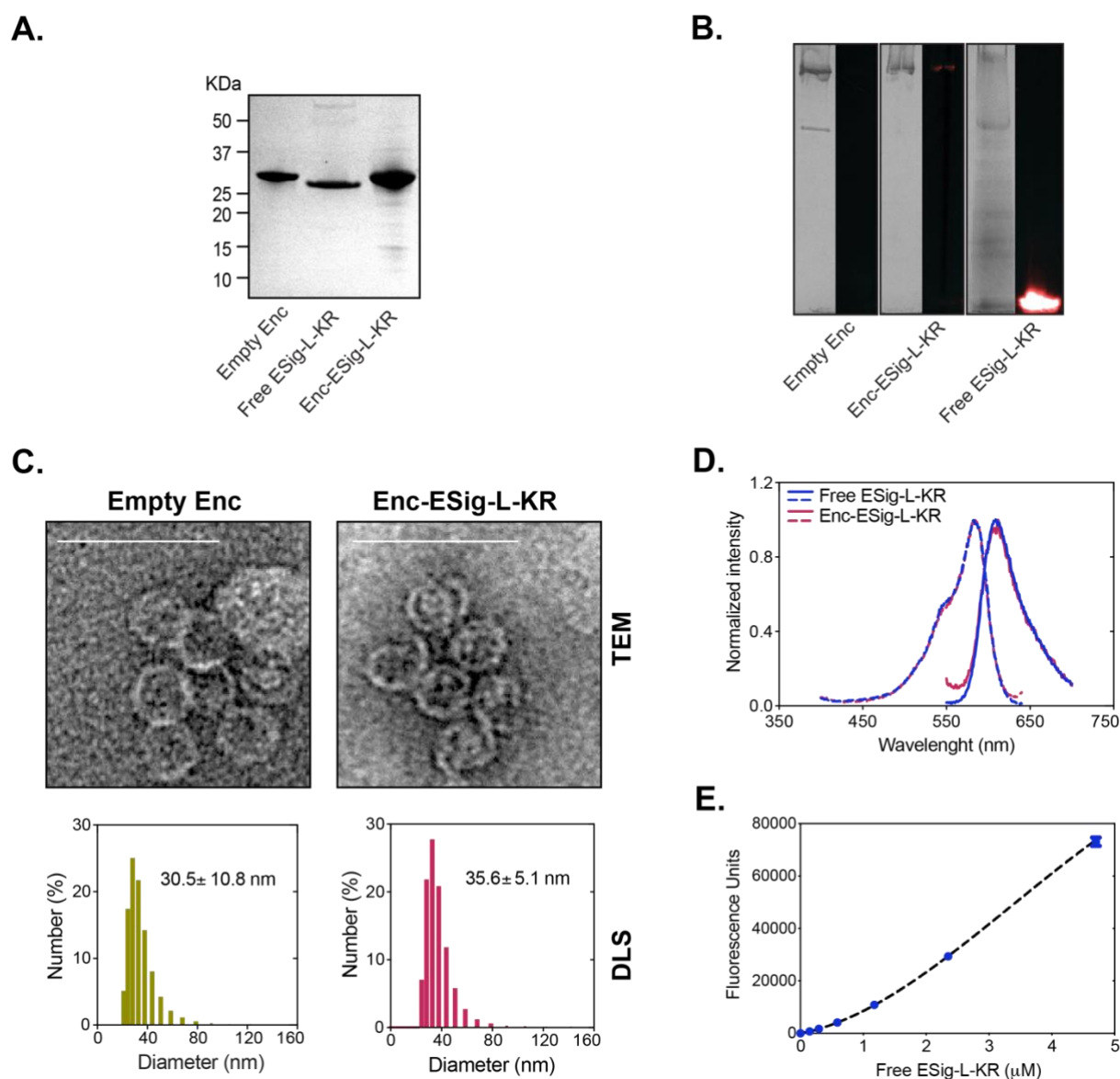


Fig. 2. Biophysical characterization of ESig-L-KR. **A.** Coomassie-stained SDS-PAGE showing the purification and co-purification of the EncSubunit (31.9 KDa) and ESig-S-KR (32.9 KDa) cargo proteins. **B.** Native-PAGE of SEC purified Empty Enc, Enc-ESig-L-KR and free Enc-ESig-L-KR. **(Left panel)** Coomassie-stained gel verifying the self-assembly of Enc-ESig-L-KR into cargo-loaded nanocompartments. **(Right panel)** The in-gel fluorescence confirming the encapsulation of fluorescent ESig-L-KR cargo. **C. (Upper panel)** TEM images of empty Enc and ESig-L-KR show their self-assembly into spherical nanocompartments (Scale bars = 50 nm). **(Lower panel)** size distributions measured by DLS indicate that their diameters range between ~30 and 36 nm. **D.** Fluorescence excitation (dash line) and emission (solid line) spectra of free and encapsulated ESig-L-KR. **E.** Standard curve: fluorescence vs. Concentration of free ESig-L-KR third polynomial regression: $Y = -12.30 + 4554x + 4421x^2 + (-436.3x^3)$ for calculation of the ESig-L-KR loading inside encapsulin.

Production of ROS by encapsulated KillerRed (KR)

Encapsulin surface pores allow the selective flow of small substrates in and out its inner cavity. Thus, we assumed that molecular oxygen (O_2) can flow inside the internal cavity of the nanocompartment and interact with the encapsulated ESig-L-KR cargo. Under green light activation, KR converts O_2 into ROS, which then diffuses out of the same open surface pores (Fig. 3A). To evaluate the photoactivated generation of ROS by Enc-ESig-L-KR we used the 2'-7'-dichlorofluorescein diacetate (DCFH-DA) fluorometric assay. ROS readily oxidizes DCFH-DA, converting it into highly fluorescent 2'-7'-dichlorofluorescein (DHF) with Ex_{max}/Em_{max} of 504/529 nm. This emission is proportional to the amount of ROS³¹. The samples were exposed to green light irradiation (35 mW/cm² for 10 min) at 520 nm, then DCFH-DA was added to a final concentration of 5 μ M and the DHF formed was measured at 485/520 nm (excitation/emission). Fig. 3B shows the ROS production after irradiation with green light. As expected, empty Enc did not generate ROS under laser irradiation. In contrast, both Enc-ESig-L-KR and free ESig-L-KR generated significant amounts of ROS. Interestingly, the levels of ROS produced by free and encapsulated ESig-L-KR were highly similar, indicating that the encapsulation of KR within encapsulin nanocompartments does not have a negative effect on its ROS-generating function.

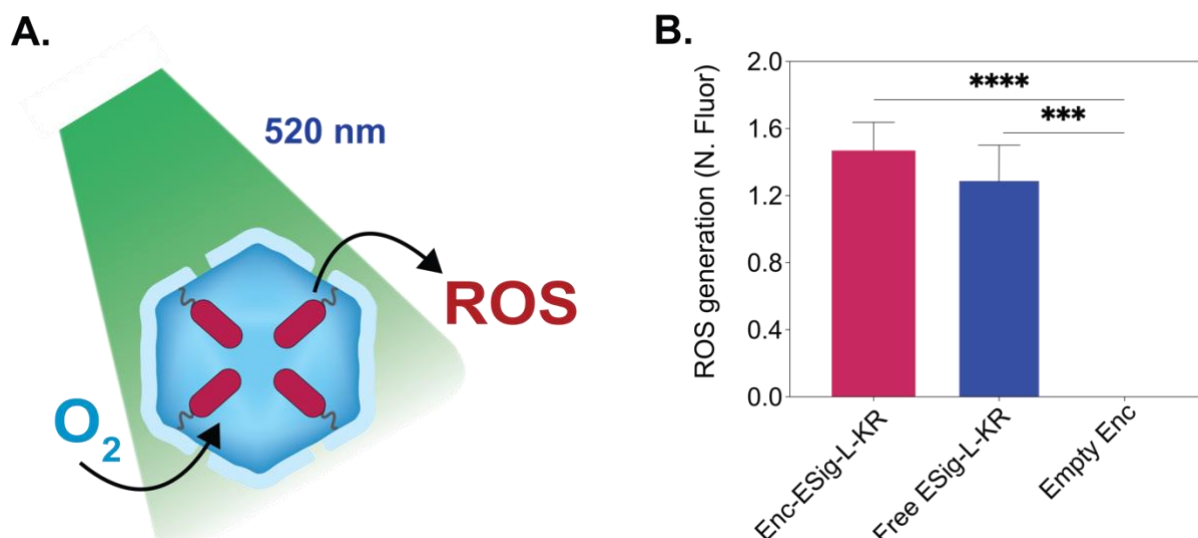


Figure 3. The light-activated ROS generation by ESig-L-KR loaded encapsulin (Enc-ESig-L-KR). **A.** Illustration showing the generation of ROS by a light-activated Enc-ESig-L-KR nanocompartment. In this process, molecular oxygen (O_2) enters the internal cavity of the nanocompartment via open surface pores where it interacts with encapsulated ESig-L-KR. Upon irradiation with green laser light, the ESig-L-KR cargo converts O_2 (substrate) into ROS (product), which subsequently diffuses out of the same open surface pores. **B.** ROS production from encapsulated and free ESig-L-KR and unloaded Enc upon irradiation with a green laser (520 nm) at ~ 34 mW/cm 2 for 10 min. ROS production was determined by the accumulated fluorescence intensity of oxidized DCFH-DA, with the fluorescence intensity of each reaction normalized to the intrinsic fluorescence of each protein (N. Fluor). Error bars represent the mean \pm standard deviation (** $p < 0.001$, **** $p \leq 0.0001$), one-way ANOVA, Tukey, $n \geq 3$.

Discussion

In this work, we successfully encapsulated the fluorescent photosensitizing protein KillerRed inside encapsulin nanocompartments. We also demonstrated that *Tm* ESig with a C-terminal linker peptide inserted on the N-terminal of KR allows the successful loading of the protein inside encapsulin. Additionally, we confirmed that encapsulated ESig-L-KR exhibits almost identical fluorescent properties and ROS-generating functions as its free counterpart.

In nature, the *Tm* ESig is found on the C-terminus of its cargo protein (i.e. ferritin-like protein). Thus, our first approach to achieve encapsulation was to insert the ESig to the C-terminal of KR. This resulted in minimal expression of the protein and no fluorescence was observed. We used fluorescence as an indication of the proper protein expression and folding, which can obviously affect KR's ROS-generating

functionality. A peptide linker was introduced between KR and the ESig to avoid steric hindrance and improve the folding ESig and KR. Although addition of this linker resulted in slightly improved protein expression, no fluorescence was observed. This could be explained by the structure of KR. In its native form, KR tends to dimerize into a homodimer composed of two monomers, A and B. It has been proposed that monomer B remains in a green-emitting state, while most monomer A chromophores mature to the red fluorescent state. Thus, the fluorescence emitted by KR is due to the fluorescence resonance energy transfer (FRET) that occurs from monomer B to A upon light excitation ¹⁷. The dimerization of KR could be disturbed by changes at the C-terminus of the protein monomer, given that the C-terminal region of one monomer interacts with the cylindrical surface of its counterpart, contributing to the stability of the interface between monomers ¹⁶. Therefore, the insertion of a C-terminal ESig in our initial studies might have hampered the structure and/or formation of the KR homodimer, causing low expression and a loss of fluorescence. As an alternative, the ESig was moved to the N-terminus of the protein with or without the addition of the peptide linker. These two KR variants (ESig-KR and ESig-L-KR) showed the expected red fluorescence and were successfully co-expressed with Enc. Upon IMAC purification it seemed that the presence of the linker increased the loading of the KR inside Enc as N-terminally ESig-tagged KR without the linker did not show signs of encapsulation, but ESig-L-KR did. In this case, the peptide linker most likely help expose the ESig allowing it to selectively interact with hydrophobic binding pockets on the inner surface of the Enc ⁵. It is worth noting that to the extent of our knowledge, the use of N-terminal ESigs to mediate the encapsulation of foreign proteins has not been reported for the *Tm* encapsulin system ^{10, 32}. Our results consequently open the door for the encapsulation of proteins that have functional modules near their C-terminus, which includes other biological photosensitizers e.g. KillerOrange ³³.

One of the structural features that permit the generation of ROS in KR is the presence of a funnel-shaped channel that extends from the chromophore all the way to the bottom of the β -barrel. Due to its composition, this channel is believed to allow the access and/or storage of oxygen while simultaneously facilitating the exit of ROS (mainly O₂^{•-}) produced by electron transfer to from KR's excited chromophore to O₂ (Type I photoconversion) ^{16, 18}. Our study showed that after the encapsulation of

ESig-L-KR, its fluorescent properties and ROS generation remained almost the same as free ESig-L-KR. This might indicate that during encapsulation, the KR's chromophore and its funnel-shaped channel did not undergo any structural changes that affected their functionality. The results also suggest that the loading inside encapsulin did not disrupt the dimerization of the ESig-L-KR, which is consistent with the native ability of encapsulins to load multimeric cargo proteins such as decameric FLPs ⁵.

These findings, while preliminary, show that KR-loaded Enc is functional as a light-activatable ROS-generator and that further development of this technology could lead to the construction of an encapsulin-based delivery system for KR. The ROS generated by this technology can interact (oxidize) with nearby molecules in a process known as 'photosensitization'. Thus, this technology has the potential to be utilized as a photosensitizing platform for a range of applications. For example, the platform could be useful for photodynamic therapy (PDT) of cancer, given that KR has been reported to have phototoxicity against cancer cells (e.g. breast cancer and leukemia cells) ^{25, 34}. Similarly, the light-induced production of ROS by encapsulated KR could be explored for photodynamic inactivation or antimicrobial PDT, which is a novel approach to combat pathogenic microorganism, this could be applied in the treatment of bacterial and wound infections ^{35, 36}. Additionally, to extend the properties of Enc as a ROS-producing nanocompartment, other KR variants that exhibit different light activation wavelengths such as KillerOrange or are slightly better at type II photoconversion (production $^1\text{O}_2$) such as the monomeric SuperNova could be loaded inside Enc ^{33, 37}.

References

1. Murat, D.; Byrne, M.; Komeili, A., Cell biology of prokaryotic organelles. *Cold Spring Harbor Perspective Biology* **2010**, 2 (10), a000422-a000422.
2. Giessen, T. W.; Silver, P. A., Widespread distribution of encapsulin nanocompartments reveals functional diversity. *Nature microbiology* **2017**, 2, 17029.
3. Contreras, H.; Joens, M. S.; McMath, L. M.; Le, V. P.; Tullius, M. V.; Kimmey, J. M.; Bionghi, N.; Horwitz, M. A.; Fitzpatrick, J. A.; Goulding, C. W., Characterization of a Mycobacterium tuberculosis nanocompartment and its potential cargo proteins. *The Journal of Biological Chemistry* **2014**, 289 (26), 18279-89.
4. He, D.; Hughes, S.; Vanden-Hehir, S.; Georgiev, A.; Altenbach, K.; Tarrant, E.; Mackay, C. L.; Waldron, K. J.; Clarke, D. J.; Marles-Wright, J., Structural characterization of encapsulated ferritin provides insight into iron storage in bacterial nanocompartments. *eLife* **2016**, 5.
5. Sutter, M.; Boehringer, D.; Gutmann, S.; Gunther, S.; Prangishvili, D.; Loessner, M. J.; Stetter, K. O.; Weber-Ban, E.; Ban, N., Structural basis of enzyme encapsulation into a bacterial nanocompartment. *Nature Structural & Molecular Biology* **2008**, 15 (9), 939-47.
6. McHugh, C. A.; Fontana, J.; Nemecek, D.; Cheng, N.; Aksyuk, A. A.; Heymann, J. B.; Winkler, D. C.; Lam, A. S.; Wall, J. S.; Steven, A. C.; Hoiczky, E., A virus capsid-like nanocompartment that stores iron and protects bacteria from oxidative stress. *Embo Journal* **2014**, 33 (17), 1896-911.
7. Giessen, T. W.; Orlando, B. J.; Verdegaaal, A. A.; Chambers, M. G.; Gardener, J.; Bell, D. C.; Birrane, G.; Liao, M.; Silver, P. A., Large protein organelles form a new iron sequestration system with high storage capacity. *eLife* **2019**, 8, e46070.
8. Sigmund, F.; Pettinger, S.; Kube, M.; Schneider, F.; Schifferer, M.; Schneider, S.; Efremova, M. V.; Pujol-Martí, J.; Aichler, M.; Walch, A.; Misgeld, T.; Dietz, H.; Westmeyer, G. G., Iron-Sequestering Nanocompartments as Multiplexed Electron Microscopy Gene Reporters. *ACS Nano* **2019**, 13 (7), 8114-8123.
9. Rahmanpour, R.; Bugg, T. D. H., Assembly in vitro of Rhodococcus jostii RHA1 encapsulin and peroxidase DypB to form a nanocompartment. *The FEBS Journal* **2013**, 280 (9), 2097-2104.
10. Cassidy-Amstutz, C.; Oltrogge, L.; Going, C. C.; Lee, A.; Teng, P.; Quintanilla, D.; East-Seletsky, A.; Williams, E. R.; Savage, D. F., Identification of a Minimal Peptide Tag for in Vivo and in Vitro Loading of Encapsulin. *Biochemistry* **2016**, 55 (24), 3461-8.
11. Rurup, W. F.; Snijder, J.; Koay, M. S. T.; Heck, A. J. R.; Cornelissen, J. J. L. M., Self-Sorting of Foreign Proteins in a Bacterial Nanocompartment. *Journal of the American Chemical Society* **2014**, 136 (10), 3828-3832.
12. Tamura, A.; Fukutani, Y.; Takami, T.; Fujii, M.; Nakaguchi, Y.; Murakami, Y.; Noguchi, K.; Yohda, M.; Odaka, M., Packaging guest proteins into the encapsulin nanocompartment from Rhodococcus erythropolis N771. *Biotechnology and Bioengineering* **2015**, 112 (1), 13-20.
13. Sigmund, F.; Massner, C.; Erdmann, P.; Stelzl, A.; Rolbieski, H.; Desai, M.; Bricault, S.; Worner, T. P.; Snijder, J.; Geerlof, A.; Fuchs, H.; Hrabe de Angelis, M.; Heck, A. J. R.; Jasanoff, A.; Ntziachristos, V.; Plitzko, J.;

- Westmeyer, G. G., Bacterial encapsulins as orthogonal compartments for mammalian cell engineering. *Nature Communications* **2018**, 9 (1), 1990.
14. Lau, Y. H.; Giessen, T. W.; Altenburg, W. J.; Silver, P. A., Prokaryotic nanocompartments form synthetic organelles in a eukaryote. *Nature Communications* **2018**, 9 (1), 1311.
 15. Abrahamse, H.; Hamblin, Michael R., New photosensitizers for photodynamic therapy. *Biochemical Journal* **2016**, 473 (4), 347-364.
 16. Pletnev, S.; Gurskaya, N. G.; Pletneva, N. V.; Lukyanov, K. A.; Chudakov, D. M.; Martynov, V. I.; Popov, V. O.; Kovalchuk, M. V.; Wlodawer, A.; Dauter, Z.; Pletnev, V., Structural basis for phototoxicity of the genetically encoded photosensitizer KillerRed. *The Journal of Biological Chemistry* **2009**, 284 (46), 32028-39.
 17. Bulina, M. E.; Chudakov, D. M.; Britanova, O. V.; Yanushevich, Y. G.; Staroverov, D. B.; Chepurnykh, T. V.; Merzlyak, E. M.; Shkrob, M. A.; Lukyanov, S.; Lukyanov, K. A., A genetically encoded photosensitizer. *Nature Biotechnology* **2006**, 24 (1), 95-9.
 18. Carpentier, P.; Violot, S.; Blanchoin, L.; Bourgeois, D., Structural basis for the phototoxicity of the fluorescent protein KillerRed. *FEBS Letters* **2009**, 583 (17), 2839-2842.
 19. Roy, A.; Carpentier, P.; Bourgeois, D.; Field, M., Diffusion pathways of oxygen species in the phototoxic fluorescent protein KillerRed. *Photochemical & Photobiological Science* **2010**, 9 (10), 1342-50.
 20. Vegh, R. B.; Solntsev, K. M.; Kuimova, M. K.; Cho, S.; Liang, Y.; Loo, B. L.; Tolbert, L. M.; Bommaris, A. S., Reactive oxygen species in photochemistry of the red fluorescent protein "Killer Red". *Chemical Communications (Camb)* **2011**, 47 (17), 4887-9.
 21. Collin, F., Chemical Basis of Reactive Oxygen Species Reactivity and Involvement in Neurodegenerative Diseases. *International journal of molecular sciences* **2019**, 20 (10), 2407.
 22. Miller, A. F., 8.19 - Superoxide Processing. In *Comprehensive Coordination Chemistry II*, McCleverty, J. A.; Meyer, T. J., Eds. Pergamon: Oxford, 2003; pp 479-506.
 23. Bulina, M. E.; Lukyanov, K. A.; Britanova, O. V.; Onichtchouk, D.; Lukyanov, S.; Chudakov, D. M., Chromophore-assisted light inactivation (CALI) using the phototoxic fluorescent protein KillerRed. *Nature protocols* **2006**, 1 (2), 947-53.
 24. Buckley, C.; Carvalho, M. T.; Young, L. K.; Rider, S. A.; McFadden, C.; Berlage, C.; Verdon, R. F.; Taylor, J. M.; Girkin, J. M.; Mullins, J. J., Precise spatio-temporal control of rapid optogenetic cell ablation with mem-KillerRed in Zebrafish. *Scientific Reports* **2017**, 7 (1), 5096.
 25. Serebrovskaya, E. O.; Edelweiss, E. F.; Stremovskiy, O. A.; Lukyanov, K. A.; Chudakov, D. M.; Deyev, S. M., Targeting cancer cells by using an antireceptor antibody-photosensitizer fusion protein. *Proceedings of the National Academy of Sciences* **2009**, 106 (23), 9221-9225.
 26. Whitefield, D. B.; Spagnol, S. T.; Armiger, T. J.; Lan, L.; Dahl, K. N., Quantifying site-specific chromatin mechanics and DNA damage response. *Scientific Reports* **2018**, 8 (1), 18084.
 27. Moon, H.; Lee, J.; Min, J.; Kang, S., Developing genetically engineered encapsulin protein cage nanoparticles as a targeted delivery nanoplatform. *Biomacromolecules* **2014**, 15 (10), 3794-801.

28. Serebrovskaya, E. O.; Ryumina, A. P.; Boulina, M. E.; Shirmanova, M. V.; Zagaynova, E. V.; Bogdanova, E. A.; Lukyanov, S. A.; Lukyanov, K. A., Phototoxic effects of lysosome-associated genetically encoded photosensitizer KillerRed. *Journal of Biomedical Optics* **2014**, 19 (7), 071403.
29. Lawrence, A.-M.; Besir, H. U. S., Staining of proteins in gels with Coomassie G-250 without organic solvent and acetic acid. *Journal of visualized experiments* **2009**, (30), 1350.
30. Schneider, C. A.; Rasband, W. S.; Eliceiri, K. W., NIH Image to ImageJ: 25 years of image analysis. *Nature Methods* **2012**, 9 (7), 671-5.
31. Bourré, L.; Thibaut, S.; Briffaud, A.; Rousset, N.; Eléouet, S.; Lajat, Y.; Patrice, T., Indirect detection of photosensitizer ex vivo. *Journal of Photochemistry and Photobiology B: Biology* **2002**, 67 (1), 23-31.
32. Lagoutte, P.; Mignon, C.; Stadthagen, G.; Potisopon, S.; Donnat, S.; Mast, J.; Lugari, A.; Werle, B., Simultaneous surface display and cargo loading of encapsulin nanocompartments and their use for rational vaccine design. *Vaccine* **2018**, 36 (25), 3622-3628.
33. Sarkisyan, K. S.; Zlobovskaya, O. A.; Gorbachev, D. A.; Bozhanova, N. G.; Sharonov, G. V.; Staroverov, D. B.; Egorov, E. S.; Ryabova, A. V.; Solntsev, K. M.; Mishin, A. S.; Lukyanov, K. A., KillerOrange, a Genetically Encoded Photosensitizer Activated by Blue and Green Light. *PLOS ONE* **2015**, 10 (12), e0145287.
34. Yuan, M.; Liu, C.; Li, J.; Ma, W.; Yu, X.; Zhang, P.; Ji, Y., The effects of photodynamic therapy on leukemia cells mediated by KillerRed, a genetically encoded fluorescent protein photosensitizer. *BMC Cancer* **2019**, 19 (1), 934.
35. Sperandio, F. F.; Huang, Y. Y.; Hamblin, M. R., Antimicrobial photodynamic therapy to kill Gram-negative bacteria. *Recent Patents on Anti-infective Drug Discovery* **2013**, 8 (2), 108-20.
36. Hamblin, M. R., Antimicrobial photodynamic inactivation: a bright new technique to kill resistant microbes. *Current Opinion in Microbiology* **2013**, 33, 67-73.
37. Takemoto, K.; Matsuda, T.; Sakai, N.; Fu, D.; Noda, M.; Uchiyama, S.; Kotera, I.; Arai, Y.; Horiuchi, M.; Fukui, K.; Ayabe, T.; Inagaki, F.; Suzuki, H.; Nagai, T., SuperNova, a monomeric photosensitizing fluorescent protein for chromophore-assisted light inactivation. *Science Reports* **2013**, 3, 2629.

Acknowledgments

D.D. is supported by an international Macquarie University Research Excellence Scholarship, Sydney Vital Research Scholar Award and the Commonwealth Scientific and Industrial Research Organisation (CSIRO) Ph.D. Scholarship Program in Synthetic Biology. A.C. is supported by a Cancer Institute New South Wales Early Career Fellowship (Project Number: ECF171114) and the Australian Research Council (CE140100003).

Author Contributions

D.D co-designed the research, generated all constructs, conducted all biophysical characterization work and ROS production experiments, analyzed the data and wrote the manuscript. X.V. Constructed the laser set-up and supported laser irradiation experiments. A.S. Supervised the project and wrote the manuscript. A.C. conceptualized and co-designed the study, supervised the project and wrote the manuscript.

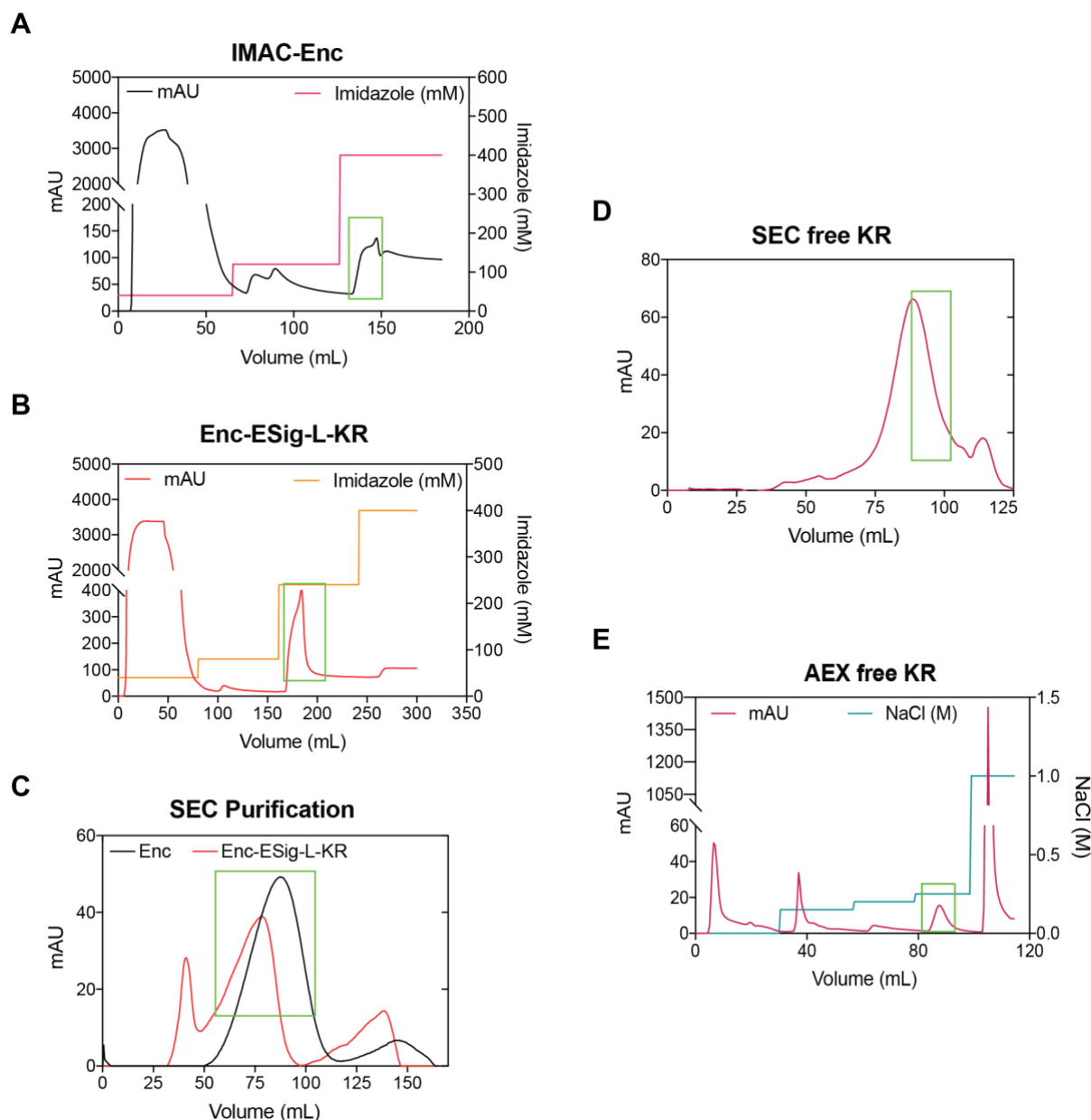
Supplementary information

Engineering encapsulin as a ROS-generating nanocompartment

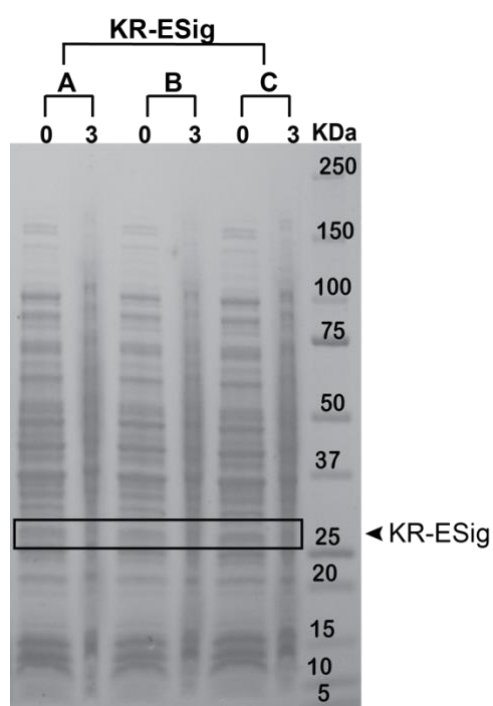
Dennis Diaz, Xavier Vidal, Anwar Sunna, Andrew Care *

Table S1. Expression vectors constructed for this study

Vector	Description	Protein ID
pACYC-Duet-1_Enc	Encapsulin from <i>Thermotoga maritima</i> 138-GGGGGGHHHHHGGGGG-139	UniProt: Q9WZP3
-	Encapsulation signal (ESig)	UniProt: R4NZH3
-	KillerRed	UniProt: Q2TCH5
-	Linker (SGLRSRAE)	-
pPETDuet-1_ESig-KR	LFTDKPITEIEEETSGGSENTG GDLGIRKL- KillerRed	
pPETDuet-1_ESig-S-KR	LFTDKPITEIEEETSGGSENTG GDLGIRKL- linker- KillerRed	
pPETDuet-1_KR-ESig	KillerRed-LFTDKPITEIEEETSGGSENTG GDLGIRKL	
pPETDuet-1_KR-S-ESig	KillerRed-Linker-LFTDKPITEIEEETSGGSENTG GDLGIRKL	



Supplementary Fig. 1. Examples Purification Chromatograms. **A** and **B**. nickel-immobilized metal-affinity chromatography (IMAC) of Enc-ESig-L-KR and empty Enc, respectively. The green square highlights the peak corresponding to the protein of interest. **C**. Size exclusion chromatography (SEC) of IMAC-purified empty and Enc-ESig-L-KR. Empty Enc elutes between 72 mL-100 mL and Enc-ESig-L-KR 61 mL-90 mL. **D**. SEC of partially purified free ESig-L-KR. The protein of interest elutes between 90 mL-105 mL. **E**. Anion Exchange Chromatography (AEX) of SEC purified free ESig-L-KR.



Supplementary Fig. 2. Expression of KR-ESig. SDS-PAGE of the total protein obtained after expression of KR-ESig before induction (0) with IPTG and after 3 h of induction (3). A, B and C represent three different BL21 (DE3) clones expressing KR-ESig.

4

Engineering encapsulin for the loading and controlled release of drugs

Introduction

Conventional drug-based therapies often lack the capacity to selectively target their site-of-action, resulting in adverse side-effects in healthy tissues and a reduction in clinical efficacy ¹. Drug delivery systems (DDS) aim to minimize these limitations by enhancing a drug's physicochemical properties, pharmacokinetic profile and biodistribution ². Nanoparticles (NPs) are a well-known type of DDS, which due to their conformation, can provide selective targeting and protective coatings for increased circulation times and protection from degradation/sequestration ^{1, 2}. Furthermore, the controlled release of therapeutic cargo at their primary site-of-action can be achieved by the incorporation of disassembly and degradation mechanisms that are triggered by specific external stimuli ¹⁻³. Unfortunately, the clinical translation of DDS that rely on synthetic NPs remains poor, mainly due to problematic site-specific functionalization and their heterogeneous physicochemical properties (e.g. size and shape), which limits their stability and biocompatibility⁴.

In contrast, the protein nanocompartment encapsulin represents an exciting new class of biological NPs. Encapsulins self-assemble from multiple protein sub-units into hollow spherical capsids, which are uniform in size and shape, soluble and monodisperse, biocompatible and biodegradable ⁵. They also possess three distinct components that can be readily engineered to have functionalities that lend themselves to drug delivery i.e. an interior cavity, an exterior surface, and interfaces between the protein subunits that form the overall structure ⁶. The interior cavity can be used for encapsulation of therapeutics; the exterior surface can be genetically or chemically functionalized to display ligands for drug targeting; and the protein subunit interfaces can be engineered to allow disassembly for controlled drug release ⁷. Furthermore, unlike other protein nanocompartments, encapsulins selectively encapsulate proteins tagged with a unique C-terminal encapsulation peptide signal (ESig) ⁵. Cargo loading inside encapsulin can be achieved via two approaches (i) *in vivo* (during self-assembly), by co-expressing encapsulin and a ESig-tagged protein in a heterologous host; or (ii) *in vitro* (during reassembly) by disassembling empty encapsulin (i.e. under strong acidic and basic conditions) and then reassembling it by dilution in biological buffers in the presence of ESig-tagged cargo ⁸. There are several examples in which proteins have been loaded inside

encapsulins, which has been discussed extensively in Chapter 2 and 3. However, the *in vitro* loading of small-molecule drugs inside encapsulins and the controlled release of their cargo has remained unexplored until now.

The localized and controlled release of a drug enhances its therapeutic efficacy while reducing its harmful side-effects. However, drug release strategies for self-assembling protein nanocompartments tend to be controlled by simple diffusion of the drug from the nanocompartment, biodegradation of the protective protein shell (e.g. proteolysis), reducing environments and pH ⁹. Alternatively, NDDS that release a drug upon application of an external stimulus offer superior spatial and temporal control in dynamic biological systems, minimizing drug-related toxicity ¹⁰.

Photoresponsive switches that undergo structural changes upon light excitation could be used to disrupt a protein nanocompartment's macrostructure triggering the release of encapsulated cargo within. Azobenzene is a photoswitch that undergoes a reversible *cis-trans* photochemical isomerization. Irradiation at 335 nm converts the 'longer' *trans* form to the shorter *cis* form, which can revert to its *trans* form again upon irradiation at 420 nm ¹¹. The azobenzene moiety has been chemically conjugated to phenylalanine producing the unnatural amino acid (UAA) phenylalanine-4'-azobenzene (AzoPhe), which has been biologically incorporated into proteins using the amber codon suppression approach¹¹. The amber stop codon (TAG) is a great choice for codon reassignment given that it has been reported to be minimally used in *Escherichia coli* (~7%) and infrequently found as a termination signal in essential genes ¹². Additionally, the discovery of organisms such as *Methanococcus jannaschii* for which TAG encodes for the amino acid tyrosine instead of a stop codon, has resulted in the directed evolution of orthogonal TAG-tRNA/aminoacyl-tRNA synthase pairs that allow the inclusion of UAAs into *E. coli* proteins¹². Subsequently, AzoPhe has been used to coordinate the light-controlled regulation of protein function i.e. switching between *cis/trans* causes switches between 'active/inactive' protein conformations ¹³. Thus, if accurately positioned within the interface between encapsulin's protein subunits, AzoPhe could induce the assembly/disassembly of the encapsulin macrostructure.

In this chapter, I aimed to develop an encapsulin nanocompartment whose disassembly/reassembly can be triggered by light to release an encapsulated drug. To achieve this function, I implemented a pH disassembly/reassembly approach to test the encapsulation of small-molecule drugs into the encapsulin *from the bacterium Thermotoga maritima*. In addition, the amber codon suppression approach was proved to incorporate AzoPhe into permissive regions of the encapsulin's structure. Finally, use protein modelling to identify three residues located at the interfaces of encapsulin subunits, which could be substituted with AzoPhe to potentially mediate light-triggered disassembly.

Materials and methods

Materials

Reagents were purchased from Sigma-Aldrich unless stated otherwise. HEPES-free acid was purchased from Chem-Supply Pty. Restriction enzymes and competent *E. coli* cells were purchased from New England Biolabs unless stated otherwise. All chromatography columns were purchased from GE Healthcare, USA unless stated otherwise. All purifications were carried out on an Äkta™ start or Äkta™ pure chromatography system (GE Healthcare, USA). Phenylalanine 4' azobenzene was synthesized by Dr Victoria Peddie from the University of Adelaide.

Molecular biology and cloning

All inserts were codon optimized for recombinant expression in *E. coli*. The gene corresponding to native empty encapsulin (nEnc) from *Thermotoga maritima* (Uniprot: Q9WZP3) was synthesized as gBlock Gene Fragments (Integrated DNA Technologies). To generate expression vectors, nEnc was ligated into plasmid pETDuet-1 (+) (Merck) via NcoI/BamHI restriction sites. To introduce Phenylalanine 4' azobenzene (AzoPhe) inside proteins the amber stop codon (TGA) was inserted inside the gene encoding the protein of interest. All genes modified with the incorporation of the amber codon were synthesized and ligated into pETDuet-1 via NcoI/BamHI restriction sites by GeneScript®. Additionally, the pEVOL-AzoPhe (+) Chloramphenicol plasmid encoding the tRNA synthetase/tRNA pair for the incorporation of AzoPhe in response of the amber codon in *E. coli* was obtained as a gift from Prof. Peter Schultz (The Scripps Research Institute, USA) ¹¹.

In the case of Superfolder Green Fluorescent Protein¹⁴ (sfGFP), the TGA codon was inserted between residues 21-22. For nEnc, a loop region was modified with the amber codon inside a flexible linker (GGGGGAMBERGGGGG) between residues 42-43 and for easier purification a hexahistidine tag (GGGGGGHHHHHHGGGGGG) was additionally inserted into a surface-exposed loop region between residues 138-139 as previously described¹⁵. *E. coli* α -Select (Bioline) was used as a host for general gene cloning and vector storage. Gene insertion was verified by performing PCR using the primers pairs pETUpstream/DuetDOWN or DuetUP2/T7 Terminator (Merck). All gene constructions used in this study are summarised in Table 1. *E. coli* BL21 (DE3) cells were used for recombinant protein expression of all constructs.

Table 1. Expression vectors constructed for this study

Vector	Description	Protein ID
pETDuet-1_nEnc	Encapsulin from <i>Thermotoga maritima</i>	UniProt: Q9WZP3
pETDuet-1_His-Enc-42 amber	Encapsulin from <i>Thermotoga maritima</i> 42- GGGGGAMBERGGGGG-43 138-GGGGGGHHHHHHGGGGGG-139	UniProt: Q9WZP3
pETDuet-1_sfGFP21amber	21-AMBER-22	GFP UniProt: P42212

Protein expression and purification

In this study, protein expression (or co-expression) experiments were carried out in LB medium supplemented with carbenicillin (100 μ g/ml), chloramphenicol (35 μ g/ml) or both. In order to evaluate the protein expression or co-expression of the constructs, 10 ml LB (1:100) was inoculated with an overnight culture of cells harbouring the expression plasmid(s). Cultures were grown aerobically at 37 °C to an optical density at 600 nm (OD₆₀₀) of 0.6-0.8 and induced by the addition of 0.8 mM isopropyl- β -D-thiogalactopyranoside (IPTG) and/or galactose (0.02%, w/v) and/or AzoPhe (1 mM). The cultures were incubated at 20 °C for 18 h in the dark. Next, cells were harvested by centrifugation (10,000 x g 15 min, 4 °C) and stored at -30 °C. The cells were resuspended in 1 mL 100 mM HEPES buffer pH 7.4 with 1 U/mL Benzonase® nuclease. Cell lysis was performed with glass beads using a cell disruptor. Afterwards, the glass beads were spun down at 100 x g for 30 seconds and the supernatant was transferred to a new tube. The cell lysate was spun down again at 13,000 x g for 5 min, to separate the cell debris (insoluble fraction) from the

soluble fraction. For the partial purification of His-tagged proteins, the gravity flow purification Ni-NTA Fast Start Kit (Qiagen) was used following the manufacturer's recommendations. The fluorescence in each fraction was observed in a Safe Imager™ 2.0 Blue Light Transilluminator (ThermoFisher Scientific).

For the expression of nEnc, 50 ml of LB was inoculated (1:100) with an overnight culture of cells harbouring the expression plasmid and grown aerobically at 37 °C to an optical density OD₆₀₀ of 0.6-0.9. nEnc protein expression was induced by the addition of 0.1 mM IPTG. The expression was performed at 37 °C for 4 h. Finally, cells were harvested by centrifugation (10,000 x g 15 min, 4 °C) and stored at -30 °C.

For the purification of nEnc, the harvested cells were resuspended in 10 mL lysis buffer (100 mM Hepes, 1 U/mL Benzonase® nuclease, pH 7.4) and lysed by three rounds through a French press. After centrifugation at 10,000 x g for 15 min, the supernatant was heat treated at 65 °C for 15 min. Denatured proteins were removed by centrifugation (10000 x g, 10 min, 4 °C). PEG8000 and NaCl to a final concentration of 10% and 2% (w/v), respectively, were added to the soluble fraction (supernatant) obtained after centrifugation. After incubation for 15 min on ice, the precipitated proteins were centrifuged at 10,000 x g for 15 min and the pellet was resuspended in 3 mL of 100 mM HEPES buffer pH 7.5. This protein sample was subjected to size exclusion chromatography (SEC) on a HiPrep™ 16/60 Sephacryl® S-400 HR column using 100 mM HEPES as the running buffer. The fractions containing nEnc were concentrated with Amicon Ultra-15 centrifugal filter units (100 KDa cut-off). The final protein concentration concentrations were determined by measuring absorbance at 280 nm.

Polyacrylamide gel electrophoresis (PAGE)

The Bio-Rad mini-protean system (Bio-Rad laboratories) was used for all SDS-PAGE and Native-PAGE analysis. For SDS-PAGE, samples were diluted in 2X Laemmli sample buffer with 50 mM 1,4-dithiothreitol, incubated at 95 °C for 5 min, loaded into pre-cast Bio-Rad Mini-PROTEAN® TGX™ gels (4-15%) and run at 200V for 30 min. For Native-PAGE, samples were diluted in 4X native sample buffer (200 mM Tris-HCl pH 6.8, 40% glycerol, and 0.08% bromophenol blue), loaded into

pre-cast Bio-Rad Mini-PROTEAN® TGX™ gels (4-20%) and run at 200V for a minimum of 2 h. In-gel fluorescence of proteins was observed on a G-BOX gel documentation system (Syngene). All gels were stained following the Coomassie G-250 safe stain protocol¹⁶.

Transmission electron microscopy (TEM)

10 µL of the protein samples (~100 µg/ml) were adsorbed onto formvar-carbon coated copper grids for 2 min and negatively stained with uranyl acetate replacement stain (UAR-EMS) for 1 h. Grids were then washed with ultrapure water and allowed to dry for 15 min. Finally, the grids were observed under a Philips CM10 TEM operated at 100 kV accelerating voltage.

In vitro disassembly/reassembly of nanocompartments

In order to induce the disassembly of the nanocompartment, the pH of SEC-purified nEnc was dropped or increased by adding 2 M HCL or 0.5 M NaOH, respectively. The final pH of the samples was confirmed using pH strips (Merck), after which samples were incubated for 90 min at room temperature (RT). Any precipitated proteins were separated by centrifugation (13000 x g, 10 min, 4 °C). For reassembly experiments, the pH of the soluble part of all samples was brought back to neutral pH by diluting the sample (1:10) in 100 mM HEPES pH 7.5 follow by overnight incubation at RT. Samples were concentrated using Amicon Ultra-0.5 mL centrifugal filter units (10 KDa cut-off) before loading the re-assembled samples onto a Native-PAGE gel.

In vitro drug loading

A sample containing nEnc was disassembled at extreme acidic or basic pH and subsequently reassembled upon return to neutral pH, following the protocol described above (see 2.7). For *in vitro* drug loading and to initiate the reassembly process, the fluorescent anticancer drug doxorubicin hydrochloride (DOX) was added to the dissembled nEnc at an nEnc:DOX ratio of 1:50. As a control, DOX was incubated with untreated assembled nEnc. All samples were eventually loaded onto a native-PAGE gel and evaluated for correct reassembly and drug loading i.e. fluorescence.

Rational design of light-triggered disassembly of encapsulin

Amino acid residues for the potential incorporation of AzoPhe into nEnc were identified using the Rosetta modelling software ¹⁷. This work was performed in collaboration with Prof Ingemar André from Lund University and Prof Sinisa Bjelic Linneus University, Sweden. Briefly, the crystal structure of *T. maritima* encapsulin (PDB: 3KDT) was used to model the nanocompartment *in silico* as a completely symmetric T=1 icosahedral capsid. To avoid steric clashes and symmetrize the structure, energy optimization of the system was performed. The *trans* and *cis* conformation of the AzoPhe residue was then introduced and modelled at the interface between encapsulin subunits. To optimize the search for ideal positions to incorporate AzoPhe, all amino acids with a maximum distance of 8 Å from a neighbouring subunit were scanned. Afterwards, the change of energy of introducing AzoPhe (*trans* or *cis*) was recorded.

Results and Discussion

pH-mediated disassembly and reassembly of encapsulin

The encapsulin from *T. maritima* is a very robust nanocompartment (~24 nm in diameter) which can be recombinantly-produced in microbial host organisms such as *E. coli* as a hollow shell ¹⁸. In a report from the Savage lab at the University of California, the *T. maritima* encapsulin was shown to disassemble under strong acidic and basic conditions and to reassemble when brought back to neutral pH₈ (see Figure 1A). The report also mentions that disassembly with a strong acidic pH (1.0) results in 95% reassembly of the protein₈. In order to confirm these results, the native encapsulin gene from *T. maritima* (nEnc) was expressed in *E. coli* and purified it as described in the “Materials and Methods”. In preliminary experiments, nEnc was exposed to different acidic pHs and its disassembly analyzed by Native-PAGE gel (Figure 1B). All acidic pH conditions tested showed some protein precipitation, with pH 4.5 exhibiting the most precipitation. This was expected as pH 4.5 is very close to Enc’s theoretical isoelectric point (pI) of pH 4.9 (ExPASy). At pH 3.5 to pH 1.0, nEnc started to disassemble and form presumably smaller oligomers and monomers (Figure 1B). As a result, pH 3.0 and 1.0 were used to mediate disassembly in subsequent experiments (Figure 1C). At pH 3.0 the protein seemed to precipitate completely as no protein could be seen on the gel, whereas at pH 1.0

the protein disassembled completely and was visible of the gel. When returned to neutral pH, the acid-dissembled nEnc did not appear to reassemble, which is contrary to the findings of previously reports. This disassembly/reassembly experiment was repeated using either acidic (pH 1.0) or basic (pH 13) conditions to initiate nEnc disassembly (Figure 1D). pH 13 has been reported to also induce the disassembly with subsequent reassembly at neutral pH of *T. maritima* encapsulin⁸. Again, reassembly of nEnc was not observed after disassembly at pH 1.0, while nEnc was did reassemble following disassembly at basic pH 13. Thus, these preliminary experiments confirmed that disassembly of the nanocompartment at pH 1.0 does not allow the subsequent reassembly of nEnc. To evaluate the correct formation of nEnc after treatment at pH 13, the samples obtained before, during and after reassembly were visualized by TEM. As shown in Figure 1E, after *in vitro* disassembly, nEnc protein shells could not be seen. However, upon return to neutral pH the spherical nanocompartments were observed, indicating their ability to refold and reassemble into the original macrostructure after their previous disassembly at pH 13. Therefore, this pH-mediated disassembly/reassembly protocol was chosen to perform the *in vitro* loading of small-molecule drugs into encapsulin.

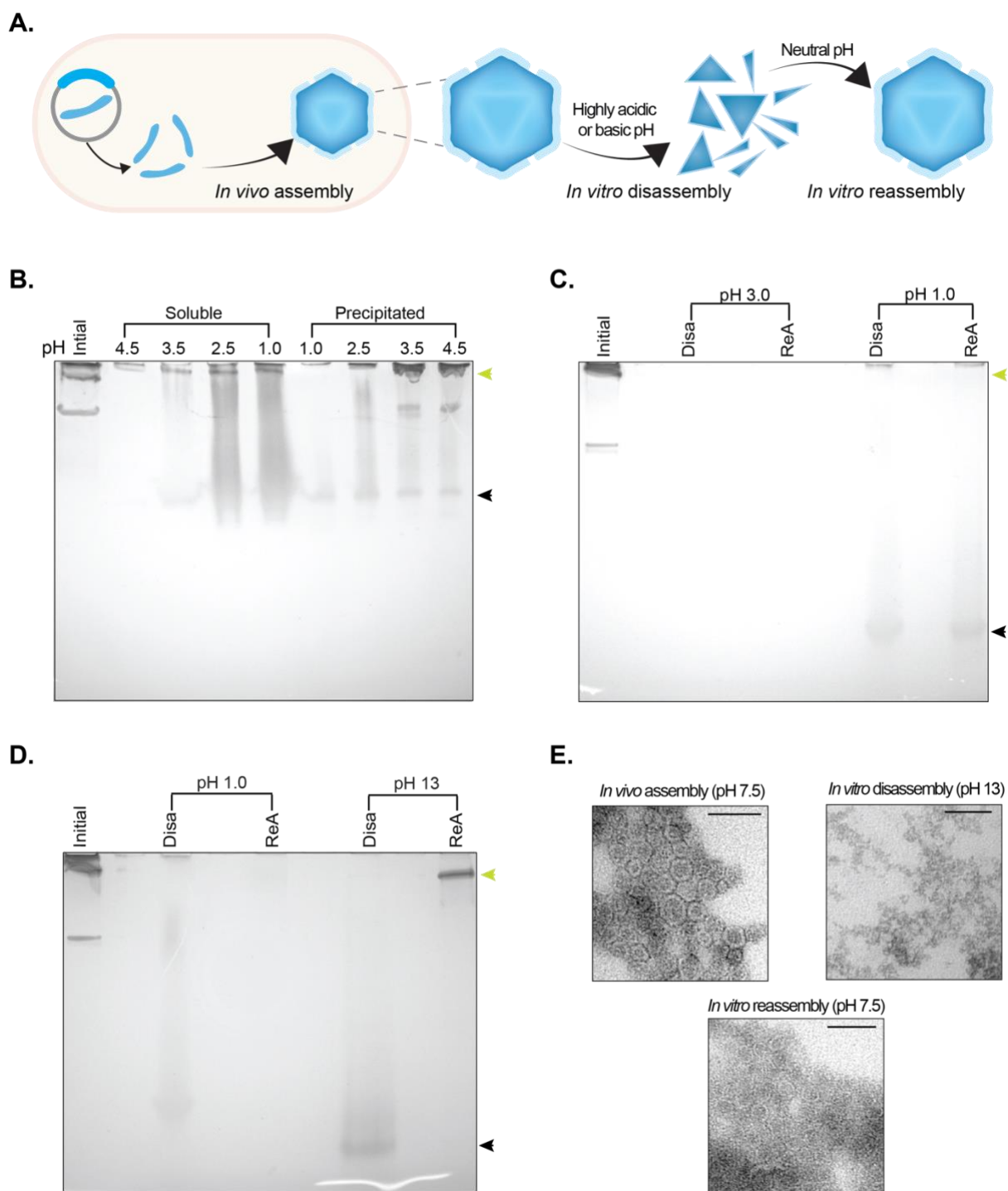


Figure 1. pH triggered disassembly/reassembly of empty *T. maritima* encapsulin. **A.** Illustration showing the *in vivo* self-assembly and *in vitro* disassembly/reassembly of encapsulin nanocompartments. For *in vivo* assembly, the encapsulin monomers are expressed in a heterologous host (e.g. *E. coli*) where they self-assemble into a nanocompartment. In *in vitro* assembly, the *in vivo* produced nanocompartment is disassembled under strong acidic or basic conditions and then reassembled by dilution in buffers at neutral pH. **B.** Coomassie-stained Native-PAGE of: The initial SEC-purified nEnc sample followed by 'Soluble' and 'precipitated' protein after exposure to different acidic pHs. **C and D:** Coomassie-stained Native-PAGE of the initial SEC-purified nEnc and disassembly (Disa) at **C.** pH 1.0 and 3.0 and **D.** pH 1.0 and 13 - with subsequent reassembly at pH 7.5 (ReA). Green arrows highlight the assembled nEnc and black arrows highlight the disassembled nEnc. **E.** TEM images of the *in vivo* self-assembled; and *in vitro* disassembled/reassembled nEnc nanocompartments (Scale bars = 50 nm).

In vitro loading of small-molecule drugs inside encapsulin

The pH-mediated disassembly/reassembly of ferritin, a well-characterised protein nanocompartment, has been widely utilised to encapsulate small-molecule drugs (e.g. doxorubicin, DOX) inside ferritin's internal cavity. Consequently, drug-loaded ferritins have been shown to mediate cancer therapy in both *in vitro* and pre-clinical studies^{19, 20}. Recently, the outer surface of encapsulin was crosslinked with the prodrug derivative of DOX – aldoxorubicin (AlDox). This drug-coated encapsulin was shown to deliver AlDox into liver cancer cells, where it had a killing effect¹⁵. Despite showing promise as a drug delivery vehicle, the loading of small-molecule drugs inside the inner cavity of encapsulins remains unexplored. This loading approach offers several advantages as it protects a drug from degradation and leaves the exterior surface free for further functionalization with targeting molecules (e.g. antibodies and peptides).

To further extend the utility of encapsulin as a drug delivery platform, we aimed to load the chemotherapeutic drug DOX into nEnc nanocompartments using the pH disassembly/reassembly protocol detailed above process depicted in Figure 2A. As shown in Figure 2B, the presence of DOX altered the quality of the protein band that was previously obtained after reassembly of nEnc (Figure 1D). DOX has intrinsic fluorescence (470/595 excitation/emission maxima)²¹ which means that if DOX is packaged inside nEnc during reassembly the protein band observed in the Native-page gel should exhibit fluorescence. However, no fluorescence was observed in the reassembled sample, suggesting that DOX was not packaged inside nEnc during its reassembly. This indicates that the pH-mediated disassembly/reassembly approach is not suitable for the encapsulation of small-drug molecules inside encapsulin. To solve this challenge, other disassembly methods could be evaluated such as denaturation with the denaturant guanidine hydrochloride, which has been successfully applied for the *in vitro* loading of ESig-tagged proteins inside *T. maritima* encapsulin⁸.

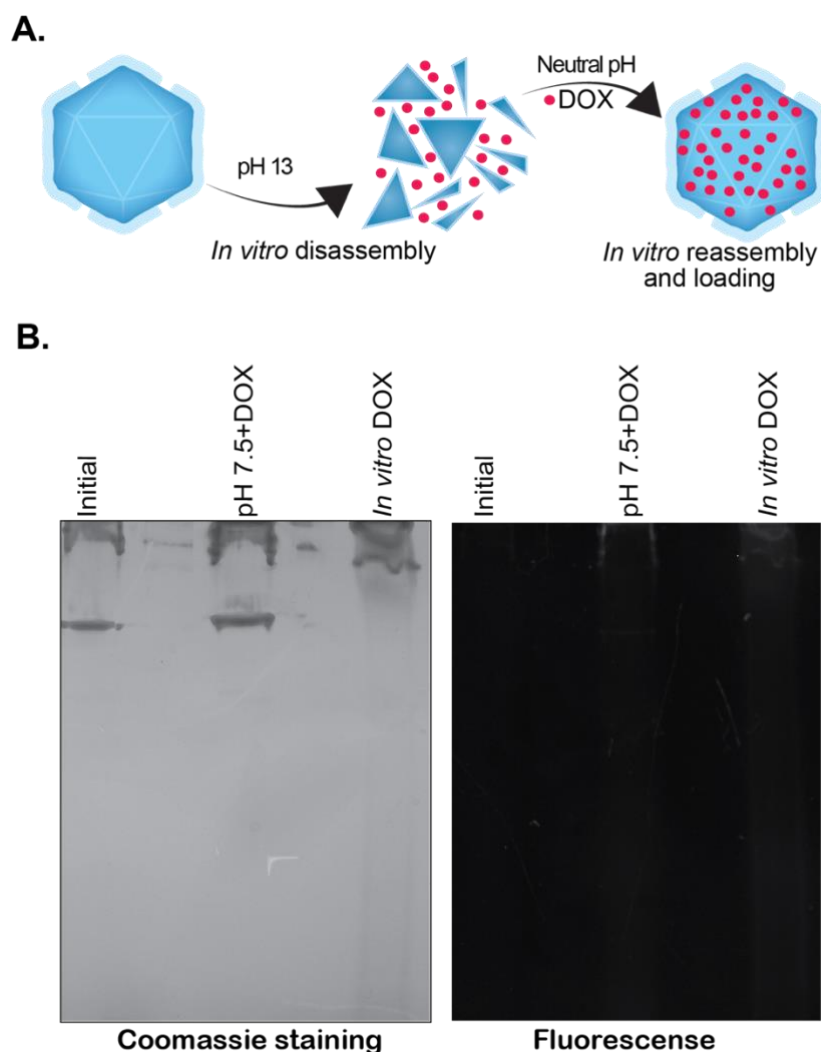


Figure 2. pH triggered loading of DOX inside encapsulin. **A.** Illustration depicting the *in vitro* loading of DOX inside *TmEnc*. In this process, pH 13 triggers the disassembly of the nanocompartments. The small-molecule drug (e.g. DOX) in buffer at neutral pH is then added, diluting the solution and initiating the reassembly of Enc while simultaneously permitting the drug encapsulation. **B.** Coomassie-stained (**Left panel**) and in-gel fluorescence (**Right panel**) of a Native-PAGE, showing SEC-purified *TmEnc* sample: without treatment (Initial), incubated with DOX without pH disassembly (pH 7.5 +DOX), and disassembly/reassembly in the presence of DOX (*in vitro* DOX).

Incorporation of AzoPhe into encapsulin

An alternative method to load drugs inside encapsulin and control their release could be to develop an encapsulin nanocompartment that can be triggered by light to disassemble/reassemble. In pursuit of this objective, we designed a system in which the photoswitchable unnatural amino acid phenylalanine-4'-azobenzene (AzoPhe) is incorporated into the encapsulin nanocompartment at positions essential to its assembly (i.e. subunit interfaces) (Figure 3A). Upon light excitation at a specific wavelength, AzoPhe would controllably 'switch' from *cis* (short) to *trans* (long) isomers, disrupting encapsulin's macrostructure resulting in its disassembly into

individual subunits. This will be achieved by using the suppression of the amber stop codon by an orthogonal AzoPhe tRNA/ aminoacyl tRNA synthase pair, which instead of stopping the protein translation, incorporates AzoPhe, allowing the target protein to be expressed and functional¹¹. The three primary components required to produce an AzoPhe-containing protein are: (i) the pEVOL-AzoPhe vector that encodes the tRNA synthase/tRNA pair that incorporate AzoPhe; (ii) the chemically synthesized AzoPhe UAA; and (iii) a recombinant gene that contains the amber codon.

Accordingly, we verified the functionality and compatibility of these components using the model fluorescent protein sfGFP. Herein, a gene sequence encoding sfGFP with an amber codon mutation at the beginning of the protein (insertion between residues 21- 22) was used. To verify the incorporation of AzoPhe into sfGFP (AzoPhe-sfGFP) during its recombinant expression in *E. coli*, we performed two control expressions: (1) without IPTG (sfGFP) and galactose (tRNA synthase/tRNA pair) induction and no AzoPhe supplementation; or (2) with IPTG and galactose induction and no AzoPhe supplementation. As shown in Figure 3B, both control expressions showed small amounts of sfGFP production and fluorescence, even though the presence of the amber codon should prevent translation of the complete protein. This result could be due to heterogenous readthrough of the amber codon, which has been previously reported in *E. coli* ²². Alternatively, following induction with both IPTG and galactose and supplementation with AzoPhe, we observed significant expression of AzoPhe-sfGFP and its corresponding bright fluorescence (Figure 3B). These results match those observed in previous studies where AzoPhe and other UAAs have been incorporated into GFP variants ^{11, 23}. In summary, the amber codon system and all our components can successfully incorporate AzoPhe into proteins.

Next, we tested whether the amber codon system could incorporate AzoPhe into a permissive outer surface loop region located on *T. maritima* encapsulin structure, which has been reported to accept modifications without any negative impact on the nanocompartment's auto-assembly properties ¹⁵. This encapsulin variant, AzoPhe-Enc, carried a His-tag for easier purification. In order to confirm the introduction of AzoPhe into encapsulin, protein expression experiments were carried out as

described previously, with an additional final Ni-NTA purification step for the recognition of His-tagged proteins. SDS-PAGE analysis (Figure 3C) showed no readthrough of the amber codon in the negative expression controls. In contrast, the correct expression of encapsulin subunits was observed upon supplementation with AzoPhe. This suggests the successful incorporation of AzoPhe into the encapsulin's structure.

Other protein nanocompartments have been modified for the incorporation of UAA inside their structure, mainly with the objective to have an array of reactive moieties (e.g. azides and alkynes) that are not available in nature and can be used for the bioconjugation of different ligands (e.g. antibodies) ²⁴. For more examples please refer to Chapter 1. Thus, our study provides further evidence for the possibility to explore the incorporation of other UAA that could expand the functionalities of encapsulin.

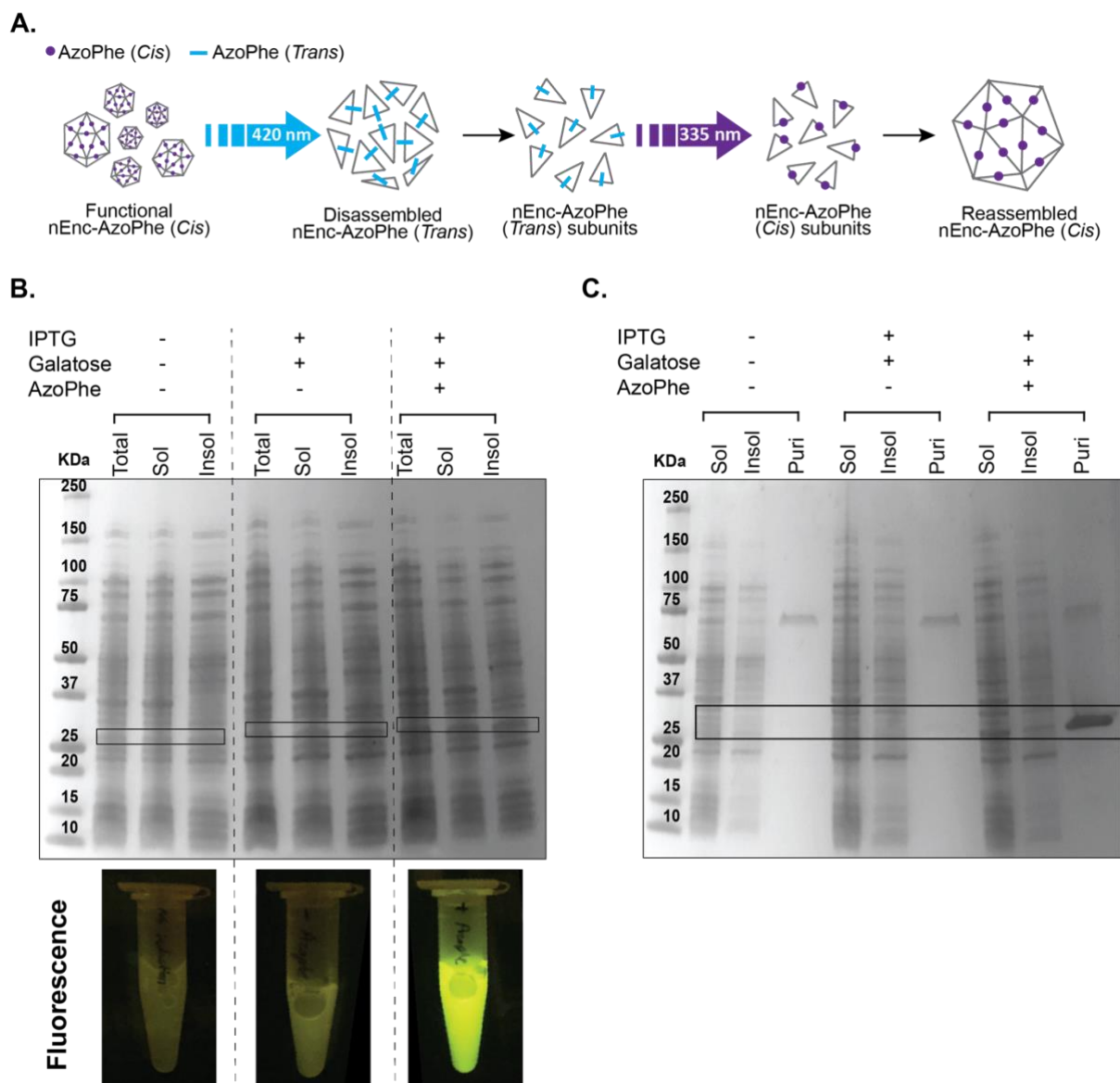


Figure 3. Expression of proteins with the incorporation of AzoPhe. **A.** Illustration showing a light-triggered mechanism for the disassembly/reassembly of encapsulin. To achieve this, a rationally designed AzoPhe-containing encapsulin variant is irradiated at 420 nm changing the AzoPhe isoform from short *cis* to long *trans*, disrupting its macrostructure. By switching the light wavelength to 365 nm AzoPhe reverses from long *trans* to short *cis* conformation to allow reassembly of encapsulin. **B** and **C.** SDS-PAGE analysis of the incorporation of AzoPhe into sfGFP and His-tagged encapsulin (Enc), respectively. The expression of the protein was performed with or without the induction of the protein of interest (IPTG) and the tRNA synthetase/tRNA pair (Galactose) and/or the addition of AzoPhe. **B.** The total protein before lysis (Total), and the soluble proteins (Sol) and cell debris (Insol) after cell lysis were observed via Coomassie-stained SDS-PAGE. The fluorescence of the soluble fraction, under blue light excitation, for each experiment is also presented. **C.** After cell lysis the soluble proteins (Sol), the cell debris (Insol) and the partially purified AzoPhe-Enc were observed via Coomassie-stained SDS-PAGE.

The Rosetta modelling software was used to model amino acid residues located within the interface between encapsulin subunits that could be substituted with AzoPhe for potential light-triggered disassembly. Potential incorporation sites were identified based on the energy change caused by the substitution with AzoPhe in *cis* or *trans* conformation. A threshold of more than 5 for energy change was used to account for a change that is costly enough to modify the nanocompartment structure. Thus, for the selection of the potential mutation sites, the substitution with AzoPhe in *cis* should be less likely to cause a major structural impact (<5) but in *trans* should cause structural changes (>5). Out of 96 possible residues just 3 complied with the selection criteria (Table 2).

Table 2. Positions for AzoPhe mutations in encapsulin

Res No ¹	Res ²	Codon	Mut ³	Δ Trans ⁴	Δ Cis ⁵
14	K	AAA	AzoPhe	12.8974	4.47412
74	P	CCG	AzoPhe	1839.59	0.64505
95	G	GGU	AzoPhe	1676.07	1.58007

¹Residue position, ²Residue, ³Mutation, ⁴Energy change for AzoPhe *trans* isomer, ⁵Energy change for AzoPhe *cis* isomer

The structural impact of the AzoPhe substitution modelling at these potential sites was observed in PyMOL. As shown in Figure 4, when AzoPhe is introduced in *cis* isoform there are no evident clashes between neighbouring amino acids whilst in *trans* conformation AzoPhe causes steric clashes with surrounding residues. These results contribute to the hypothesis that these mutations sites might enable the light-controlled regulation of the disassembly and potential reassembly of encapsulin. The genes encoding these mutations were designed, ligated into the pET-Duet-1 expression vector and co-transform with pEVOL-AzoPhe plasmid into BL21(DE3) *E. coli* cells but due to time constraints we were not able to evaluate them.

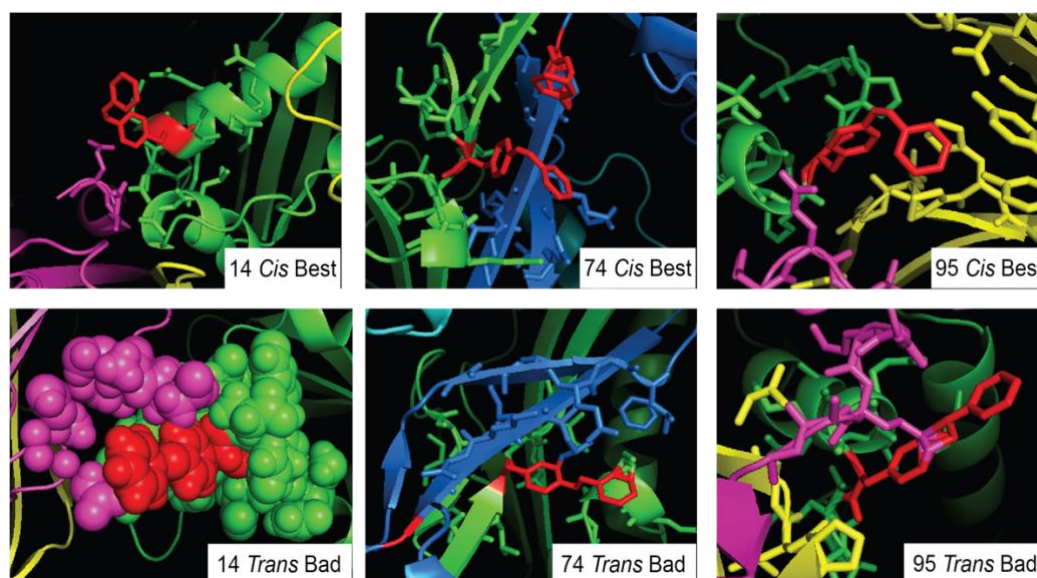


Figure 4. Potential residues for the incorporation of AzhoPhe inside encapsulin. Molecular visualization (PyMOL) of the potential mutations that allow the assembly of the protein when AzoPhe is in *cis* isoform (Residue No *Cis* best) and cause steric clashes with neighbouring residues in *trans* conformation (Residue No *Cis* Bad).

Conclusions

We confirmed the ability of *T. maritima* encapsulin to disassemble at strong basic pH 13 and reassemble upon returning to neutral pH. However, the previously reported encapsulin disassembly strategy at pH 1 with subsequent reassembly could not be reproduced in this study. The loading of nEnc with a small-molecule drug (DOX) using the *in vitro* pH disassembly/reassembly protocol was unsuccessful. Based on these results we believe that this method is not suitable for the loading of small-molecule drugs inside encapsulin and that other approaches such as the use of denaturants (e.g. guanidine hydrochloride) for disassembly or the conjugation of DOX to the encapsulation signal could achieve better results. Additionally, the light-triggered system for the disassembly/reassembly could also allow the loading of drugs inside encapsulin as well as their controlled release.

With regards to the construction of the light-triggered system, it was determined that the three components required for AzoPhe incorporation into proteins (i.e. vector for the incorporation of AzoPhe, chemically synthesized AzoPhe, and gene constructs) are compatible. This was confirmed by the successful incorporation of AzoPhe into sfGFP and a permissive loop region located in his-tagged encapsulin.

Protein modelling using the Rosetta software led to the identification of 3 residues within each encapsulin sub-unit that could be substituted with AzoPhe to potentially enable light-triggered disassembly. However, due to time constraints of this PhD project, the evaluation and characterization of these constructs was not possible.

References

1. Schoonen, L.; van Hest, J. C. M., Functionalization of protein-based nanocages for drug delivery applications. *Nanoscale* **2014**, 6 (13), 7124-7141.
2. Sahandi Zangabad, P.; Karimi, M.; Mehdizadeh, F.; Malekzad, H.; Ghasemi, A.; Bahrami, S.; Zare, H.; Moghooei, M.; Hekmatmanesh, A.; Hamblin, M. R., Nanocaged platforms: modification, drug delivery and nanotoxicity. Opening synthetic cages to release the tiger. *Nanoscale* **2017**, 9 (4), 1356-1392.
3. Gu, W.; Wu, C.; Chen, J.; Xiao, Y., Nanotechnology in the targeted drug delivery for bone diseases and bone regeneration. *International Journal of Nanomedicine* **2013**, 8, 2305-2317.
4. Bertrand, N.; Wu, J.; Xu, X.; Kamaly, N.; Farokhzad, O. C., Cancer nanotechnology: the impact of passive and active targeting in the era of modern cancer biology. *Advanced drug delivery reviews* **2014**, 66, 2-25.
5. Sutter, M.; Boehringer, D.; Gutmann, S.; Gunther, S.; Prangishvili, D.; Loessner, M. J.; Stetter, K. O.; Weber-Ban, E.; Ban, N., Structural basis of enzyme encapsulation into a bacterial nanocompartment. *Nature Structural & Molecular Biology* **2008**, 15 (9), 939-47.
6. Giessen, T. W., Encapsulins: microbial nanocompartments with applications in biomedicine, nanobiotechnology and materials science. *Current Opinion in Chemical Biology* **2016**, 34, 1-10.
7. Choi, B.; Moon, H.; Hong, S. J.; Shin, C.; Do, Y.; Ryu, S.; Kang, S., Effective Delivery of Antigen–Encapsulin Nanoparticle Fusions to Dendritic Cells Leads to Antigen-Specific Cytotoxic T Cell Activation and Tumor Rejection. *ACS Nano* **2016**, 10 (8), 7339-7350.
8. Cassidy-Amstutz, C.; Oltrogge, L.; Going, C. C.; Lee, A.; Teng, P.; Quintanilla, D.; East-Seletsky, A.; Williams, E. R.; Savage, D. F., Identification of a Minimal Peptide Tag for in Vivo and in Vitro Loading of Encapsulin. *Biochemistry* **2016**, 55 (24), 3461-8.
9. Molino, N. M.; Wang, S. W., Caged protein nanoparticles for drug delivery. *Current Opinion in Biotechnology* **2014**, 28, 75-82.
10. Liu, D.; Yang, F.; Xiong, F.; Gu, N., The Smart Drug Delivery System and Its Clinical Potential. *Theranostics* **2016**, 6 (9), 1306-1323.
11. Bose, M.; Groff, D.; Xie, J.; Brustad, E.; Schultz, P. G., The Incorporation of a Photoisomerizable Amino Acid into Proteins in *E. coli*. *Journal of the American Chemical Society* **2006**, 128 (2), 388-389.
12. Wals, K.; Ovaa, H., Unnatural amino acid incorporation in *E. coli*: current and future applications in the design of therapeutic proteins. *Frontiers in Chemistry* **2014**, 2, 15-15.
13. Padilla, M. S.; Young, D. D., Photosensitive GFP mutants containing an azobenzene unnatural amino acid. *Bioorganic & Medical Chemistry Letter* **2015**, 25 (3), 470-473.

14. Pedelacq, J. D.; Cabantous, S.; Tran, T.; Terwilliger, T. C.; Waldo, G. S., Engineering and characterization of a superfolder green fluorescent protein. *Nature Biotechnology* **2006**, *24* (1), 79-88.
15. Moon, H.; Lee, J.; Min, J.; Kang, S., Developing genetically engineered encapsulin protein cage nanoparticles as a targeted delivery nanoplatform. *Biomacromolecules* **2014**, *15* (10), 3794-801.
16. Lawrence, A.-M.; Besir, H. U. S., Staining of proteins in gels with Coomassie G-250 without organic solvent and acetic acid. *Journal of visualized experiments* **2009**, (30), 1350.
17. Kortemme, T.; Kim, D. E.; Baker, D., Computational alanine scanning of protein-protein interfaces. *Sci STKE* **2004**, *2004* (219), pl2.
18. Ferlez, B.; Sutter, M.; Kerfeld, C. A., A designed bacterial microcompartment shell with tunable composition and precision cargo loading. *Metabolic Engineering* **2019**, *54*, 286-291.
19. Zhen, Z.; Tang, W.; Chen, H.; Lin, X.; Todd, T.; Wang, G.; Cowger, T.; Chen, X.; Xie, J., RGD-Modified Apoferritin Nanoparticles for Efficient Drug Delivery to Tumors. *ACS Nano* **2013**, *7* (6), 4830-4837.
20. Cutrin, J. C.; Crich, S. G.; Burghilea, D.; Dastrù, W.; Aime, S., Curcumin/Gd Loaded Apoferritin: A Novel "Theranostic" Agent To Prevent Hepatocellular Damage in Toxic Induced Acute Hepatitis. *Molecular Pharmaceutics* **2013**, *10* (5), 2079-2085.
21. Shah, S.; Chandra, A.; Kaur, A.; Sabnis, N.; Lacko, A.; Gryczynski, Z.; Fudala, R.; Gryczynski, I., Fluorescence properties of doxorubicin in PBS buffer and PVA films. *Journal of photochemistry and photobiology. B, Biology* **2017**, *170*, 65-69.
22. Fan, Y.; Evans, C. R.; Barber, K. W.; Banerjee, K.; Weiss, K. J.; Margolin, W.; Igoshin, O. A.; Rinehart, J.; Ling, J., Heterogeneity of Stop Codon Readthrough in Single Bacterial Cells and Implications for Population Fitness. *Molecular Cell* **2017**, *67* (5), 826-836.e5.
23. Wandrey, G.; Wurzel, J.; Hoffmann, K.; Ladner, T.; Büchs, J.; Meinel, L.; Lühmann, T., Probing unnatural amino acid integration into enhanced green fluorescent protein by genetic code expansion with a high-throughput screening platform. *Journal of biological engineering* **2016**, *10*, 11-11.
24. Khoshnejad, M.; Greineder, C. F.; Pulsipher, K. W.; Villa, C. H.; Altun, B.; Pan, D. C.; Tsourkas, A.; Dmochowski, I. J.; Muzykantov, V. R., Ferritin Nanocages with Biologically Orthogonal Conjugation for Vascular Targeting and Imaging. *Bioconjugate Chemistry* **2018**, *29* (4), 1209-1218.

5

Summary and Future Perspectives

In this work we reprogrammed the *T. maritima* encapsulin to create two light-induced ROS-generating nanoreactors with potential use in nanomedicine and biocatalysis. To achieve this, two biological fluorescent photosensitizers were successfully loaded inside a His-tagged encapsulin retaining their ROS-generating ability. From our results we can conclude that three main variables can affect the loading of cargo proteins and their functionality after encapsulation: I) structural changes upon both fusion of the cargo protein to the encapsulation signal (ESig) and loading inside encapsulin. II) overcrowding caused by high loading efficiency. III) substrate and product diffusion in and out of the nanocompartment. Furthermore, we present preliminary data of the loading of small-molecule drugs inside *T. maritima* encapsulin and the development of a light-triggered mechanism for the disassembly of the nanocompartment.

Chapter 1 describes innovative and existing tools and approaches for the reengineering and *de novo* construction of protein nanocompartments (PNC). The review first touches on the identification, production hosts and purification strategies that have been developed for PNC. It also highlights the great progress that has been accomplished by computational modelling tools, presenting examples of rational redesign of existing proteins to form PNC and the construction of *de novo* protein-protein interfaces permitting protein building blocks to self-assemble into PNC with defined architectures. A closer examination is given to the different strategies of chemical (bioconjugation) and genetic modifications used to impart new functionalities to PNC considering the advantages and challenges faced by these methods. Lastly, reports of the potential applications of PNC for vaccine development, drug delivery, and biocatalysis are mentioned.

In **Chapter 2** and **3** encapsulin was reprogrammed into two ROS-generating nanoreactors that can be activated by light. The presence of the ESig in different forms was studied for both mSOG and KR. mSOG variants were designed with two different lengths of ESig and tested whilst for KR the position inside the protein (C- or N- terminus) and the presence of a peptide linker were evaluated. All variants reached different results in terms of loading efficiency which can affect the cargo's functionality. This was particularly true for encapsulated C-terminally ESig-tagged mSOG. Drastic differences were observed in loading efficiencies (up to 30%)

between mSOG1 and mSOG2, with mSOG2 versions having the highest loading efficiencies but presenting the lowest singlet oxygen ($^1\text{O}_2$) generation. The differences in loading seemed more likely due to conformational changes that ESig took upon fusion to the cargo protein, obstructing the exposure of the residues that interact with the inner surfaces of encapsulin. This was confirmed when loading KR inside encapsulin, where N-terminally ESig-tagged KR benefit from a flexible peptide linker that presumably improved the folding of ESig and consequently KR's encapsulation. The use of the ESig on the N-terminus of KR could allow to explore the N-terminus as an alternative for proteins that have functional moieties towards the C-terminus. Additionally, it is unclear if the positioning of the ESig at the N- or C-terminus of the cargo has an impact on the affinity of ESig towards encapsulin. Recently, it was reported that an encapsulin system found exclusively in Firmicutes present one C-terminally ESig-tagged core cargo (Iron-Mineralizing Encapsulin-Associated Firmicute (IMEF) and a secondary N-terminally ESig-tagged cargo (Ferredoxin, Fer). Expression of the encapsulin, IMEF and Fer genes from the strain *Bacillaceae bacterium* MTCC10057, resulted in the encapsulation of just IMEF while when expressing just Fer and encapsulin, Fer was encapsulated ¹. This could suggest that the N-terminally tagged proteins have lower affinity towards encapsulin than C-terminal ESig, explaining why there is a preference for the loading of IMEF. Nevertheless, this assumption does not consider the fact that these are different proteins and as it is shown in our study, even very similar proteins tagged with the same ESig can show marked cargo loading differences. Based on this, it would be interesting to test if the cargo loading of mSOG2 tagged with a N-terminal ESig results in lower number of molecules encapsulated. Another approach to control the amount of cargo loaded inside encapsulin could involve using different promoters to regulate the induction and expression of the cargo and encapsulin in *E. coli*. In order to do this, the cargo and encapsulin genes could be cloned in BlgBrick vectors which allow to test protein expression with several combinations of plasmid copy number, promoter strength, inducible expression system, and selection markers ². Controlling the cargo loading inside encapsulin could provide the opportunity to find the perfect balance between amount of protein loaded and production of ROS.

Other ways to achieve higher ROS generation could be by substituting the cargo protein and/or the protein shell. Recently, there has been a growing interest in modifying mSOG1 and KR to enhance or change some of their features. For example, mSOG1 was rationally designed to create the singlet oxygen photosensitizing protein (SOPP3). This protein showed a $^1\text{O}_2$ quantum yield (~ 0.6) comparable to FMN (~ 0.65) which is 20-fold higher than the parental protein ³. In the case of KR, monomeric versions have been created such as SuperNova (SN) and monomeric KillerOrange (mKO) ^{4, 5}. SN presents similar fluorescence properties to KR and has been reported to produce a higher ROS quantum yield than tandem KR ^{4, 6}. Additionally, its monomeric state is advantageous when protein fusion and subcellular localization are required (e.g. chromophore-assisted light inactivation experiments) ⁴. mKO is the monomeric version of KillerOrange a variant of KR that display orange fluorescence and its ROS production can be activated at a different light range (450-550 nm) ^{5, 7}.

In terms of the protein shell, about 900 encapsulin systems have been discovered from all genomes available. However, very few of them have been characterized ¹. Therefore, there is a plethora of encapsulins system that might have evolved features that allow a higher resistance to ROS production. For example, the encapsulin from *Quasibacillus thermotolerans* have inner and outer diameters of ~ 43 nm and ~ 30 nm, respectively. It also presents pores of ~ 1 nm in diameter at the 5-fold and 3-fold axes ⁸. The larger size of *Q. thermotolerans* encapsulin could hold a higher amount of cargo and the presence of larger pores could benefit the diffusion of O_2 and ROS in and out the nanocompartment, respectively. Additionally, other encapsulin systems reported to have cargoes related to ROS protection could be screened for enhanced ROS resisting qualities.

In **Chapter 2** we also show the potential of our light-activated $^1\text{O}_2$ -producing nanoreactor (Enc-mSOG1-ESig $_{\text{T}}$) for applications in PDT. In contrast to free mSOG1-ESig $_{\text{T}}$, which did not present phototoxicity, Enc-mSOG1-ESig $_{\text{T}}$ decreased the viability of A549 lung cancer cells up to ~ 34 % after 8-12h of incubation. These findings suggest that encapsulation facilitated the cellular uptake of mSOG1. Nevertheless, mSOG1 has been modified with cancer targeting moieties that have increased its phototoxicity reaching a 79% viability reduction in SK-BR-3 breast

adenocarcinoma cells. In order to increase the phototoxicity of Enc-mSOG1-ESigT, its outer surface could be modified with cell penetrating peptides such as RGD and TAT that have been successful in mediating the cell uptake of other PNC (e.g. ferritin and virus like particles) ⁹⁻¹¹. Alternatively, more specific targeting peptides could be used such as the newly discovered lung cancer peptide 1 (AWRTHTP) which shows high binding affinity towards A549 lung cancer cells ¹². This would increase the amount of Enc-mSOG1-ESigT inside the cell. Another variable that can affect the efficacy of the treatment with PNC is the route of cellular internalization. PNC are internalized via endocytosis, which is divided into four subcategories macropinocytosis, the clathrin-mediated pathway, the caveolae-mediated pathway, and the clathrin/caveolae independent pathway ¹³. The uptake of PNC can be mediated by one or more of these pathways and the preference for any of them is determined by a PNC's structural features, surface chemistry and interactions with the cytoplasmic membrane ¹³. Excluding the caveolae-mediated pathway, all these pathways result in trafficking from early endosomes to lysosomes which is known to present acidic pHs (5.5-4.5) and proteolytic enzymes. This harsh environment can result in the degradation of a PNC ¹³. For further application of Enc-mSOG1-ESigT and future improved versions it is essential to characterize their internalization pathways, for example by fluorescent microscopy. Additionally, if the endo-lysosomal pathway happens to be the internalization route, encapsulin can be modified to display on its surface membrane fusion peptides used for endosomal escape. For instance, the amphiphilic pH-sensitive GALA peptide (WEAALAEALAEALAEHLAEALAEALEALAA) structure changes from random to α -helical when the pH drops from 7.0 to 5.0. This can result in destabilization of lipid membranes and consequently it might cause endosomal release ¹⁴. The display of GALA on the surface of a bio-nanocapsule derived from the Hepatitis B virus envelope L protein was proven to allow the bio-nanocapsules release into the cytoplasm of cancer cells ¹⁵.

In **Chapter 3** we show that encapsulated KR (Enc-ESig-L-KR) has similar features in terms of fluorescence and ROS-production as its free counterpart. Thus, suggesting that Enc-ESig-L-KR could have the same photocytotoxic properties as free KR. KR exhibits a strikingly high phototoxicity in KR-expressing *Escherichia coli* and mammalian cells when compared to other fluorescent proteins (e.g. dsred,

mCherry)^{16, 17}. Enc-ESig-L-KR phototoxic activity on bacteria could be explored for photodynamic inactivation (antimicrobial PDT), which is a novel approach to combat pathogenic microorganism¹⁸. Additionally, KR's ROS-production has been used for light-induced killing of cancer cells by delivery of either the KR gene, the recombinant protein or KR-expressing *E. coli* cells¹⁹⁻²¹. To improve specific delivery and to enhance its phototoxicity, KR has been tagged with the antibody 4D5scFV, which specifically targets tumors that overexpress HER2/neu. 4D5scFV-KR, selectively killed HER2/neu expressing ovarian carcinoma SKOV-3 cells²². Therefore, Enc-ESig-L-KR could be modified to display targeting peptides on its outer surface to evaluate its light-activated PDT effect on cancer cells.

One challenge of PDT is the restricted penetration of light into deep tissue which limits the applications of most photosensitizers. To extend the application of KR and mSOG to treat deep-seated tumours, these biological photosensitizers can be paired with molecules that emit the excitation light needed to trigger their ROS production in those environments. One example of this approach is the use of upconversion nanoparticles (UCNPs). UCNPs can be excited with deep-penetrating near infrared light (NIR) causing the emission of light at different wavelengths in the UV-visible range (depending on their composition)²³. The emitted light can be used to activate the localized production of ROS from photosensitizers. For instance, UCNPs have been conjugated to KR²⁴. A comparison between conventional KR (activated by low-penetrating light) and UCNP-mediated KR treatment of MDA-MB-231 breast cancer cells buried under 10 mm muscle tissue, showed that the KR-UCNPs photosensitisation by the NIR light was 10-fold more effective than the KR photosensitised by a light²⁴. This UCNP-based strategy could also be applied to activate ROS-generation by mSOG. For example, the activation of FMN, mSOG's chromophore, by a blue-light emitting UCNP exerted a ~90% growth inhibition of grafted breast cancer (SK-BR-3) tumours in immunocompetent mice²⁵. Although UCNPs represent a promising route to deliver light into deep-seated tumors, they can suffer from low solubility, poor biocompatibility, and a tendency to aggregate after functionalisation, which severely limits their biological safety. The encapsulation of luminescent UCNPs inside encapsulin could address these limitations by providing a soluble, biocompatible, and a functionalizable outer coating. To achieve this, UCNPs could be synthesized accurately so that they fit inside

the interior cavity of encapsulin (~20 nm diameter). An ESig-tagged protein photosensitizer could be attached to UCNPs via a ligand exchange reaction. Furthermore, by using the guanidine hydrochloride-based *in vitro* disassembly/reassembly method reported for *T. maritima* encapsulin the functionalised UCNPs might undergo selective encapsulation via the attached photosensitizer's ESigs^{26, 27}. This ESig-directed loading method has been employed to encapsulate gold nanoparticles in encapsulin²⁸. If successful, subsequent assessment of their ability to activate our ROS-generating nanoreactors will be performed.

Chapter 4 presents the preliminary results obtained for the engineering of a new approach to achieve the controlled release of therapeutics from encapsulin inner cavity. Firstly, a protocol was developed in which encapsulin was disassembled under basic conditions (pH 13) and then re-assembled by neutralizing the solution (pH 7.0). Subsequently, the aim was to determine whether this mechanism could be used to *in vitro* load the anti-cancer drug doxorubicin (DOX) into encapsulin. It was determined that DOX could not be loaded into encapsulin via this approach. Based on these results the previously mentioned guanidine hydrochloride disassembly/reassembly strategy could be evaluated for the *in vitro* loading of small-molecule drugs. In addition, DOX has been conjugated to peptides²⁹; therefore, it is presumed its conjugation to ESig might achieve a selective loading of DOX with a better encapsulation yield.

Secondly, our objective was to develop an encapsulin that can be non-invasively triggered by light to disassemble *in vivo* and release therapeutic drugs. To achieve this, the photoswitchable unnatural amino acid (UAA), phenylalanine-4'-azobenzene (AzoPhe) will be genetically incorporated into the inter-subunit space of the encapsulin macrostructure at regions essential for its assembly and stability. Upon light excitation, the AzoPhe will controllably 'switch' from *cis* (short) to *trans* (long) isomers that disrupt the encapsulin structure to release its drug cargo. To check whether the chosen strategy to incorporate AzoPhe inside proteins was feasible, sfGFP and encapsulin were mutated for the incorporation of AzoPhe. The proteins were expressed and after supplementation with AzoPhe good expression

was reached indicating the successful incorporation of AzoPhe using the amber codon system.

To determine optimal amino acid positions for AzoPhe incorporation into encapsulin, I initiated an international collaboration with Professor Ingemar André, Lund University and Prof Sinisa Bjelic, Linneus University, Sweden experts in protein modelling and design. From the modelling results 3 amino acid residues that could be substituted with AzoPhe for potential light-triggered disassembly of encapsulin were selected. Genes encoding the 3 encapsulin variants with substitutions at each of these pre-defined positions were synthesized (nEncXAzoPhe) and incorporated into an expression vector. *E. coli* BL21 strains were transformed with the expression plasmids in charge of the incorporation of AzoPhe and nEncXAzoPhe. Due to time constraints these gene constructions have not been evaluated.

Future work will require the production of rationally designed variants in *E. coli* with pre-irradiated AzoPhe (365 nm) to allow the incorporation of the shorter *cis* form of AzoPhe and the formation of the Enc macrostructure. Any assembled Enc variants will require purification and irradiation with blue light (420 nm) to initiate disassembly by converting AzoPhe into the sterically disruptive longer *trans* isoform. The integrity, assembly, and disassembly of encapsulin variants will involve assessment by Native-PAGE, TEM, and DLS techniques. From this point onward we will select the variants that can be disassemble by light and then a test if re-assembly can be activated by switching between 365 nm and 420 nm light irradiation. Moreover, if the expression in *E. coli* is found difficult because of amber codon readthrough or low expression of the proteins, cell-free approaches for production of proteins with UAA will be used. These approaches have been proven to address these challenges reaching great protein yields and high fidelity of UAA incorporation ³⁰.

Overall, this work shows the potential of encapsulins as engineerable platforms for the construction of customized nanoreactors for applications ranging from biotechnology to biomedicine. However, regulating cargo loading is a major challenge and further understanding of the variables that affect this process could broaden the possible applications of encapsulin-based technologies.

References

1. Giessen, T. W.; Silver, P. A., Widespread distribution of encapsulin nanocompartments reveals functional diversity. *Nature microbiology* **2017**, *2*, 17029.
2. Lee, T. S.; Krupa, R. A.; Zhang, F.; Hajimorad, M.; Holtz, W. J.; Prasad, N.; Lee, S. K.; Keasling, J. D., BglBrick vectors and datasheets: A synthetic biology platform for gene expression. *Journal of Biological Engineering* **2011**, *5* (1), 12.
3. Westberg, M.; Bregnhøj, M.; Etzerodt, M.; Ogilby, P. R., No Photon Wasted: An Efficient and Selective Singlet Oxygen Photosensitizing Protein. *Journal of Physical Chemistry B* **2017**, *121* (40), 9366-9371.
4. Takemoto, K.; Matsuda, T.; Sakai, N.; Fu, D.; Noda, M.; Uchiyama, S.; Kotera, I.; Arai, Y.; Horiuchi, M.; Fukui, K.; Ayabe, T.; Inagaki, F.; Suzuki, H.; Nagai, T., SuperNova, a monomeric photosensitizing fluorescent protein for chromophore-assisted light inactivation. *Science Reports* **2013**, *3*, 2629.
5. Pletneva, N. V.; Pletnev, V. Z.; Sarkisyan, K. S.; Gorbachev, D. A.; Egorov, E. S.; Mishin, A. S.; Lukyanov, K. A.; Dauter, Z.; Pletnev, S., Crystal Structure of Phototoxic Orange Fluorescent Proteins with a Tryptophan-Based Chromophore. *PLOS ONE* **2015**, *10* (12), e0145740.
6. Onukwufor, J. O.; Trewin, A. J.; Baran, T. M.; Almast, A.; Foster, T. H.; Wojtovich, A. P., Quantification of reactive oxygen species production by the red fluorescent proteins KillerRed, SuperNova and mCherry. *bioRxiv* **2019**, 777417.
7. Sarkisyan, K. S.; Zlobovskaya, O. A.; Gorbachev, D. A.; Bozhanova, N. G.; Sharonov, G. V.; Staroverov, D. B.; Egorov, E. S.; Ryabova, A. V.; Solntsev, K. M.; Mishin, A. S.; Lukyanov, K. A., KillerOrange, a Genetically Encoded Photosensitizer Activated by Blue and Green Light. *PLOS ONE* **2015**, *10* (12), e0145287.
8. Sigmund, F.; Pettinger, S.; Kube, M.; Schneider, F.; Schifferer, M.; Schneider, S.; Efremova, M. V.; Pujol-Martí, J.; Aichler, M.; Walch, A.; Misgeld, T.; Dietz, H.; Westmeyer, G. G., Iron-Sequestering Nanocompartments as Multiplexed Electron Microscopy Gene Reporters. *ACS Nano* **2019**, *13* (7), 8114-8123.
9. Lin, X.; Xie, J.; Niu, G.; Zhang, F.; Gao, H.; Yang, M.; Quan, Q.; Aronova, M. A.; Zhang, G.; Lee, S.; Leapman, R.; Chen, X., Chimeric Ferritin Nanocages for Multiple Function Loading and Multimodal Imaging. *Nano Letters* **2011**, *11* (2), 814-819.
10. Pan, Y.; Zhang, Y.; Jia, T.; Zhang, K.; Li, J.; Wang, L., Development of a microRNA delivery system based on bacteriophage MS2 virus-like particles. *The FEBS Journal* **2012**, *279* (7), 1198-1208.
11. Shan, W.; Zhang, D.; Wu, Y.; Lv, X.; Hu, B.; Zhou, X.; Ye, S.; Bi, S.; Ren, L.; Zhang, X., Modularized peptides modified HBc virus-like particles for encapsulation and tumor-targeted delivery of doxorubicin. *Nanomedicine: Nanotechnology, Biology and Medicine* **2018**, *14* (3), 725-734.
12. Bakhshinejad, B.; Nasiri, H., Identification of a Novel Tumor-Binding Peptide for Lung Cancer Through in-vitro Panning. *Iran J Pharm Res* **2018**, *17* (1), 396-407.
13. Sandra, F.; Khaliq, N. U.; Sunna, A.; Care, A., Developing Protein-Based Nanoparticles as Versatile Delivery Systems for Cancer Therapy and Imaging. *Nanomaterials* **2019**, *9* (9), 1329.

14. Nakase, I.; Kogure, K.; Harashima, H.; Futaki, S., Application of a Fusiogenic Peptide GALA for Intracellular Delivery. In *Cell-Penetrating Peptides: Methods and Protocols*, Langel, Ü., Ed. Humana Press: Totowa, NJ, 2011; pp 525-533.
15. Nishimura, Y.; Takeda, K.; Ezawa, R.; Ishii, J.; Ogino, C.; Kondo, A., A display of pH-sensitive fusogenic GALA peptide facilitates endosomal escape from a Bio-nanocapsule via an endocytic uptake pathway. *Journal of Nanobiotechnology* **2014**, 12 (1), 11.
16. Bulina, M. E.; Chudakov, D. M.; Britanova, O. V.; Yanushevich, Y. G.; Staroverov, D. B.; Chepurnykh, T. V.; Merzlyak, E. M.; Shkrob, M. A.; Lukyanov, S.; Lukyanov, K. A., A genetically encoded photosensitizer. *Nature Biotechnology* **2006**, 24 (1), 95-9.
17. Waldeck, W.; Heidenreich, E.; Mueller, G.; Wiessler, M.; Tóth, K.; Braun, K., ROS-mediated killing efficiency with visible light of bacteria carrying different red fluorochrome proteins. *Journal of Photochemistry and Photobiology B: Biology* **2012**, 109, 28-33.
18. Sperandio, F. F.; Huang, Y. Y.; Hamblin, M. R., Antimicrobial photodynamic therapy to kill Gram-negative bacteria. *Recent Patents on Anti-infective Drug Discovery* **2013**, 8 (2), 108-20.
19. Liao, Z.-X.; Li, Y.-C.; Lu, H.-M.; Sung, H.-W., A genetically-encoded KillerRed protein as an intrinsically generated photosensitizer for photodynamic therapy. *Biomaterials* **2014**, 35 (1), 500-508.
20. Yuan, M.; Liu, C.; Li, J.; Ma, W.; Yu, X.; Zhang, P.; Ji, Y., The effects of photodynamic therapy on leukemia cells mediated by KillerRed, a genetically encoded fluorescent protein photosensitizer. *BMC Cancer* **2019**, 19 (1), 934.
21. Yan, L.; Kanada, M.; Zhang, J.; Okazaki, S.; Terakawa, S., Photodynamic Treatment of Tumor with Bacteria Expressing KillerRed. *PLOS ONE* **2015**, 10 (7), e0131518.
22. Serebrovskaya, E. O.; Edelweiss, E. F.; Stremovskiy, O. A.; Lukyanov, K. A.; Chudakov, D. M.; Deyev, S. M., Targeting cancer cells by using an antireceptor antibody-photosensitizer fusion protein. *Proceedings of the National Academy of Sciences* **2009**, 106 (23), 9221-9225.
23. Gee, W. J., Recent trends concerning upconversion nanoparticles and near-IR emissive lanthanide materials in the context of forensic applications. *Australian Journal of Chemistry* **2019**, 72 (3), 164-173.
24. Liang, L.; Lu, Y.; Zhang, R.; Care, A.; Ortega, T. A.; Deyev, S. M.; Qian, Y.; Zvyagin, A. V., Deep-penetrating photodynamic therapy with KillerRed mediated by upconversion nanoparticles. *Acta Biomaterialia* **2017**, 51, 461-470.
25. Khaydukov, E. V.; Mironova, K. E.; Semchishen, V. A.; Generalova, A. N.; Nechaev, A. V.; Khochenkov, D. A.; Stepanova, E. V.; Lebedev, O. I.; Zvyagin, A. V.; Deyev, S. M.; Panchenko, V. Y., Riboflavin photoactivation by upconversion nanoparticles for cancer treatment. *Scientific Reports* **2016**, 6, 35103-35103.
26. Yao, C.; Wang, P.; Wang, R.; Zhou, L.; El-Toni, A. M.; Lu, Y.; Li, X.; Zhang, F., Facile Peptides Functionalization of Lanthanide-Based Nanocrystals through Phosphorylation Tethering for Efficient in Vivo NIR-to-NIR Bioimaging. *Analytical Chemistry* **2016**, 88 (3), 1930-1936.
27. Cassidy-Amstutz, C.; Oltrogge, L.; Going, C. C.; Lee, A.; Teng, P.; Quintanilla, D.; East-Seletsky, A.; Williams, E. R.; Savage, D. F., Identification of a Minimal Peptide Tag for in Vivo and in Vitro Loading of Encapsulin. *Biochemistry* **2016**, 55 (24), 3461-8.

28. Kunzle, M.; Mangler, J.; Lach, M.; Beck, T., Peptide-directed encapsulation of inorganic nanoparticles into protein containers. *Nanoscale* **2018**, *10* (48), 22917-22926.
29. Gao, L.; Yu, J.; Liu, Y.; Zhou, J.; Sun, L.; Wang, J.; Zhu, J.; Peng, H.; Lu, W.; Yu, L.; Yan, Z.; Wang, Y., Tumor-penetrating Peptide Conjugated and Doxorubicin Loaded T1-T2 Dual Mode MRI Contrast Agents Nanoparticles for Tumor Theranostics. *Theranostics* **2018**, *8* (1), 92-108.
30. Gao, W.; Cho, E.; Liu, Y.; Lu, Y., Advances and Challenges in Cell-Free Incorporation of Unnatural Amino Acids Into Proteins. *Frontiers in Pharmacology* **2019**, *10*, 611-611.

Appendix A: Ethics Approval

Appendix A of this thesis has been removed as it may contain sensitive/confidential content